Storage of Gases in Deep Geological Structures: Spatial and Temporal Hydrogeochemical Processes Evaluated and Predicted by the Development and Application of Numerical Modeling

D o c t o r a l T h e s i s
(D i s s e r t a t i o n)

to be awarded the degree
Doctor rerum naturalium (Dr. rer. nat.)

submitted by

M. Sc. Christina Hemme
from Hamburg, Germany

approved by the Faculty of Energy and Management Science,
Clausthal University of Technology,

Date of oral examination
26.02.2019

Chairperson of the Board of Examiners
Professor Dr. Hans-Jürgen Gursky (TU Clausthal)

Supervising tutor
Professor Dr. Klaus-Jürgen Röhlig (TU Clausthal)

Reviewer
PD Dr. Hans-Martin Schulz (Helmholtz Centre Potsdam)

Declaration

I hereby declare that I have created this Ph.D. thesis completely by my own and used no other sources that the ones listed, and I have marked any citations accordingly.

Christina Hemme Clausthal-Zellerfeld, December 2018

Acknowledgements

I would like to thank Prof. Dr. Wolfgang van Berk†, who supervised me until July 2018, for his scientific guidance, advice and helpful discussions throughout the years. He was always interested in my work and willing to share his scientific knowledge.

I highly appreciate the help of Prof. Dr. Klaus-Jürgen Röhlig who kindly took over supervision after the death of Prof. Dr. Wolfgang van Berk. Thank you for your valuable assistance and scientific support in the end phase of my Ph.D. studies.

A big thank to PD. Dr. Hans-Martin Schulz for preparing the reviews of my thesis.

Special thanks to all colleagues of the Institute of Geology and Paleontology and of the Institute of Disposal Research, especially Dr. habil. Elke Bozau.

I would like to thank my family for their help and support and - especially Nils Kollert - for your proof-reading, patience and understanding.

† Prof. Dr. Wolfgang van Berk passed away on 29.07.2018

Kurzfassung

Bei der Speicherung von Kohlenstoffdioxid und Wasserstoff in ausgeförderten Erdöl- und Erdgaslagerstätten und von Erdgas in Salzkavernen treten vielfältige hydrogeochemische Prozesse auf, die zum Verlust der Gase, zu Veränderungen der Gaszusammensetzung oder zu Problemen in der Abdichtung führen können.

Diese hydrogeochemischen Prozesse werden in der vorliegenden Arbeit identifiziert, mit reaktiven 1D- und 3D-Stofftransportmodellen quantifiziert und mit ihrer räumlich-zeitlichen Entwicklung abgebildet – auf der Grundlage i) chemisch-thermodynamischer Gesetzmäßigkeiten, ii) der Gesetzmäßigkeiten der Reaktionskinetik der bakteriellen Sulfat-Reduktion und Methanogenese und iii) der Gesetzmäßigkeiten des diffusiven Stofftransports. Die verwendeten Modellierungsprogramme sind PHREEQC und PHAST, die beide vom Geologischen Dienst der USA zur Verfügung gestellt werden.

In den Modellen werden hydrogeochemische Prozesse wie die Gas-Wasser-Gesteins Reaktionen unter gegebenen Druck- und Temperaturverhältnissen simuliert, die durch die Einspeicherung von Gasen im tiefen Untergrund ausgelöst werden. Ein mögliches Risiko entsteht durch die Auflösung von Mineralphasen in den abdichtenden Gesteinsschichten, die zu einer erhöhten Porosität und damit zu einer Verminderung der Abdichtung führt. Unter bestimmten hydrogeochemischen und Druck- und Temperaturbedingungen kann es durch Bakterien zu einer Umwandlung der gespeicherten Gase und damit zum Verlust der gespeicherten Energie kommen. Dabei nutzen Sulfat-reduzierende Bakterien das gespeicherte und gelöste Gas (Methan und/oder Wasserstoff), um vorhandene Sulfat-Ionen in den wässrigen Lösungen ($SO_4^{2-}{}_{(aq)}$) zu Sulfid-Schwefel zu reduzieren – und damit Energie für ihre Lebensprozesse zu gewinnen.

Die Modellierungsergebnisse erlauben es, Bedingungen zu ermitteln, die eine sichere Speicherung der Gase gewährleisten. Zudem können anhand der Modellierungsergebnisse diejenigen Faktoren identifiziert und deren Wirkungen quantifiziert werden, die auf die räumlich-zeitliche Entwicklung der Gasverluste einwirken. Mit der Hilfe solcher hydrogeochemischen Modellierungen kann die Speicherung von Gasen im tiefen Untergrund im Hinblick auf Sicherheit und Produktivität optimiert werden.

Abstract

Storage of carbon dioxide and hydrogen in depleted hydrocarbon reservoirs and natural gas storage in salt caverns trigger hydrogeochemical processes which can lead to a loss of the stored gas, a change in the gas composition, and a loss of the sealing capacities of the cap rock.

In this study, these different hydrogeochemical processes will be identified, quantified by 1D and 3D reactive mass transport models, and predicted in terms of their spatial-temporal development based on i) equilibrium thermodynamics, ii) kinetic reactions for sulfate reduction and methanogenesis, and iii) diffusive mass transport. The modeling codes used are PHREEQC and PHAST, both provided by the US Geological Survey.

In these models, hydrogeochemical processes, like gas–water–rock interactions under given pressure and temperature conditions induced by the storage of gases in deep geological structures, are simulated. A potential risk arises from the dissolution of mineral phases in the cap rock that can lead to an increased porosity and, therefore, to a decrease in the sealing capacity. Under specific pressure and temperature conditions, bacterial conversion of the stored gases can lead to a loss of the stored energy. Sulfate-reducing bacteria use the stored and dissolved gas (methane and/or hydrogen) to reduce available sulfate-ions in the aqueous solutions ($SO_4^{2-}{}_{(aq)}$) to sulfide-sulfur—to produce energy for growth.

The modeling results allow the identification of storage conditions that ensure safe underground gas storage. Furthermore, the modeling results help to identify the factors that influence the spatial and temporal development of gas loss and quantify their effects. Hydrogeochemical modeling provides an efficient tool for safe and productive underground gas storage in deep geological structures.

Preface

This cumulative Ph.D. thesis is based on three published (and peer-reviewed) articles. The topics were also presented at national and international conferences.

Papers

- Hemme, C., van Berk, W., 2018. Hydrogeochemical modeling to identify potential risks of underground hydrogen storage in depleted gas fields. Applied Sciences, 8(11), 2282. doi.org/10.3390/app8112282

- Hemme, C., van Berk, W., 2017. Potential risk of H_2S generation and release in salt cavern gas storage. Journal of Natural Gas Science and Engineering, 47, 114–123. doi.org/10.1016/j.jngse.2017.09.007

- Hemme, C., van Berk, W., 2017. Change in cap rock porosity triggered by pressure and temperature dependent CO_2-water-rock interactions in CO_2 storage systems. Petroleum, 3, 96–108. doi.org/10.1016/j.petlm.2016.11.010

Oral Presentations at Conferences

- Hemme, C., van Berk, W., 2017. Risk of H_2S contamination of natural gas stored in salt caverns. GeoBremen (2017).

Poster Presentations at Conferences

- Hemme, C., van Berk, W., 2017. H_2S Generation and Release in Salt Cavern Gas Storage. AAPG 2017 Annual Convention & Exhibition in Houston, Texas. http://www.searchanddiscovery.com/pdfz/documents/2017/42082hemme/ndx_hemmepdf.html

- Hemme, C., van Berk, W., 2015. One-Dimensional Reactive Transport Modeling of CO_2 Storage Systems - Change in Cap Rock Porosity Triggered by Pressure and Temperature Dependent CO_2-Water-Rock Interactions. AGU Fall Meeting, San Francisco 2015.

Contents

1 Introduction

Storage of gases in deep geological formations is of increasing interest due to the new German energy concept, which aims to reduce greenhouse gas emissions and expand renewable energies. Furthermore, increasing natural gas consumption leads to the strategic importance of future energy supply and access to efficient energy storage systems (Federal Ministry for Education and Research, 2011). This work was created in light of these debates and transformation processes. This study focuses on the hydrogeochemical processes relevant to the underground storage of gases in deep geological structures and related potentials and risks. These processes were evaluated and predicted in space and time by the development and application of numerical modeling. Therefore, the study is divided into three subtopics:

(i) carbon capture and storage (CCS),

(ii) salt cavern gas storage (SCGS),

(iii) underground hydrogen storage (UHS).

These technical means of storing gases in the underground trigger a series of hydrogeochemical processes. For successful underground gas storage, the analysis of gas–water–rock interactions is important because they can affect the storage efficiency and the sealing capacity of the cap rocks as well as the stored gas composition.

1.1 Review of Underground Gas Storage—State of Research

Storing gases in the underground has a long history starting with the first gas implementation in 1915 in Welland County, Ontario (Canada) in a depleted gas reservoir (Evans, 2008). Since that point, both research and practical experience in underground gas storage have evolved. Research in underground gas storage links a wide field of disciplines, including geology, geochemistry, oil and gas geology, engineering, mechanics, and social sciences.

Natural gas storage in the underground is used to provide flexibility in times of increasing dependence on natural gas imports. Germany imports around 91% of its natural gas and operates 57 storage facilities in total; 20 depleted oil and gas fields, 31 salt caverns, and 6 aquifers in 2016 (LBEG, 2016). In comparison, the global number of underground storage facilities amounts to 498 depleted oil and gas fields, 97 salt caverns, and 77 aquifers at the end of 2016 (Cornot-Gandolphe, 2017). The total volume of working gas capacity is 23.9 bcm in Germany versus 424 bcm worldwide (Cornot-Gandolphe, 2017). The storage of natural gas

in salt caverns has been studied with respect to the design of storage caverns (Crotogino et al., 2006), the geomechanics to analyze potential cavern instability and collapse (DeVries et al., 2002), and the economic aspects regarding low investment costs (Farahani et al., 2015). Furthermore, the interaction of storage gas with surface facilities, including computational-fluid-dynamics and heat-transfer-modeling, have been analyzed (Barajas and Faruk, 2014).

In addition to natural gas, the storage of carbon dioxide in the underground has gained in importance because of rising global carbon dioxide emissions. With CCS, the consequences of the additional greenhouse gases on climate change could be mitigated (IPCC, 2005). Germany operated only the in-situ testing site Ketzin, whereas worldwide carbon dioxide is stored in several projects e.g. Sleipner (North Sea), Weyburn (Canada) or In Salah (Algeria). Intensive studies on CCS were performed, including numerical simulation studies of CO_2 leakage (Pruess, 2013), related monitoring studies to detect leaks of carbon dioxide (Arts et al., 2004; Blackford et al., 2015), and the migration of carbon dioxide (Arts et al., 2004). Furthermore, seismic studies were conducted to discuss seismic activity due to CCS (Verdon and Stork, 2016). CCS technologies, like post-combustion, pre-combustion and oxy-combustion, are also the subject of debate (Araújo and de Medeiros, 2017; Leung et al., 2014). The possibility of enhanced oil recovery (EOR) by injection of compressed carbon dioxide into oil reservoirs is widely discussed (Emberley et al., 2005; Reichl et al., 2015).

Another gas that is discussed for potential storage in deep geological structures is hydrogen to balance the demand for energy from renewable energy sources. Hydrogen storage is known from town-gas storage, where a gas composed of $H_{2(g)}$, $CO_{2(g)}$, $CO_{(g)}$, $CH_{4(g)}$ and $N_{2(g)}$ is stored in an underground reservoir (Šmigáň et al., 1990). It is also known from Russia where it is stored for the aerospace industry (Panfilov, 2010; Ponomarev-Stepnoi, 2004) and from the US and the UK where hydrogen is already stored in salt caverns (Crotogino et al., 2010; Henkel et al., 2013; Panfilov, 2010; Stone et al., 2009). Special focus is also given in the literature on the capacity and efficiency of UHS (Crotogino et al., 2010), on the effects of hydrogen storage on the reservoir and cap rocks (Henkel et al., 2014; Truche et al., 2013), and on the integrity of wells as well as on material durability (Somerday and Gangloff, 2012). Furthermore, experimental studies have been performed in which the reactivity of hydrogen in sandstone was evaluated (Yekta et al., 2018). Additionally, possible biotic and abiotic reactions are analyzed in detail by Panfilov et al. (2006) and Panfilov (2016).

1.1.1 Underground Gas Storage—Risks and Potentials

Generally, gases can be stored in depleted oil and gas fields, aquifers, and salt caverns. All these storage options show advantages and disadvantages. The main advantages for depleted oil and gas fields are that the fields are fully explored, the technical installations and infrastructure are already available from production and the sealing capacity over geological timescales is verified. Disadvantages are the low operational flexibility and a high amount of cushion gas (Crotogino, 2011). Furthermore, hydrocarbons remaining from production are still present in the fields and could contaminate the stored gas and pose a risk for its quality. Another disadvantage is the possible risk of reactions between the stored gas and the rocks, fluids, and microorganisms present in depleted oil and gas fields (Crotogino, 2011).

Storing gases in aquifers entails the risk of reaction between the stored gas and the original rocks, fluids, and microorganisms as well. A high amount of cushion gas and low flexibility are further disadvantages of storing gas in aquifers. Furthermore, the pressure loss is increased when the injection and production rates are high. The information density about the aquifers is very low in most cases; therefore, the costs of exploring and verifying the sealing capacity are high (Crotogino, 2011).

The main advantage of storing gases in salt caverns is the high sealing capacity of the salt rock and its impermeability below 300 m (Evans, 2008; Yang et al., 2013). Another advantage is the high deliverability rate because of the high pressure in salt caverns. Furthermore, the ability to shift between injection and withdrawal is possible in a short period (Foster Associates Inc., 1995). The main disadvantages are that the caverns must be created in advance and that the construction period could last a few years. Additionally, the created brine must be disposed of in an environmentally friendly way (Crotogino, 2011).

The health, environmental and economic risks that could arise when storing gases underground are discussed in detail by Evans (2008), who focuses on the risk of stored product leakage to overlying formations or to the surface. However, all storage options have in common that the underground structures selected for gas storage should have the capacity to store the gases with no significant leakage. If large quantities of gas have to be stored, it is cheaper to store it underground than in containers (Panfilov, 2010). Storage in salt caverns is the cheapest solution, followed by storage in aquifers. The most expensive is storage in depleted gas reservoirs (Taylor et al., 1986).

A general problem arising from underground gas storage is the social implications. Storage of gases underground leads to an area of conflict between science, politics, economy, and public opinion. Public acceptance is a fundamental prerequisite for underground gas storage. Stone

et al. (2009) describe that the public of the UK accepts underground gas storage in principle as long as it does not affect their locality. For that reason, salt cavern gas storage in Thornton has been stopped (Beutel and Black, 2005; Stone et al., 2009). In general, acceptance depends mainly on the societal benefit and the political conflict (Pietzner, 2012). Comprehensive communication with the public is recommended (Pietzner, 2012), as has been done in the German Ketzin CCS pilot-project (Schilling et al., 2009). However, public acceptance and the concrete inclusion of CCS in the political energy concept is missing in Germany (Pietzner, 2012; Vögele et al., 2018). The difficulties when striving for acceptance of underground gas storage is also seen in other underground operations like fracking and radioactive waste disposal.

In addition to natural gas, hydrogen and carbon dioxide, substances like compressed air, thermal energy, crude oil, geothermal energy, and radioactive waste must be stored in the underground. Therefore, the demand for underground storage options rises. In some cases, the same storage options are possible for different storage mediums (Crotogino, 2011) so that multiple conflicts of interest regarding the demand of underground storage capacities come up (Zander-Schiebenhöfer et al., 2014). To counter this, subsurface spatial planning is required, (Schulze et al., 2015) and a range of conditions for safe storing options for each storage product must be identified.

1.1.2 Hydrogeochemical Processes—Mineral Dissolution and Precipitation

An important aspect of underground gas storage is the reaction of the stored gases with the minerals of the reservoir rock and the cap rock, which can lead to mineral dissolution and precipitation and resulting in porosity changes, as is known from CCS (e.g. Bildstein et al. (2010), Gaus et al. (2008), Mohd Amin et al. (2014)) and from UHS (Amid et al., 2016). Porosity changes in the cap rock can either improve or deteriorate its sealing capacity (Gaus et al., 2005). Furthermore, the precipitation of minerals at the well equipment may cause scaling (Reitenbach et al., 2015).

1.1.3 Pressure and Temperature Conditions

In Germany, salt caverns are at depths of 500–2000 m and depleted gas fields are at depths of 350–2930 m (LBEG, 2016). Temperature and pressure conditions are correspondingly high, considering the geothermal gradient of 33.3 °C per kilometer of depth and the pressure

increase of 100 atm per kilometer of depth under hydrostatic conditions. These higher pressure and temperature conditions must be considered when modeling CCS, SCGS, and UHS because temperature and pressure could strongly affect the mass-action law constants of the equilibrium reactions and the kinetic rate constants. Authors like Bildstein et al. (2010) and Van Pham et al. (2012) considered higher pressure and temperature conditions at starting conditions when modeling CO_2 storage in deep geological structures but disregarded that temperature and pressure conditions change along the path of diffusive transport of the stored gases.

1.1.4 Microbial Processes in Underground Gas Storage

Some important processes when storing gases in the underground are the microbial activities, including bacterial sulfate reduction, methanogenesis, acetogenesis, and iron(III)-reduction, summarized by Hagemann et al. (2016). The stored gases are microbially catalyzed and converted by bacteria. The activity of the different bacteria depends on the availability of different electron acceptors such as sulfate or carbon dioxide (Ebigbo et al., 2013). The energy that is gained from conversion is used by the bacteria for cell growth (Cord-Ruwisch et al., 1987; Šmigáň et al., 1990; Whitman et al., 2006). The influences of these processes in underground gas storage systems are extensively discussed in the literature (Ebigbo et al., 2013; Hagemann et al., 2016; Kleinitz and Böhling, 2005; Panfilov, 2010).

An important microbial process when storing natural gas and hydrogen in deep geological structures is the bacterial sulfate reduction (BSR). BSR occurs in low-temperature geological settings ranging from 0 °C to a maximum of 110 °C (Bernardez et al., 2013; Ehrlich, 1990; Jorgensen et al., 1992; Machel, 2001; Postgate, 1984). The sulfate-reducing bacteria (SRB) use sulfate as an electron acceptor to oxidize organic compounds and generate sulfide in aqueous anoxic environments. Even if the optimal growth conditions for SRB are at near-neutral pH (Cord-Ruwisch et al., 1987), SRB also occur in more acidic environments of pH 3–4 (Church et al., 2007; Tuttle et al., 1969). The activity of SRB has been observed in a wide range of environments, for example, in hydrocarbon reservoirs (Machel, 2001), in underground gas storage in porous media (Kleinitz and Böhling, 2005), in the underground storage of town gas (Postgate, 1979) and in salt caverns filled by hydrogen gas (Panfilov, 2016).

Another microbial process that is important for hydrogen storage is methanogenesis. Here, hydrogen is the electron donor and carbon dioxide the electron acceptor, which is reduced to form methane. Methanogenic bacteria have been found in environments with temperatures up to 97 °C (Gusev and Mineeva, 1992; Panfilov, 2016). The existence of methanogenic bacteria

has been observed, for example, in anoxic sediments, flooded soils (Whitman et al., 2006), and in town gas storages (Šmigáň et al., 1990).

1.1.5 Chemical and Physical Properties of the Stored Gases

The chemical and physical properties of the stored $CO_{2(g)}$, $CH_{4(g)}$ and $H_{2(g)}$ are extensively discussed in the literature, including e.g. the effective diffusion coefficients, the viscosity, and the solubility in water. For a comparison of these gases, the properties are summarized in Table 1.1.

Table 1.1 Chemical and physical properties of the stored gases.

	Carbon dioxide	**Methane**	**Hydrogen**
Chemical formula	CO_2	CH_4	H_2
Effective diffusion coefficient (m^2 s^{-1})	3.33×10^{-10} [a]	$2.35\text{-}2.49 \times 10^{-10}$ (in clayey rocks at 21 °C)[b]	3.0×10^{-11} (in clayey rocks at 25 °C)[c]
Diffusion coefficient in pure water at 25 °C (m^2 s^{-1})	1×10^{-9} [a]	1.85×10^{-9} [d]	5.13×10^{-9} [d]
Solubility in pure water at 25 °C and 1 atm (mol kgw^{-1})	3.5×10^{-2} [d]	1.4×10^{-3} [d]	7.9×10^{-4} [d]
Viscosity (kg m^{-1} s^{-1})	9.41×10^{-5} (at 197.4 atm; 26.85 °C)[e]	1.81×10^{-5} (at 197.4 atm; 76.85 °C)[f]	1.01×10^{-5} (at 167.8 atm; 76.85 °C)[g]
Solubility constant log *K*	-1.468[d]	-2.8502[d]	-3.1050[d]
Critical temperature (°C)	31.05[d]	-82.55[d]	-239.95[d]
Critical pressure (atm)	72.86[d]	45.40[d]	12.80[d]

[a]: based on assumptions made by Mohd Amin et al. (2014): diffusion coefficient in pure water of 1×10^{-9} m^2 s^{-1} divided by an averaging tortuosity of 3
[b]: Jacops et al. (2013)
[c]: Krooss (2008)
[d]: based on phreeqc.dat
[(e)]: Laesecke and Muzny (2017)
[f]: Friend et al. (1989)
[g]: McCarty et al. (1981)

Considered as a whole, the modeling of hydrogeochemical processes induced by gas storage becomes increasingly important. Hydrogeochemical studies were performed for CCS by e.g. Gaus et al. (2005) and Bildstein et al. (2010) and for UHS by Amid et al. (2016). These processes are still not fully understood and need further research to gain a comprehensive process understanding.

1.2 Aims of This Study

The aim of this study is to contribute to a general system and process understanding of the hydrogeochemical effects related to underground gas storage in deep geological structures on aqueous solutions, mineral phases and gas compositions in the storage systems. Furthermore, one main objective is to provide hydrogeochemical model approaches which can be used and adapted to various underground gas storage systems and conditions to answer and solve practical oriented questions and problems. This includes the identification and analysis of the hydrogeochemical processes induced by the storage of $CO_{2(g)}$, $CH_{4(g)}$, and $H_{2(g)}$ in deep geological formations. Special attention is given to the gas–water–rock interactions, spatial and temporal dependence, and on temperature and pressure influenced reactions. Thereby, the risks and potentials of storing gases in the underground will be analyzed with the aim to answer the following main questions:

1) How does the storage of $CO_{2(g/sc)}$ influence the sealing capacity of the cap rocks?

To answer this question, the hydrogeochemical processes, including gas–water–rock interactions, induced by carbon capture and storage are identified. The change in porosity of the cap rock because of geochemical reactions are quantified in dependence on pressure and temperature.

2) Is $H_2S_{(g)}$ generation a risk when storing natural gas in salt caverns?

The aim of the second part of this study is to draw the attention to the possible risk of $H_2S_{(g)}$ pollution in salt caverns filled with natural gas, to clarify and quantify time-dependent $H_2S_{(g)}$ generation processes, and to analyze the limiting factors for $H_2S_{(g)}$ generation and release. In the course of this, the viability of reducing or inhibiting $H_2S_{(g)}$ generation and release is tested.

3) Which factors influence the loss of hydrogen in depleted gas storage?

The aim of the third part of the study is to investigate the loss of hydrogen by bacterial conversion over storage times at reservoir scale and to describe qualitatively and quantitatively which reservoir and cap rock minerals dissolve or newly form because of hydrogen storage. Furthermore, the loss of hydrogen by diffusion is analyzed.

1.3 Hydrogeochemical Reactive Mass Transport Modeling

1.3.1 Basics of Hydrogeochemical Modeling

A model is a representation of a real system or process (Konikow and Bredehoeft, 1992). The basis of a model is the definition of a conceptual model with the hypothesis for how a system or process operates (Konikow and Bredehoeft, 1992). Modeling is based on a multistage process of abstraction whereby the results of each stage can be understood as a model of the previous stage. A conceptual model can be expressed quantitatively by mathematical models, where abstractions replace objects, events, and forces, and also by using expressions that involve mathematical constants, variables, and parameters (Konikow and Bredehoeft, 1992; Krumbein and Graybill, 1965). The results of the numerical computer model are subsequently compared with the real system or process.

Hydrogeochemical systems are defined by one or more phases which can be aqueous$_{(aq)}$, gaseous$_{(g)}$ and/or solid$_{(s)}$ (Stumm and Morgan, 1981). Reactions take place in single phases$_{(aq, g, s)}$ as well as between the phases like i) aqueous species$_{(aq)}$ and solid$_{(s)}$ phases, ii) aqueous species$_{(aq)}$ and gases$_{(g)}$ and iii) solid$_{(s)}$ phases and gases$_{(g)}$, the so-called gas–water–rock interactions.

For numerical modeling of gases stored in deep geological formations, chemical-thermodynamic or kinetically based model approaches can be chosen. Thermodynamic systems are defined by variables like pressure, temperature, density, volume, concentration of dissolved components, viscosity, etc. Chemical-thermodynamic based models describe the initial and final state of irreversible reactions. The kinetic-based model must be chosen, when the change in concentrations of the involved chemical substances in an irreversible reaction must be considered.

Models should always be tested with sensitivity and parameter studies to identify the main influencing factors (Konikow and Bredehoeft, 1992). For building confidence in the model, different approaches can be applied. This includes quality assurance (of e.g. the scientific bases), comparison with other models (e.g. code verification), and real systems (including laboratory experiments, field tests, and natural analogs). With the help of models, a critical analysis is provided (Konikow and Bredehoeft, 1992) and modeling approaches could be tested.

1.3.2 Thermodynamic Equilibrium Reactions

With the thermodynamics of chemical equilibrium, reactions and their direction and conversion until equilibration are described. Chemical equilibrium is defined by the law of mass action (Equation (1.1)) and related equilibrium constants. Equilibrium constants are based on the properties of the atoms, molecules, ions, and phases which are involved in the reactions. They are functions of temperature, pressure, and composition (Stumm and Morgan, 1981) and are independent of the hydrogeochemical environment (van Berk and Hansen, 2006). The data required for equilibrium models, apart from equilibrium constants, are the Gibbs free energies, enthalpies, entropies, and heat capacities (Stumm and Morgan, 1981).

The law of mass action describes reversible equilibrium reactions (Equation (1.1)).

$$K = \frac{\{C\}^c \cdot \{D\}^d}{\{A\}^a \cdot \{B\}^b} \tag{1.1}$$

where *K* is the thermodynamic equilibrium constant (-), *a*, *b*, *c*, and *d* are stoichiometric coefficients (-), *A* and *B* are the reactants (mol L^{-1}), and *C* and *D* are the reaction products (mol L^{-1}).

The dissolution of a mineral *AB* to its components *A* and *B* is described by the law of mass action as follows (Equation (1.2)):

$$K = \frac{\{A\} \cdot \{B\}}{\{AB\}} \tag{1.2}$$

Because the activity of solid phases is assumed to be constant at 1, the solution product *L* or the ion activity product *IAP* is derived from the thermodynamic equilibrium constant *K* (Equation (1.3)).

$$L = IAP = \{A\} \cdot \{B\} \tag{1.3}$$

Based on *L* and *IAP*, the saturation index (*SI*) of a mineral phase can be calculated. *SI* describes if a mineral phase is in equilibrium with the aqueous solution or if the aqueous solution is over- or undersaturated regarding a specific mineral phase (Equation (1.4)). If *SI* < 0 the mineral phase dissolves. If *SI* = 0 the phase is in equilibrium and with SI > 0 the mineral phase precipitates.

$$SI = log_{10}\left(\frac{IAP}{L}\right) \tag{1.4}$$

IAP is calculated from the concentrations of a given water sample by recalculation as activity and *L* is defined as the maximal solubility (given in databases). The temperature dependence must be considered.

1.3.3 Reaction Kinetics

While the thermodynamic-equilibrium reaction assumes a time-independent stable state for a system, with reaction-kinetics an unstable chemical state at any time of reaction can be calculated. This can be relevant if slow irreversible, reversible or heterogeneous reactions (reactions between the different phases: aqueous, gaseous, and solid) are included in the system (Merkel and Planer-Friedrich, 2002). For kinetic-based models, either the values for the rate constants or half-lives are needed. The rate constants are functions of pressure, temperature and solution composition (Stumm and Morgan, 1981). These rate constants and half-lives describe the reaction rates and the mechanisms of the defined reaction. Because they are dependent on pressure, temperature, and solution composition, they are not universally valid constants. These constants were determined in laboratory and field studies and are, unlike the equilibrium constants, dependent on the hydrogeochemical environment.

1.3.4 Reactive Mass Transport

Reactive mass transport models simulate the transport of aqueous species coupled with the chemical reactions to show the temporal and spatial development of hydrogeochemical processes. With the help of reactive mass transport coupled chemical, physical and biological processes can be analyzed (Steefel et al., 2005). The main transport processes of aqueous species are advection, dispersion, and molecular diffusion. Advection describes the movement of aqueous species with the velocity of the flowing fluid (Equation (1.5)).

$$j_{adv} = v \cdot C \tag{1.5}$$

where j_{adv} is the advective mass transport (mol s^{-1} m^{-2}), v is the flow velocity (m s^{-1}), and C is the species concentration (mol L^{-1}).

Dispersion describes the changes in aqueous species concentration by advective mass transport in the fluid induced by differences in geometry and structure of the rock (Equations (1.6) and (1.7)).

$$j_{dispL} = -D_L \frac{\delta C}{\delta s_L} \tag{1.6}$$

$$j_{dispT} = -D_T \frac{\delta C}{\delta s_T} \tag{1.7}$$

where j_{dispL} is the longitudinal dispersive mass transport (mol s^{-1} m^{-2}), j_{dispT} is the transversal dispersive mass transport (mol s^{-1} m^{-2}), D_L is the longitudinal dispersion coefficient (m^2 s^{-1}), D_T is the transversal dispersion coefficient (m^2 s^{-1}), $\delta C/\delta s_L$ is the species concentration gradient in longitudinal direction (mol L^{-1}), and $\delta C/\delta s_T$ is the species concentration gradient in transversal direction (mol L^{-1}).

The diffusion is described by Fick´s law (Equation (1.8)). The diffusive mass transport is induced by concentration gradients.

$$j_{diff} = -D_e \frac{\delta C}{\delta x} \tag{1.8}$$

where j_{diff} is the diffusive mass transport (mol s^{-1} m^{-2}), D_e is the effective diffusion coefficient (m^2 s^{-1}), and $\delta C/\delta x$ is the species concentration gradient in x-direction (mol L^{-1}).

Reactive mass transport can be explained by transport equations in 1D (Equation (1.9), Section 1.3.5.1) or 3D (Equation (1.10), Section 1.3.5.2).

1.3.5 Modeling Tools

The programs used in this study for hydrogeochemical modeling are PHREEQC (Parkhurst and Appelo, 2013) and PHAST (Parkhurst et al., 2010), both provided by the US Geological Survey. PHREEQC and PHAST connect hydrogeochemical and geohydraulic models to reactive mass transport. Further programs with the capability for hydrogeochemical modeling are The Geochemist´s Workbench (Bethke and Yeakel, 2009), EQ 3/6 (Wolery, 1992), MINTEQA2 (Allison et al., 1991), and WATEQ4F (Ball and Nordstrom, 1991).

1.3.5.1 PHREEQC

PHREEQC (= **pH**-**Re**dox-**Eq**uilibrium written in the **C** programming language) is a computer simulation program with the capability to calculate batch-reaction, one-dimensional (1D) transport, speciation, and inverse geochemical calculations. It is written in the programming languages C and C++ and can be used for aqueous geochemical modeling in a wide field of application and in a wide range of hydrogeochemical environments (Parkhurst and Appelo, 2013). The basis of PHREEQC is the equilibrium chemistry of aqueous solutions that interact with gases, minerals, solid solutions, sorption surfaces, and exchangers, but it is also possible to include kinetically-controlled reactions whereby the interconnection of equilibrium and kinetic reactants is possible.

The transport calculations (1D) in PHREEQC are used to model the movement of solutions through a column, where the initial compositions of aqueous solutions, minerals, and gases are pre-defined and the changes induced by transport (Appelo and Postma, 2005) are simulated and are coupled with irreversible and reversible chemical reactions (Parkhurst and Appelo, 2013). PHREEQC has the capability to simulate advective-transport calculations as well as advective-dispersive and/or diffusive transport calculations (Parkhurst and Appelo, 2013). Reactive mass transport in one dimension can be explained by the Advection-Reaction-Dispersion Equation (ARD) (1.9), which is a second order partial differential equation.

$$\frac{\partial C}{\partial t} = -v\frac{\partial C}{\partial t} + D_L\frac{\partial^2 C}{\partial x^2} - \frac{\partial q}{\partial t} \tag{1.9}$$

where C is the concentration in water (mol kgw^{-1}), t is the time (s), v is the pore water flow velocity (m s^{-1}), D_L is the hydrodynamic dispersion coefficient [m^2 s^{-1}, $D_L = D_e + \alpha_L v$, with D_e the effective diffusion coefficient and α_L the dispersivity (m)], x is the distance (m), and q is the concentration in the solid phase (expressed as mol kgw^{-1} in the pores). Numerical solution methods for the mass-transport-equation coupled to chemical reactions use the finite volume, finite element, or finite difference method.

1.3.5.2 PHAST

With PHAST (= **PH**REEQC **A**nd H**ST**3D), 3D models with 3D mass transport, diffusion, and chemical reactions can be simulated. Using PHAST, multicomponent geochemical reactions, solute transport, and groundwater flow can be modeled (Parkhurst et al., 2010). The geochemical reactions in PHAST are simulated with PHREEQC, and the flow and transport

calculations are based on HST3D; both programs are embedded in PHAST (Parkhurst et al., 2010). The results are visualized using the software Model Viewer (Hsieh and Winston, 2002).

The transport equation used in PHAST is different from that in PHREEQC because a 3D transport equation, which considers equilibrium and kinetic reactions, is applied (Equation (1.10)). The equation is modified by Parkhurst et al. (2010) from Bear (1972) and Kirkner and Reeves (1988).

$$\frac{\delta}{\delta_t}\left(\varepsilon\rho c_j\right) = \nabla\cdot\varepsilon D\nabla\rho c_j - \nabla\cdot\varepsilon v\rho c_j - \sum_{e=1}^{N_E} v_{j,e}^{E}\frac{\delta}{\delta t}\left(\varepsilon\rho\bar{c}_e\right) + \sum_{k=1}^{N_K} v_{j,k}^{K}\,\varepsilon\rho R_k + \mathrm{q}\varepsilon\rho\hat{c}_j \qquad (1.10)$$

$$j = 1, \ldots, N_C$$

where ε is the saturated porosity (-), ρ is the density of water (kg m^{-3}), v is the interstitial velocity (m s^{-1}), c_j is the total aqueous concentration of component j (mol kgw^{-1}), t is the time (s), D is the tensor of the dispersion-coefficient (m^2 s^{-1}), N_E is the number of heterogeneous equilibrium reactions, $v_{j,e}^{E}$ is the stoichiometric coefficient of component j in the heterogeneous equilibrium reaction e (-), $\bar{c}_e$ is the concentration of solid reactant e (mol kgw^{-1}), N_K is the number of kinetic reactions, $v_{j,k}^{K}$ is the stoichiometric coefficient of component j in kinetic reaction k (-), R_k is the kinetic reaction rate k (mol kgw^{-1} s^{-1}), $\hat{c}_j$ is the total aqueous concentration of component j in the source water (mol kgw^{-1}), and N_C is the number of the chemical components in the system (Parkhurst et al., 2010).

For both, PHREEQC and PHAST, the accuracy of the modeling results must be manually checked by evaluating the mass balance. Numerical stability/instability must be proven manually by discretization studies and by refining grid and time steps. For spatial and temporal discretization, finite-difference techniques are used in PHREEQC and PHAST. Further detailed information about PHREEQC and PHAST are given in Parkhurst and Appelo (2013) and Parkhurst et al. (2010).

1.3.5.3 Databases

The programs PHREEQC and PHAST are based on databases and come with nine different databases (Parkhurst and Appelo, 2013): phreeqc.dat (Parkhurst et al., 1980), wateq4f.dat (Ball and Nordstrom, 1991), pitzer.dat (Pitzer, 1973), llnl.dat (derived from databases for

The Geochemist´s Workbench and EQ3/6 using thermodynamic data prepared by the Lawrence Livermore National Laboratory), minteq.dat (Allison et al., 1991), minteqv4.dat (U.S. Environmental Protection Agency, 1999), sit.dat (Grenthe et al., 1997), iso.dat (Thorstenson and Parkhurst, 2002; Thorstenson and Parkhurst, 2004), and amm.dat (same as phreeqc.dat, but ammonia is considered as a separate component). Additional developed databases are the “gebo”-database from Bozau (2013) which extends pitzer.dat for solutions with high ionic strength and the thermochemical database thermoddemv1.10_11dec2014 from the BRGM institute, French Geological Survey (Blanc et al., 2012). The database used in this study is phreeqc.dat which is extended by data from llnl.dat.

1.4 Hydrogeochemical Modeling Approaches—Similarities and Differences

The numerical modeling of the hydrogeochemical processes induced by the storage of gases in the underground is based on the equilibrium thermodynamics of chemical gas–water–rock interactions, including kinetic reactions. The diffusive transport of aqueous species through the solutions in the respective underground gas storage system is modeled to evaluate the time- and space-dependent development in such reactive mass transport models. With the help of the codes PHREEQC and/or PHAST, the effects of the hydrogeochemical processes induced by gas storage on the hydrogeochemical compositions of the aqueous solutions, partial pressure of stored gas phases, and on the mineralogical composition of the reservoir and cap rocks are calculated, partly considering the changing porosities in reservoir and cap rocks. The similarities and differences in these three subtopics are summarized in Figure 1.1 and details are given in Table 1.2.

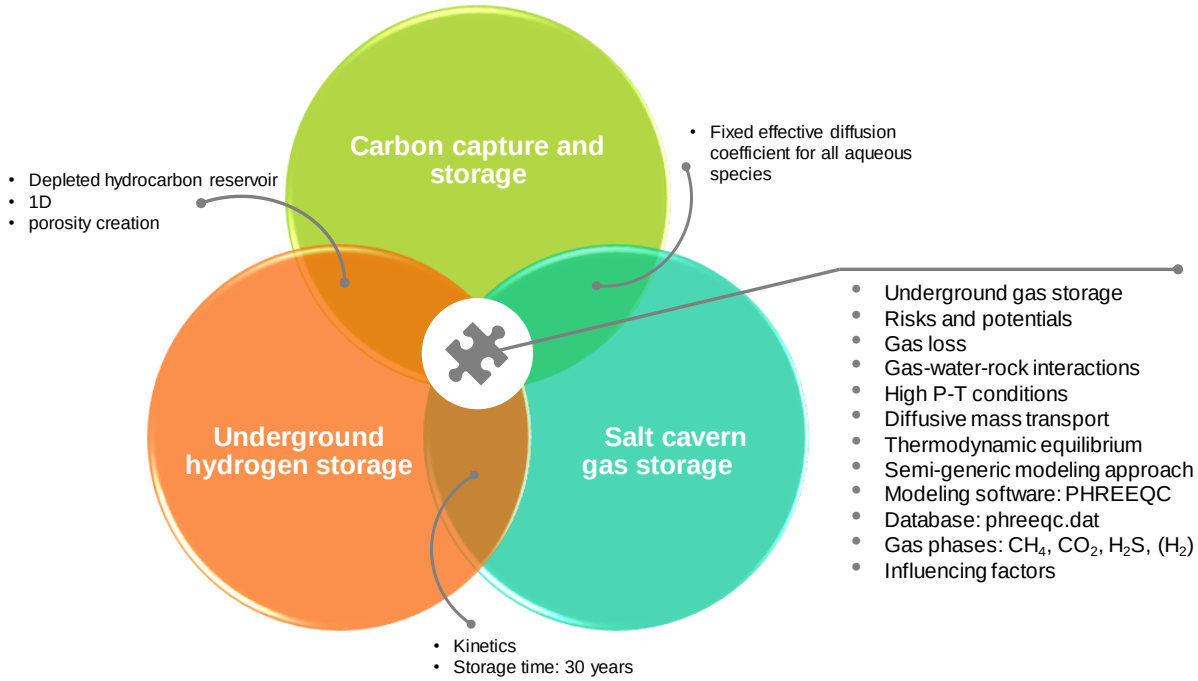

Figure 1.1 Intersections of the three subtopics CCS, SCGS, and UHS showing conceptual similarities and differences.

In all three subtopics of this study—CCS, SCGS and UHS—hydrogeochemical processes in deep geological formations are modeled and analyzed. The modeling approaches are semi-generic in nature but, whenever data from real geosystems and/or experimental data are available, these data are used to check the plausibility of the models. In CCS a depleted hydrocarbon reservoir, in SCGS a salt cavern, and in UHS a depleted gas reservoir is considered. The mineralogical compositions of the reservoir rocks and the cap rocks are different in CCS and SCGS and, of course, different from the mineralogical composition of the salt cavern. However, typical minerals like quartz, calcite, pyrite, and barite are considered in all three models. The considered brines are pre-calculated in separate batch models (CCS and SCGS) and in a one-dimensional reactive transport model for UHS.

The multi-component gas compositions that are analyzed when storing gases in the underground are different in their partial pressures but not in their composition. In all three modeled gas storage systems $CO_{2(g)}$, $CH_{4(g)}$, and $H_2S_{(g)}$ are considered. Additionally, $N_{2(g)}$ is given in SCGS and UHS models and, of course, $H_{2(g)}$ in the UHS system.

All three systems are modeled as one-dimensional reactive mass transport (1DRMT) models. Additionally, the SCGS system is modeled using a three-dimensional reactive mass transport

(3DRMT) model as well. The modeling tool for the 1DRMT models is PHREEQC, while PHAST is used for the 3DRMT model.

The mass transport mechanism in the underground gas storage models is molecular diffusion of all aqueous species. Dispersion is not considered and advection is only considered in an alternative model scenario in CCS. While the UHS model considers multi-component diffusion (where each species has an individual temperature-dependent diffusion coefficient), the CCS model uses an effective diffusion coefficient for all aqueous species of 3.33×10^{-10} m^2 s^{-1}, and the SCGS model uses 5.0×10^{-9} m^2 s^{-1}.

The prerequisite for all considered models (and PHREEQC applicability) is the availability of water; it is given as irreducible water and, additionally, as a brine in SCGS.

In all three models, high pressure and temperature conditions (> 40 °C and > 40 atm) are simulated. Using the phreeqc.dat database, the temperature and pressure effect on the equilibrium constants are considered for almost all phases and aqueous species—with the exception of the acetate-bearing species and a few aqueous silicon- and aluminum-bearing species.

The changes in the porosity of the cap rock are addressed for CCS and UHS. Additionally, porosity changes in the reservoir rock are addressed for UHS. These changes in porosity are calculated based on volume changes from the PHREEQC modeling results.

To calculate the loss of the stored gas is, from different points of view, the aim for all modeled systems. In CCS, the potential loss of carbon dioxide is investigated by the analysis of gas–water–rock interactions which could lead to higher porosity in the cap rock and favor $CO_{2(sc/g)}$ pathways. In SCGS the loss of natural gas is analyzed by regarding the conversion of the stored $CH_{4(g)}$ to $H_2S_{(g)}$ by bacterial sulfate reduction. In UHS the loss of hydrogen is modeled by aqueous diffusion, gas–water–rock interactions that bond the stored $H_{2(g)}$, and by bacterial conversion.

All models are tested with sensitivity studies to identify the main influencing factors, including pressure and temperature conditions (SCGS, CCS, UHS), kinetic rate constants (SCGS, UHS), tortuosity (SCGS), gas compositions (SCGS, CCS, UHS), mineralogical compositions (CCS), initial cap rock porosities (CCS), effective diffusion coefficients (CCS), transport mechanisms (CCS), and storage time (CCS, UHS).

Differences in the three subtopics arise in the modeled storage time. While CCS is the final disposal of a waste product, SCGS and UHS are used for seasonal storage. The modeling

time considered is 1,000,000 years for CCS and 30 years for SCGS and UHS. The 1,000,000 years for CCS is chosen based on the discretization results of the model and follows the safety regulations for final disposal of radioactive waste in Germany, where the evidence of long-term safety for one million years has to be provided (BMU, 2010). The chosen time of 30 years for SCGS results from the typical operating lifetime of a salt cavern and for UHS from the equipment lifetime.

Table 1.2 Underground gas storage models and their parameters.

	CCS	**SCGS**	**UHS**
Model type / modeling tool	Batch/PHREEQC 1D-transport/PHREEQC	Batch/PHREEQC 1D-transport/PHREEQC 3D-transport/PHAST	1D-transport/PHREEQC
Database	Extended phreeqc.dat	Extended phreeqc.dat	Extended phreeqc.dat
Reaction modeling type	Spontaneous equilibration	Spontaneous equilibration and kinetics for BSR	Spontaneous equilibration and kinetics for BSR and methanogenesis
Storage facility	Depleted hydrocarbon reservoir	Salt cavern	Depleted gas reservoir
Gases considered	$CO_{2(g/sc)}$, $CH_{4(g)}$, $H_2S_{(g)}$	$CO_{2(g)}$, $CH_{4(g)}$, $H_2S_{(g)}$, $N_{2(g)}$	$CO_{2(g/sc)}$, $CH_{4(g)}$, $H_2S_{(g)}$, $N_{2(g)}$, $H_{2(g)}$
Number of aqueous species	11	14	12
Effective diffusion coefficient (m^2 s^{-1})	3.33×10^{-10}	5.0×10^{-9}	Multicomponent diffusion
Pressure (atm)	100	180	40
Temperature (°C)	40	50	40
Storage time (a)	1,000,000	30	30
Transport mechanisms	Diffusion	Diffusion	Diffusion

2 Carbon Capture and Storage (CCS)

Change in Cap Rock Porosity Triggered by Pressure and Temperature Dependent CO_2–Water–Rock Interactions in CO_2 Storage Systems

Publication I

Authors of the original paper: Christina Hemme, Wolfgang van Berk

Originally published in: Petroleum 3 (2017), 96–108

Summary added for the purpose of this thesis.

Author Contributions:

Conceptual model:	Christina Hemme[1]
Modeling:	Christina Hemme[1] and Wolfgang van Berk[2]
Result evaluation:	Christina Hemme[1] and Wolfgang van Berk[2]
Analysis of results:	Christina Hemme[1] and Wolfgang van Berk[2]
Visualization of results:	Christina Hemme[1]
Writing—original draft preparation:	Christina Hemme[1]
Writing—review and editing:	Christina Hemme[1] and Wolfgang van Berk[3]
Supervision:	Wolfgang van Berk[1]

[1] substantial; [2] medium; [3] minor

Summary

In this part of the study, the gas–water–rock interactions triggered by carbon dioxide storage are considered. The focus is on the diffusive mass transport of CO_2 along a gradient of changing pressure and temperature conditions through the cap rock brine. In addition, the change in porosity due to mineral dissolution and precipitation is simulated to analyze the sealing capacity of the cap rock.

In carbon capture and storage systems, supercritical CO_2 is injected into a reservoir and dissolves in the reservoir brine. Subsequently, aqueous $CO_{2(aq)}$ diffuses into the cap rock to regions of lower total pressure and temperature and triggers CO_2–water–rock interactions that are coupled with mass transport and result in precipitation and/or dissolution of minerals along the CO_2 migration path. Such hydrogeochemical interactions cause porosity changes and are responsible for the improvement, or the risk of deterioration, of the long-term integrity of the system.

This part of the study presents a semi-generic hydrogeochemical model based on chemical equilibrium thermodynamics, data from several CO_2 storage systems, and plausible assumptions regarding non-available data. One-dimensional reactive transport modeling is performed using the PHREEQC code (phreeqc.dat database) to develop a general system and process understanding of the hydrogeochemical effects of underground CO_2 storage in depleted hydrocarbon reservoirs on the aqueous solutions, mineral phases, and gas compositions in the storage systems. Furthermore, the loss or gain of total porosity affected by hydrogeochemical reactions driven by diffusive mass transport exposed to pressure and temperature gradients is identified and quantified. A fine spatial and temporal discretization and the use of non-reactive tracers enable calculation over the relevant timescale for simulations of long-term storage of CO_2.

Modeling results show that the relevant timescale for simulations of long-term storage of CO_2 is on the order of 10^6 years, and that pressure/temperature conditions, heterogeneities (veins and fractures), and the mineralogical composition of the cap rock have the strongest influence on the increase in cap rock porosity (maximum increase from the initial 5% to 7.5%). Critical parameter combinations could put long-term integrity at risk. Nevertheless, a wide range of conditions and parameter combinations for safe CO_2 storage are identified by other modeling scenarios. This model approach can be used and adapted to various underground CO_2 storage conditions to answer and solve practically oriented questions and problems (Hemme and van Berk, 2015).

Abstract

Carbon capture and storage in deep geological formations is a method to reduce greenhouse gas emissions. Supercritical CO_2 is injected into a reservoir and dissolves in the brine. Under the impact of pressure and temperature (P–T) the aqueous species of the CO_2-acidified brine diffuse through the cap rock where they trigger CO_2–water–rock interactions. These geochemical reactions result in mineral dissolution and precipitation along the CO_2 migration path and are responsible for a change in porosity and therefore for the sealing capacity of the cap rock. This study focuses on the diffusive mass transport of CO_2 along a gradient of decreasing P–T conditions. The process is retraced with a one-dimensional hydrogeochemical reactive mass transport model. The semi-generic hydrogeochemical model is based on chemical equilibrium thermodynamics. Based on a broad variety of scenarios, including different initial mineralogical, chemical and physical parameters, the hydrogeochemical parameters that are most sensitive for safe long-term CO_2 storage are identified. The results demonstrate that P–T conditions have the strongest effect on the change in porosity and the effect of both is stronger at high P–T conditions because the solubility of the mineral phases involved depends on P–T conditions. Furthermore, modeling results indicate that the change in porosity depends strongly on the initial mineralogical composition of the reservoir and cap rock as well as on the brine compositions. Nevertheless, a wide range of conditions for safe CO_2 storage is identified.

2.1 Introduction and Aim

A solution to reduce CO_2 emissions into the atmosphere is the storage of CO_2 in the reservoir rocks of depleted hydrocarbon reservoirs, coal seams and deep saline aquifers (Holloway, 1997). For the storage of CO_2 four different trapping mechanisms are known: (i) structural trapping, (ii) residual trapping, (iii) dissolution trapping, and (iv) mineral trapping (Gaus et al., 2008; IPCC, 2005). Black et al. (2015) stated that the effects of mineral dissolution and precipitation are the key factors for safe CO_2 storage. The injection of CO_2 leads to CO_2–water–rock interactions that result in the precipitation and dissolution of minerals which in turn result in a change in porosity and permeability of the cap rock. This change leads to the improvement or deterioration of the sealing capacity of the cap rock. Mineral dissolution results in an increase in porosity and enables the creation of pathways for CO_2 migration. Mineral precipitation leads to a decrease in porosity and increases the sealing effect (Gaus et al., 2005). In the discussion about carbon capture and storage (CCS) many studies focus on CO_2–water–rock interactions in reservoir rocks but much less attention has been paid on these

interactions in the cap rock. Consequently, forecasting and quantifying such CO_2–induced processes in cap rocks rank high on the agenda for successful carbon capture and storage in deep geological formations. Thus, various modeling and experimental studies aim to retrace and reproduce such hydrogeochemical reactions in cap rocks (Alemu et al., 2011; Bildstein et al., 2010; Black et al., 2015; Bolourinejad and Herber, 2015; Credoz et al., 2009; Fleury et al., 2011; Gaus et al., 2005; Gherardi et al., 2007; Szabó et al., 2016; Tian et al., 2014; Tian et al., 2015; Wollenweber et al., 2010).

Knowledge of cap rock properties is important for these studies. Cap rocks are characterized by specific mineralogical and physical properties like low porosity and permeability. The often clay-bearing cap rocks have to be saturated with brine and must have a capillary entry pressure that prevents the cap rock from supercritical CO_2 entering (Mohd Amin et al., 2014) and prevents CO_2 from escaping towards overlying aquifers needed for water supply (Liu et al., 2015).

Our study is based on equilibrium thermodynamics of chemical CO_2–water–rock interactions to fundamentally reveal where a carbon capture and storage system inevitably develops in terms of porosity alteration resulting from mineral dissolution and precipitation. It is not our aim to reproduce a real complex geological system. Correspondingly, our modeling approach is of semi-generic nature. We aim to identify long-term inorganic hydrogeochemical processes including CO_2–water–rock interactions and to quantify the change in porosity due to the effects of geochemical reactions in dependence on pressure and temperature. This process is retraced with a one-dimensional hydrogeochemical reactive mass transport model based on a hypothetical concept. Authors like Bildstein et al. (2010) have modeled porosity creation in the cap rock at constant temperature and pressure conditions. Generally, temperature and pressure conditions change along the path of diffusive transport of CO_2 (van Berk et al., 2015) and could strongly affect the mass-action law constants for the equilibrium reactions between mineral phases and CO_2. Therefore, it is important to consider not only different temperature and pressure conditions at the starting point of diffusive CO_2 migration, like those modeled by Van Pham et al. (2012), but also the change of temperature and pressure along the diffusive pathway of CO_2 through the cap rock. Therefore, this study will focus on the diffusive mass transport of CO_2 along a gradient of decreasing pressure and temperature conditions. A broad variety of modeling scenarios, including different initial mineralogical and physical parameters, is calculated to identify the hydrogeochemical parameters most sensitive for safe CO_2 storage. In addition, the numerical accuracy of our model is tested by a detailed grid convergence study.

2.2 Kinetic or Thermodynamic Equilibrium Modeling for Long-Term CO_2 Storage?

Various modeling studies related to cap rocks in CCS systems apply batch and/or reactive transport modeling approaches that include reaction kinetics (Gaus et al., 2005; Mohd Amin et al., 2014; Tian et al., 2015). These studies focus on the time-dependent progress of mineral dissolution and precipitation reactions which are characterized by associated reaction rate constants. An overview over the rate parameters of water-mineral interaction kinetics are given in a report by the US Geological Survey (Palandri and Kharaka, 2004). Kinetic simulations still show uncertainties regarding the poor knowledge of the kinetic rate constants at elevated levels of temperature, total and CO_2 partial-pressure. However, such knowledge is essential for kinetically based modeling of CCS systems, especially in this study which focuses on the diffusive mass transport of CO_2 along a gradient of decreasing P–T conditions. In addition, the rates obtained in laboratory strongly depend on the experimental devices and the chosen boundary or environmental conditions, and therefore they are difficult to compare with another (Marini, 2007). Ignoring the facts that i) hydrogeochemical conditions (e.g., pH, pε, ionic strength) evolve and change in time and space and ii) kinetic rate constants must change accordingly, makes the modeling results meaningless–especially when thermodynamically impossible reactions are modeled.

Approaches based on kinetics start from the assumption that kinetically characterized reactions actually proceed–whether any driving force in terms of system thermodynamics allows these reactions to proceed or not. In contrast, thermodynamically based modeling approaches only calculate the reactions, which are thermodynamically possible, until spontaneous equilibrium conditions are established. The term spontaneous implies that the equilibrium is established for the residence time of CO_2 in a spatially discrete compartment. Stumm and Morgan (1981) argued that applying thermodynamically based approaches allow to “identify reactions that are possible”. In consequence, the authors developed “first equilibrium and then kinetic frameworks for natural water systems”. Moreover, Marini (2007) stated that equilibrium thermodynamics seem to be a good modeling tool for the analysis of chemical reactions in CO_2 storage systems. This appraisal is based on the studies performed by Helgeson (Barnes, 1979; Helgeson, 1967, 1968; Helgeson et al., 1969; Helgeson et al., 1970; Helgeson, 1979) which show that a separation of the overall reaction path into a series of partial equilibrium states enables successful modeling based on chemical equilibrium thermodynamics.

One of the main differences between thermodynamically based modeling studies and approaches including reaction kinetics (Gaus et al., 2005; Mohd Amin et al., 2014; Tian et al.,

2015) is the total time considered by the modeling of specific reactive transport processes. In their kinetically based modeling study, Mohd Amin et al. (2014) considered a total time of 10,000 years referring to the fact that Bowden and Rigg (2005) and Credoz et al. (2009) asserted that such a timescale is relevant for the long-term safety assessment of CO_2 storage. However, this determination of Bowden and Rigg (2005) and Credoz et al. (2009) is presented without any retraceable justification. Tian et al. (2015) performed all their simulations considering a total time of 1000 years while Gaus et al. (2005) considered 15,000 years. Gaus et al. (2005) concluded that when using kinetically based calculations the system is still far from equilibrium after 15,000 years. However and in contrast, to justify a relevant timescale our study calculates the diffusive transport of a non-reactive tracer through the model system for various total times and time step lengths–prior to any reactive transport modeling (for details, see Section 2.4.1). From the time-dependent spatial spreading of this tracer we conclude that a total time of 1,000,000 years is the timescale relevant for the long-term safety assessment of CO_2 storage systems similar to our semi-generic modeling systems.

Considering these facts, we decide to perform modeling based on thermodynamics, although we are aware that the progress of various heterogeneous reactions is actually controlled by kinetics. It is not our aim to connect thermodynamically driven hydrogeochemical processes with temporal aspects. Our aim is to identify and quantify the long-term hydrogeochemical processes. Provided that thermodynamic equilibrium is established, the thermodynamically based modeling approach enables us to test where the CCS system is inevitably going in terms of porosity alteration.

2.3 Conceptual Numerical Model and Modeling Parameters

2.3.1 Model Setup

The hydrogeochemical, one-dimensional reactive mass transport (1DRMT) modeling approach presented in this study is based on a semi-generic concept. It includes available data from several real CO_2 storage systems and is based on assumptions regarding non-available data for the sake of simplicity. Alternative scenarios for selected parameters are performed to reveal how strongly the parameters affect the CO_2–water–rock interactions (for details, see Section 2.5.2).

The geological structure in this model is a depleted hydrocarbon reservoir in an anticlinal fold (Figure 2.1). Carbon dioxide is injected into the reservoir rock at a depth of about 800 m. At this depth CO_2 is supercritical ($CO_{2(sc)}$) and dissolves until the reservoir brine is saturated with

respect to $CO_{2(aq)}$. The critical point for CO_2 lies at a temperature of 304.21 K (31.06 °C) and at a pressure of 73.825 bars (72.859 atm) according to Angus et al. (1976) and Salimi et al. (2012). At temperature and pressure conditions above this critical point, the $CO_{2(sc)}$ is present in a dense phase which is lighter than the brine in the reservoir rock and migrates from the point of injection to the reservoir/cap rock contact where a $CO_{2(sc)}$ plume builds up (Figure 2.1) (Lindenberg and Wessel-Berg, 1997). During this process the reservoir brine is displaced by the supercritical $CO_{2(sc)}$. At the contact with the cap rock CO_2 is available as $CO_{2(sc)}$ in the plume and as dissolved CO_2 ($CO_{2(aq)}$ and corresponding aqueous species e.g. HCO_3^-, CO_3^{2-}, $CaHCO_3^+$, H^+) in the reservoir brine beneath the plume. The $CO_{2(sc)}$ dissolves in the cap rock brine and an acidic solution is created. Molecular diffusion of aqueous species through the cap rock brine leads to $CO_{2(aq)}$–water–rock interactions in the cap rock that cause mineral dissolution and precipitation and therefore a change in the porosity and permeability of the cap rock. The mass-action law constants for the equilibrium reactions between mineral phases and $CO_{2(aq)}$ depend on temperature and pressure, and therefore they change along the $CO_{2(aq)}$ migration path (van Berk et al., 2015).

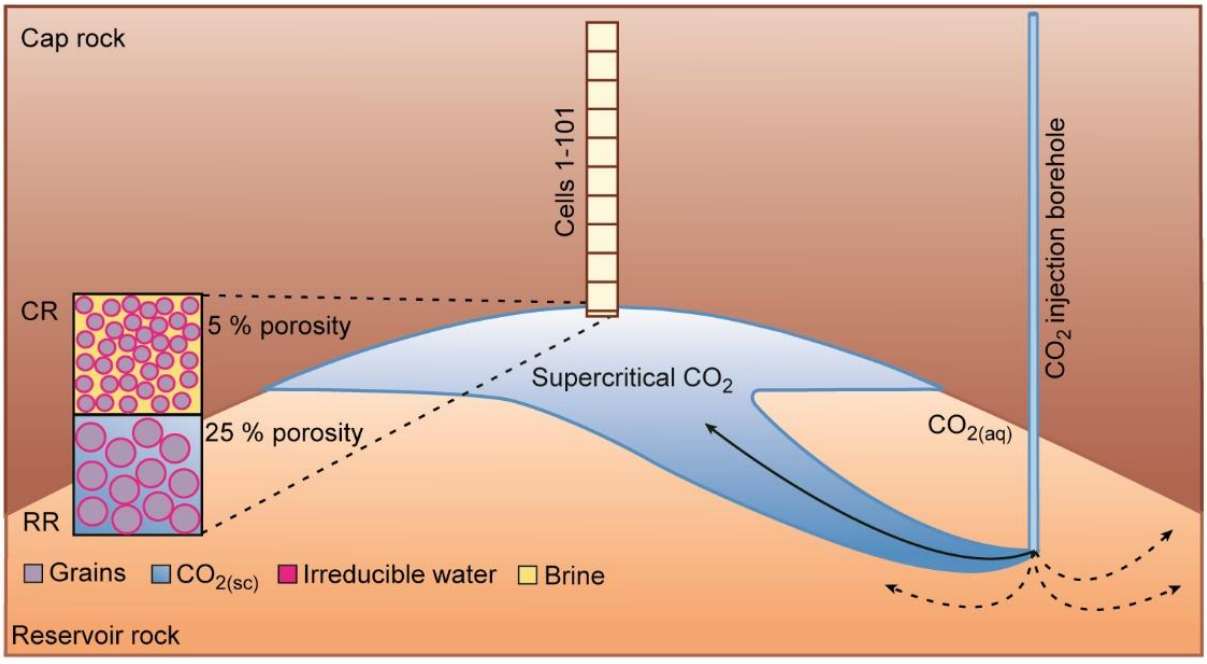

Figure 2.1 System sketch of the model. CR = cap rock, RR = reservoir rock, $CO_{2(sc)}$ = supercritical CO_2 and $CO_{2(aq)}$ = aqueous CO_2.

Our hydrogeochemical model is based on thermodynamic equilibrium reactions and the local equilibrium assumption. Kinetic aspects of mineral dissolution/precipitation are not considered. Even if CO_2 is supercritical under the assumed reservoir conditions, this model uses gaseous CO_2 as an analog. This simplifying assumption is based on the study of Rochelle and Moore

(2002) that shows results of supercritical CO_2 solubility experiments at different pressure and temperature conditions. We retraced these experiments using PHREEQC Interactive 3.1.4-8929 and its database phreeqc.dat, with the difference that we used gaseous CO_2 instead of supercritical CO_2. The solubility constants for $CO_{2(g)}$ used in PHREEQC and $CO_{2(sc)}$ measured by Rochelle and Moore (2002) are similar and consequently the following reactions apply (Equations (2.1) and (2.2)):

$$CO_{2(g)} = CO_{2(aq)} \qquad \log K = -1.468;\ \text{at } 25\ °C;\ 1\ \text{bar} \tag{2.1}$$

$$CO_{2(sc)} = CO_{2(aq)} \qquad \log K = -1.468;\ \text{at } 25\ °C;\ 1\ \text{bar} \tag{2.2}$$

Furthermore, to prove and quantify this assumption a separate sensitivity analysis is presented in Section 2.5.3.

In the model the migration path is demonstrated by a column of 101 cells, with a cell length of 1 m. One cell is located in the reservoir rock and one hundred cells are located in the cap rock (Figure 2.1). For both ends of the column the modeling boundary conditions are defined as flux. Due to a constant pCO_2 in the plume, the lower boundary can be interpreted as a constant concentration boundary. By adding five extra cells at the upper end of the column, the influence of the upper boundary condition can be minimized, considering that only the 101 cells are evaluated. The only mass transport mechanism in this model is molecular diffusion of all aqueous species through the cap rock brine. The process of diffusion of aqueous species is slow (Gaus et al., 2005) but allows the mass transport of dissolved species between all cells (Arning et al., 2011), depending on time and diffusivity. One diffusion coefficient for all aqueous species of 3.33×10^{-10} m^2 s^{-1} is used. This value is based on the assumption made by Mohd Amin et al. (2014) that the diffusion coefficient is made up of the diffusion coefficient in pure water of 1×10^{-9} m^2 s^{-1} divided by an averaging tortuosity of 3 (Cussler, 2009).

2.3.2 Initial Pressure and Temperature Conditions

The pressure and temperature conditions (P–T conditions) are similar to the conditions predominating at the CCS storage system at Sleipner in Norway, starting with 40.0 °C (37.0 °C at Sleipner) and 100.0 atm at reservoir conditions (100.0 atm at Sleipner). The temperature decreases from the reservoir depth up along the geothermal gradient, at 33.3 °C per kilometer of depth, and the pressure decreases accordingly with 100.0 atm per kilometer under hydrostatic conditions. Consequently, each of the 101 cells is associated with a specific pressure/temperature condition (for example, cell 1: 40.0 °C and 100.0 atm, cell 2: 39.967 °C

and 99.9 atm). We assume a constant partial pressure of the $CO_{2(sc)}$ plume over time because $CO_{2(sc)}$ is delivered continuously by the plume for a long time and, for the sake of simplicity, we equate the partial pressure with the hydrostatic pressure.

2.3.3 Initial Mineralogical Composition of the Reservoir and Cap Rock and Initial Brine Compositions

Each cell is defined by specific mineralogical, hydrochemical and physical properties. A homogeneous distribution of relevant parameters in the cap rock (cells 2–101) such as mineralogical composition is assumed. Table 2.1 summarizes the selected initial mineralogical composition in all cells. Assuming an initial total porosity of 25.0%, cell 1, representing the reservoir rock, is filled with 1.0 L of irreducible water, whereas 4.0 L of pore space are occupied by injected CO_2 ($CO_{2(sc)}$ plume).

Cells 2–101 are located in the cap rock and are characterized by a representative volume of 20.0 L with an initial porosity of 5.0% (1.0 L irreducible water and 19.0 L solid phases), where the type of porosity is neglected. The assumption of 5% initial porosity in the cap rock is based on observations from the Nordland Shale in UK Quadrant 16, northern North Sea (Gaus et al., 2005; Kemp et al., 2001) as an analog for the cap rock porosity in the CCS system Sleipner. Taking into account the specific density of each mineral phase (in g cm^{-3}), the amount of single mineral phases is calculated in mole per kg of pore water for different reservoir parts (Table 2.1). It is assumed that a small amount of CO_2 prevails in the cap rock and the reservoir rock during burial prior to $CO_{2(sc)}$ injection (pCO_2 = 1.0 atm). Before CO_2 injection and the triggered diffusion, a separate batch modeling calculates the initial composition of brines in both reservoir parts (the detailed input file for the separate batch model to calculate the cap rock brine is given in the supplementary data Input file S1). The brine composition of cell 1 (reservoir rock) is calculated by equilibrating 1 L of 1.5 M Na^+/Cl^--dominated solution with the defined primary minerals and gas phase under 40.0 °C and 100.0 atm (Table 2.2). For calculating the initial brine composition in cells 2–101 (cap rock), a 1.5 M Na^+/Cl^--dominated solution including 0.15 mol kgw^{-1} K^+ is equilibrated with the mineral phases of the cap rock and CO_2 under the pre-assigned reservoir P−T gradient (cell 2: 39.967 °C and 99.9 atm; cell 3: 39.934 °C and 99.8 atm; Table 2.2).

Table 2.1 Mineralogical composition of the reservoir rock and the cap rock.

Primary minerals	Weight percent (wt. %)	Amount mol kgw^{-1}
Reservoir rock		
K-feldspar	14.0	19.952
Albite	5.0	7.563
Quartz	75.0	495.130
Calcite	6.0	23.778
Cap rock		
K-feldspar	6.0	10.991
Albite	3.0	5.833
Quartz	55.0	466.745
Calcite	5.0	25.471
Kaolinite	25.0	49.377
Pyrite	2.0	8.499
Chlorite	2.0	1.835
Barite	2.0	4.369

Table 2.2 Initial irreducible water composition of the reservoir rock and cap rock.

Parameter	Reservoir rock	Cap rock
pH	6.064	7.912
Temperature (°C)	40.0	39.967
Elements	Concentration (mol kgw^{-1})	Concentration (mol kgw^{-1})
Al	3.544×10^{-06}	5.13×10^{-07}
Ba	-[d]	3.46×10^{-04}
C_{tot}[a]	4.254×10^{-02}	2.52
Ca	1.365×10^{-02}	1.96×10^{-05}
Cl[b]	1.500	1.61
Fe	-[d]	2.91×10^{-07}
K	7.649×10^{-03}	2.36×10^{-02}
Mg	-[d]	5.75×10^{-03}
Na[b]	1.492	4.47
S_{tot}[c]	-[d]	3.46×10^{-04}
Si	1.105×10^{-04}	6.56×10^{-05}

[a] C: summed concentration of aqueous CH_4 and C(+IV) species

[b]: Due to high Na^+ and Cl^- concentrations and the resulting high ionic strength the Pitzer database and Pitzer equations should be used but the Pitzer database does not include Si- und Al^{3+}-containing aqueous species and silicate minerals, which are important components of the cap rocks of CO_2 storage systems. Therefore, the phreeqc.dat is used, which includes such species and silicate minerals and uses the Debye–Hückel equation, even if the activity coefficients for all aqueous species are overestimated (Mohd Amin et al., 2014). Parkhurst and Appelo (1999) assert that “in sodium chloride dominated systems, the model may be reliable at higher ionic strengths”. Furthermore, the results of the different sensitivity scenarios are compared in relation to one another and not in an absolute context

[c] S: summed concentration of aqueous S(+VI) and S(-II) species

[d]: not present

2.4 Methodology

The software PHREEQC Interactive 3.1.4-8929 (Parkhurst and Appelo, 2013) and its database phreeqc.dat are the modeling tools for the one-dimensional reactive transport modeling. This software is provided by the Geological Survey of the United States. PHREEQC is based on an ion-association aqueous model and has the capability to simulate speciation, batch-reaction, one-dimensional transport and inverse geochemical calculations. The calculations are based on mass action laws that include all species used in this study (Al, Ba, C, Ca, Cl, Fe, K, Mg, Na, S, Si) and their corresponding equilibrium constants. A basic of the modeling is the thermodynamic database which includes the elements used in the model with their species (aq, s, g), mass-action equations, and equilibrium constants. The activity coefficients of species are calculated by using the Debye-Hückel equation. The one-dimensional reactive transport model calculation in PHREEQC is based on the Advection-Reaction-Dispersion Equation (2.3) (ARD):

$$\frac{\partial C}{\partial t} = -v\frac{\partial C}{\partial t} + D_L\frac{\partial^2 C}{\partial x^2} - \frac{\partial q}{\partial t} \tag{2.3}$$

where C is the concentration in water (mol kgw^{-1}), t is the time (s), v is the pore water flow velocity (m s^{-1}), x is the distance (m), D_L is the hydrodynamic dispersion coefficient [m^2 s^{-1}, D_L = D_e + $\alpha_L v$, with D_e the effective diffusion coefficient, α_L the dispersivity (m)], and q is the concentration in the solid phase (expressed as mol kgw^{-1} in the pores).

Our model considers a multiple web of hydrogeochemical reactions including 119 aqueous species, 10 mineral phases and their interplay. We use PHREEQC Version 3 which considers the pressure and the temperature dependence of the mass-action law constants for the equilibrium reactions of the aqueous, gaseous and solid species involved. Table 2.3 shows the equilibrium phases, mass-action equations and equilibrium constants used in the model. Phases like dawsonite and nahcolite that are not present in the phreeqc.dat database are taken from the llnl.dat database and added to the input files. However, the pressure dependence of both minerals is not considered.

Numerous publications confirm that PHREEQC produces correct results by comparing the results with other codes (De Windt et al., 2003; Gundogan et al., 2011; Nowack et al., 2006). A detailed comparison of modeling results of different software packages like The Geochemist´s Workbench, EQ3/6, FactStage/ChemApp and PHREEQC is given by Haase et al. (2013) with the focus on geochemical modeling of CO_2 and calcite dissolution in NaCl solutions. Furthermore, the user´s manual of PHREEQC provides calculations to verify their results (Parkhurst and Appelo, 2013).

Table 2.3 Equilibrium phases, mass-action equations and equilibrium constants used in the model. Data from phreeqc.dat, but dawsonite and nahcolite are from llnl.dat (Parkhurst and Appelo, 2013).

Equilibrium phase	Equilibrium reaction	log *K* at 25 °C, 1 bar
K-feldspar	$KAlSi_3O_8 + 8H_2O = K^+ + Al(OH)_4^- + 3H_4SiO_4$	-20.573
Albite	$NaAlSi_3O_8 + 8H_2O = Na^+ + Al(OH)_4^- + 3H_4SiO_4$	-18.002
Quartz	$SiO_2 + 2H_2O = H_4SiO_4$	3.98
Calcite	$CaCO_3 = CO_3^{2-} + Ca^{2+}$	8.48
Kaolinite	$Al_2Si_2O_5(OH)_4 + 6H^+ = H_2O + 2H_4SiO_4 + 2Al^{3+}$	7.435
Pyrite	$FeS_2 + 2H^+ + 2e^- = Fe^{2+} + 2HS^-$	-18.479
Chlorite(14A)	$Mg_5Al_2Si_3O_{10}(OH)_8 + 16H^+ = 5Mg^{2+} + 2Al^{3+} + 3H_4SiO_4 + 6H_2O$	68.38
Barite	$BaSO_4 = Ba^{2+} + SO_4^{2-}$	-9.97
Dawsonite	$NaAlCO_3(OH)_2 + 3H^+ = Al^{3+} + HCO_3^- + Na^+ + 2H_2O$	4.35
Nahcolite	$NaHCO_3 = HCO_3^- + Na^+$	-0.11
$CO_{2(g)}$	$CO_2 = CO_2$	-1.468

2.4.1 Discretization

To check the numerical accuracy of the results, the total time, number of shifts and number of cells are refined, and the model calculation for one (the same) scenario is rerun and the results are compared (Parkhurst and Appelo, 1999, 2013). Using a non-reactive tracer, induced as a peak injection into the first cell of the model, the progress of diffusion can be demonstrated. A concentration gradient for the non-reactive tracer is chosen based on CO_2 molality at the temperature and pressure conditions in the reservoir rock and in the cap rock. Thereby the diffusive mass transport progress of CO_2 can be tested, if the CO_2 would not react with the brine and the mineral phases of the cap rock. The total time, number of shifts and number of cells are refined until ions moved from regions of high concentration (cell 1) to regions of lower concentration (cells 2–101), resulting in an equal concentration in all cells (1–101).

To define the total time a non-reactive tracer is induced in the model to calculate the time at which the tracer concentration is equal in all cells. The model calculation is repeated for a total time of 10^4, 10^5, 10^6 and 10^7 years with a constant number of shifts and cells. The results show that the tracer concentration is equal in all the cells in the models at times of one million and ten million years (Table 2.4). In the following models the time scale of one million years is chosen.

In the second step of refinement the number of shifts is varied. The time is kept constant to one million years but the number of shifts (100, 1000, 10,000) and therefore the length of the time steps is varied, although PHREEQC may subdivide the “time step into smaller dispersion time steps if necessary to calculate dispersion accurately” (Parkhurst and Appelo, 2013). Table 2.4 shows identical results for all the modeled numbers of shifts in the last shift. When

comparing the tracer concentration at a fixed time for all models, differences in the progress of the diffusion are identifiable. The tracer concentration 1000 years later is equal in all cells in the 1000-shifts model to that in the model with 100 shifts. With 10,000 shifts the tracer concentration 400 years later is equal in all cells to that with 1000 shifts. The stopping criterion is set to 1 per mil, so 400 years fall below this cut-off. Therefore, the relevant number of shifts is set to 1000.

In the last step of refinement, the number of cells is varied (11, 21, 51, 101). The total time is kept constant to one million years and the number of shifts are kept constant to 1000. Table 2.4 depicts identical results for all the modeled numbers of cells in the last shift. The same procedure as for identification of the number of shifts applies here. When comparing the tracer concentration at a fixed time for all models, differences in the progress of the diffusion are identifiable. Considering the stopping criterion of 1 per mil, the results show that the relevant number of cells is 101 (Table 2.4).

These results are valid for the model of the reference scenario only and discretization studies should be done for each 1DRMT model. Numerical stability/instability is time and space dependent. To achieve numerical stability, the grid and time steps have to be refined, but due to the smaller time steps the number of solution calculations increases (Parkhurst and Appelo, 2013). Moreover, the change in concentration, which results from reactions, is small from one time step to the next (Schäfer, 2004). A disadvantage of this method is that it is not clear how many cells and which length of time step are necessary to achieve numerical stability (Schäfer, 2004).

Similar to our study, other studies like that of Mohd Amin et al. (2014) consider numerical dispersion as well, but they assert that their “results are not sensitive to numerical dispersion and other errors in the discretization of the transport and reaction equations” (Mohd Amin et al., 2014). They substantiate their assertion with a half of the grid spacing and the outcome of identical results. The results presented here show the opposite effect with a strong sensitivity to numerical dispersion in the sense of Mohd Amin et al. (2014). The reason for that difference is the assumption of a non-reactive tracer. CO_2 (used by Mohd Amin et al. (2014)) reacts with the reservoir and cap rocks and the respective formation waters, so an equal tracer concentration in all cells is reached earlier than without a non-reactive tracer. The advantage of a non-reactive tracer is that the progress of diffusion over the total time and the total distance (= number of cells) can be demonstrated independently from the chemical reactions that may occur. Furthermore, Credoz et al. (2009) assume a total time for the long-term safety assessment of CCS of 10,000 years. Based on the results of the discretization for this model, a total time of 1,000,000 years is defined. However, we are aware that the assumed physical

and chemical conditions, as well as the use of a non-reactive tracer, do not comply with a real system and cannot represent the complexity of the system. Nevertheless, checking the numerical accuracy of the modeling results is essential for all modeling studies.

Table 2.4 Results of temporal-spatial refinement rounded to two decimal places. The parameters used for the reference scenario are shown in bold.

	Tracer concentration $C_{(tracer)}$ (mol kgw^{-1})		
Parameters	Cell 1	Last cell	ΔC_{tracer}
Time $_{total}$ (years)			
0.00	0.85	0.01[a]	0.84
10,000	0.06	0.01[a]	0.05
100,000	0.03	0.01[a]	0.02
1,000,000	0.02	0.02[a]	10^{-6}
10,000,000	0.02	0.02[a]	10^{-6}
Shifts			
100	0.02	0.02[a]	10^{-6}
1000	0.02	0.02[a]	10^{-6}
10,000	0.02	0.02[a]	10^{-6}
Cells			
11	0.10	0.09[b]	0.01
21	0.06	0.04[c]	0.02
51	0.06	0.01[d]	0.05
101	1.04	0.99[a]	0.05

[a]: last cell: 101
[b]: last cell: 11
[c]: last cell: 21
[d]: last cell: 51

2.5 Results and Discussion

2.5.1 Reference Scenario

The equilibrium species distribution and the mass conversion are calculated based on the chemical thermodynamics of aqueous equilibrium reactions. The results of the 1DRMT model after 10^6 years of diffusive mass transport are shown in Figure 2.2 where the column of 101 cells and the change of porosity for the reference scenario are depicted. Cell 1 is neglected because it is positioned in the reservoir rock and has a different initial mineralogical composition, whereas all the other cells are located in the cap rock. The modeling results show that the mineral dissolution and precipitation differ from cell to cell, whereat mass conversion

occurs predominantly in cells 2–9. Therefore, the calculated results within the first ten cells are shown enlarged and are discussed in detail (Figure 2.2).

The cap rock brine dissolves the $CO_{2(sc)}$ and free H^+ are released because of carbonic acid dissociation. Due to acid attack, albite, K-feldspar and calcite dissolve and the corresponding pH increases to 8.4. Cell 2 is completely cemented after 10^6 years. The porosity is reduced from the initial 5.0% to -0.5% (Δ -5.5%). The negative value (-0.5%) implies that the amount of precipitated phases is higher than the available pore space. Consequently, the phases cement also the available pore space in the next cell. Mineral dissolution and precipitation reactions are expressed by the Saturation Index (*SI*) = log (*IAP*/*K*) (*IAP*: ion activity product; *K*: solubility product). When $CO_{2(aq)}$ migrates into cell 2 the cap rock brine is temporarily oversaturated with respect to quartz and dawsonite ($SI > 0$) and undersaturated regarding K-feldspar, albite, kaolinite, calcite, chlorite and barite ($SI < 0$). Thereupon, quartz and dawsonite precipitate in high amounts (+124.3 mol in cell 2) and K-feldspar, albite, kaolinite, calcite, chlorite and barite dissolve in small amounts (-32.6 mol in cell 2). The dissolution of albite and K-feldspar contributes Na^+, K^+, $Al(OH)_4^-$ and H_4SiO_4 to the cap rock brine. To form dawsonite, Al^{3+} and Na^+ have to react with HCO_3^- and $2H_2O$ and reach saturation with $SI_{dawsonite} > 0$. The respective equilibrium reactions are given in Table 2.3. Figure 2.2 shows that with increasing dissolution of albite and K-feldspar the precipitation of dawsonite gets stronger. Calcite dissolves in cell 2 in small amounts only. Calcite dissolves slightly more strongly when albite and K-feldspar are completely dissolved, but the amount of both in this model is high enough to buffer the pH and protect calcite against stronger dissolution.

In cell 3 the porosity decreases from the initial 5.0% to 2.7% (Δ -2.3%). The precipitation of quartz, dawsonite, calcite and kaolinite is responsible for this decrease. The dissolution of K-feldspar, albite and chlorite in comparison with the precipitation of quartz, dawsonite, calcite and kaolinite is too weak to create an increase in porosity. In cell 4 a weaker decrease in porosity from the initial 5.0% to 4.44% is observable. Quartz, dawsonite, K-feldspar, chlorite all precipitate and albite, kaolinite and calcite dissolve.

From cell 5 to cell 9 the porosity decreases from the initial 5.0% to ~4.5%. Quartz, dawsonite, K-feldspar and chlorite precipitate in these cells, whereas albite dissolves. Calcite dissolves in cells 5 and 6 but precipitates in small amounts in cells 7–9. Kaolinite precipitates in cells 5–7 and dissolves in cells 8 and 9. Cells 10 to 101 show similar results. Dawsonite precipitates as well as quartz, albite, K-feldspar, chlorite and barite. Kaolinite and calcite dissolve. Albite is completely dissolved from cells 2–8 but precipitates in small amounts from cell 9 onwards. Simultaneously, dawsonite precipitation decreases and kaolinite dissolution starts.

Precipitation and dissolution of pyrite, barite and chlorite has a low intensity and can be neglected.

Hellevang et al. (2005) discussed the potential of dawsonite to permanently trap CO_2 and assumed that “if dawsonite does precipitate at nonalkaline conditions it is only an ephemeral phase which decomposes when CO_2 pressure drops”. Using nahcolite ($NaHCO_3$) as potential secondary phase instead of dawsonite ($NaAlCO_3(OH)_2$), the decrease in porosity is with a mean of -1.0% in cells 2–10 and of -0.3% in cells 11–101 smaller than using dawsonite (-1.2% in cells 2–10 and -0.4% in cells 11–101). The difference in the results can be explained by a smaller amount of precipitated nahcolite in comparison with dawsonite. By dissolution of albite and K-feldspar, Na^+ and Al^{3+} ions are available. Nahcolite can use Na^+ ions only, whereas dawsonite uses Na^+ and Al^{3+} ions. It is striking that calcite and kaolinite precipitate when previously formed secondary nahcolite is available. The pH is 8.1 when using nahcolite as the potential secondary phase, whereas dawsonite precipitation leads to a pH of ca. 8.4.

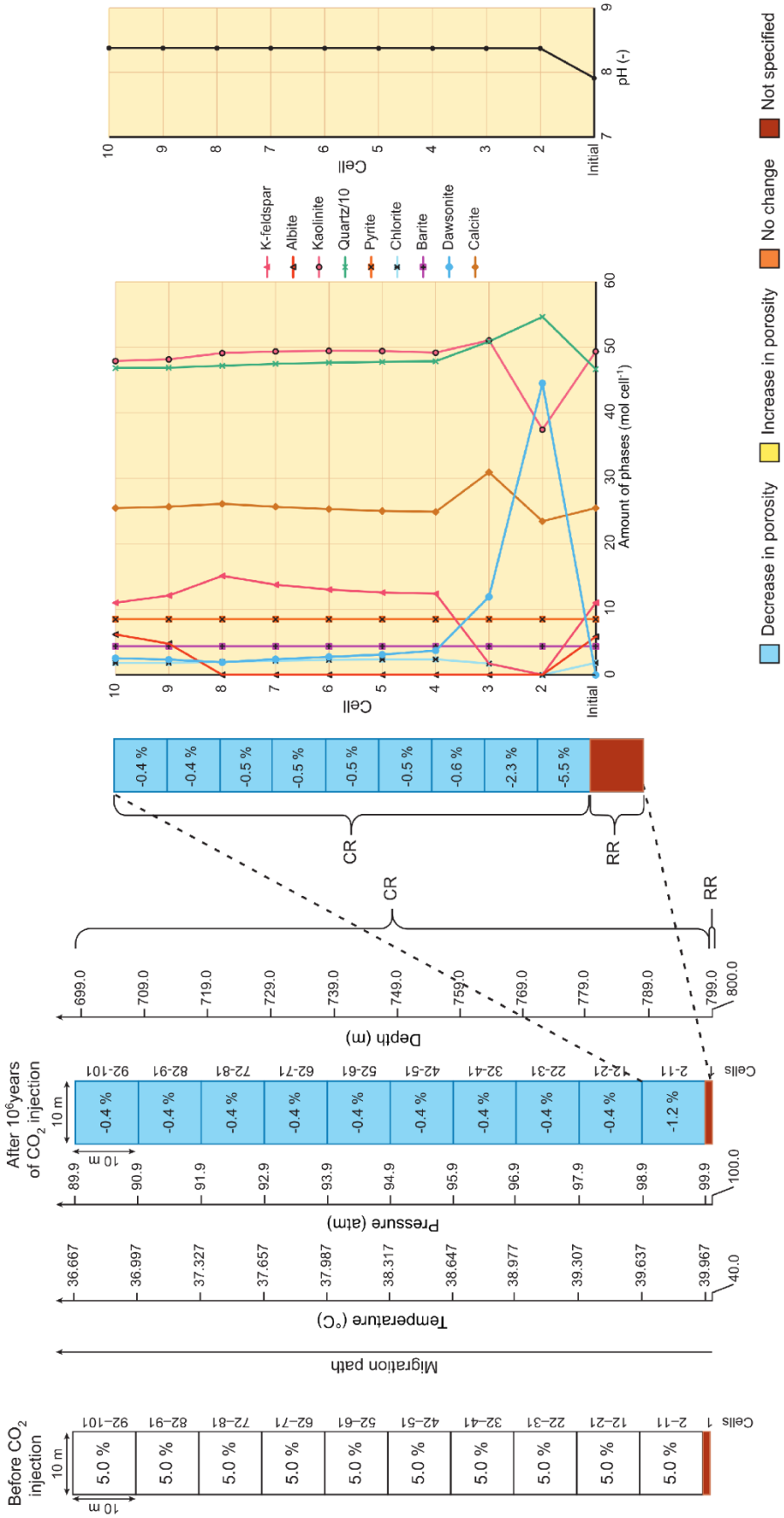

Figure 2.2 Initial conditions in the column of 101 cells and calculated distribution of changes in porosity in %, mineral amounts as well as pH for the reference scenario after 10^6 years. RR = reservoir rock, CR = cap rock. "Initial" shows the initial mineralogical composition of the cap rock and the initial pH of the cap rock brine. Cell 2 is completely cemented. The porosity is reduced from the initial 5.0% to -0.5% after 10^6 years (= decrease in porosity of --5.5%). The amount of precipitated phases is higher than the available pore space. Consequently, the phases will use the available pore space in the next cell.

2.5.2 Alternative Scenarios

Table 2.5 shows the input parameters used in the alternative scenarios. All the alternative scenarios are based on the reference scenario, and single parameters are changed to show their effects on the modeling results of each parameter. The modeling results of the alternative scenarios are presented in Figure 2.3.

Table 2.5 Parameter sensitivity analysis in alternative scenarios.

Scenario	Parameter	
reference	Temperature/pressure	40.0–36.7 °C / 100.0–90.0 atm
1a		150.0–146.7 °C / 470.0–460.0 atm
1b		60.0–56.7 °C / 150.0–140.0 atm
1c		34.0–30.7 °C / 60.0–50.0 atm
reference	Veins	No veins
2a		Quartz vein (100% quartz, 5.0% porosity)
2b		Calcite vein (100% calcite, 5.0% porosity)
2c		Calcite vein (100% calcite, 5.5% porosity)
2d		Calcite vein (100% calcite, 40.0% porosity)
reference	Initial cap rock porosity	5.0%
3a		40.0%
3b		10.0%
3c		6.0%
3d		2.0%
reference	Effective diffusion coefficient	3.33×10^{-10} m^2 s^{-1}
4a		1.00×10^{-10} m^2 s^{-1}
4b		4.50×10^{-11} m^2 s^{-1}
4c		1.00×10^{-11} m^2 s^{-1}
reference	Injected fluid composition	100% CO_2
5a		99.0% CO_2 + 1.0% CH_4
5b		50.0% CO_2 + 50.0% CH_4
5c		99.0% CO_2 + 1.0% H_2S
reference	Initial conditions according to published case study	–
6a		Mineralogical data from Bildstein et al. (2010) (see Appendix Table A 2.1, Table A 2.2)
6b		Mineralogical data + P–T conditions from Bildstein et al. (2010) (see Appendix Table A 2.1, Table A 2.2)
reference	Transport mechanism	Diffusion
7		Advection
reference	Temperature	40.0–36.7 °C / 100.0–90.0 atm
8a		150.0–146.7 °C + constant pressure (469.9 atm)
8b		34.0–30.7 °C + constant pressure (59.9 atm)
reference	Pressure	40.0–36.7 °C / 100.0–90.0 atm
9a		470.0–460.0 atm + constant temperature (149.967 °C)
9b		60.0–50.0 atm + constant temperature (33.967 °C)

2.5.2.1 Temperature / Pressure

Scenarios 1a–c (Figure 2.3a) cover a spectrum of temperature and pressure conditions, comparable to CO_2 storage systems like those at Ketzin (Germany), Frio (USA) and Lacq-Rousse (France). Changing temperature and pressure will affect the equilibrium constants, *K*, of the mass-action laws of minerals, aqueous species and gases in such CO_2 dominated systems (van Berk et al., 2015). Thus, scenarios 1a–c show the effect of temperature and pressure on the change in porosity triggered by mineral dissolution and precipitation. The pH varies for the different scenarios. It decreases in scenario 1a to 6.7 but increases in scenario 1b to 8.0 and in scenario 1c to 8.5–8.6. At a temperature of 150.0 °C and a pressure of 470.0 atm the porosity of the cap rock increases from the initial 5.0% to up to 6.7% in cells 12–101. At a temperature of 60.0 °C and a pressure of 150.0 atm the porosity of the cap rock decreases from the initial 5.0% to up to 4.8% in cells 12–101. At P–T conditions of 60.0 atm and 34.0 °C the porosity decreases from the initial 5.0% to 4.5% in cells 12–101. At temperatures between 34.0 °C and 135.0 °C and pressures between 60.0 atm and 440.0 atm the porosity decreases from the initial 5.0% to an average of 4.4%. With the help of various further temperature/pressure scenarios, a critical point is revealed where the porosity development changes from a decrease to an increase. This critical point lies between the temperatures of 135.0 °C and 150.0 °C and corresponding pressures of 440.0 atm and 470.0 atm.

Changes in temperature and pressure affect the mineral behavior. When comparing scenario 1a (150.0 °C / 470.0 atm; cell 1) with the reference scenario (40.0 °C / 100.0 atm; cell 1), differences in the porosity change are identifiable. At higher temperature and pressure conditions (scenario 1a) the porosity increases. Unlike the reference scenario where the pH increases from the initial 7.9 to 8.4, the pH decreases to 6.7 in scenario 1a. In contrast to the reference scenario, in scenario 1a chlorite is completely dissolved in cells 2−101. K-feldspar is completely consumed in the first cells but is available from cell 5, one cell earlier than in the reference scenario. Calcite, quartz and kaolinite dissolution and precipitation are less strong than in the reference scenario. The same applies for dawsonite, which precipitates with 44.5 mol in cell 2 in the reference scenario and with 23.3 mol in cell 2 of scenario 1a.

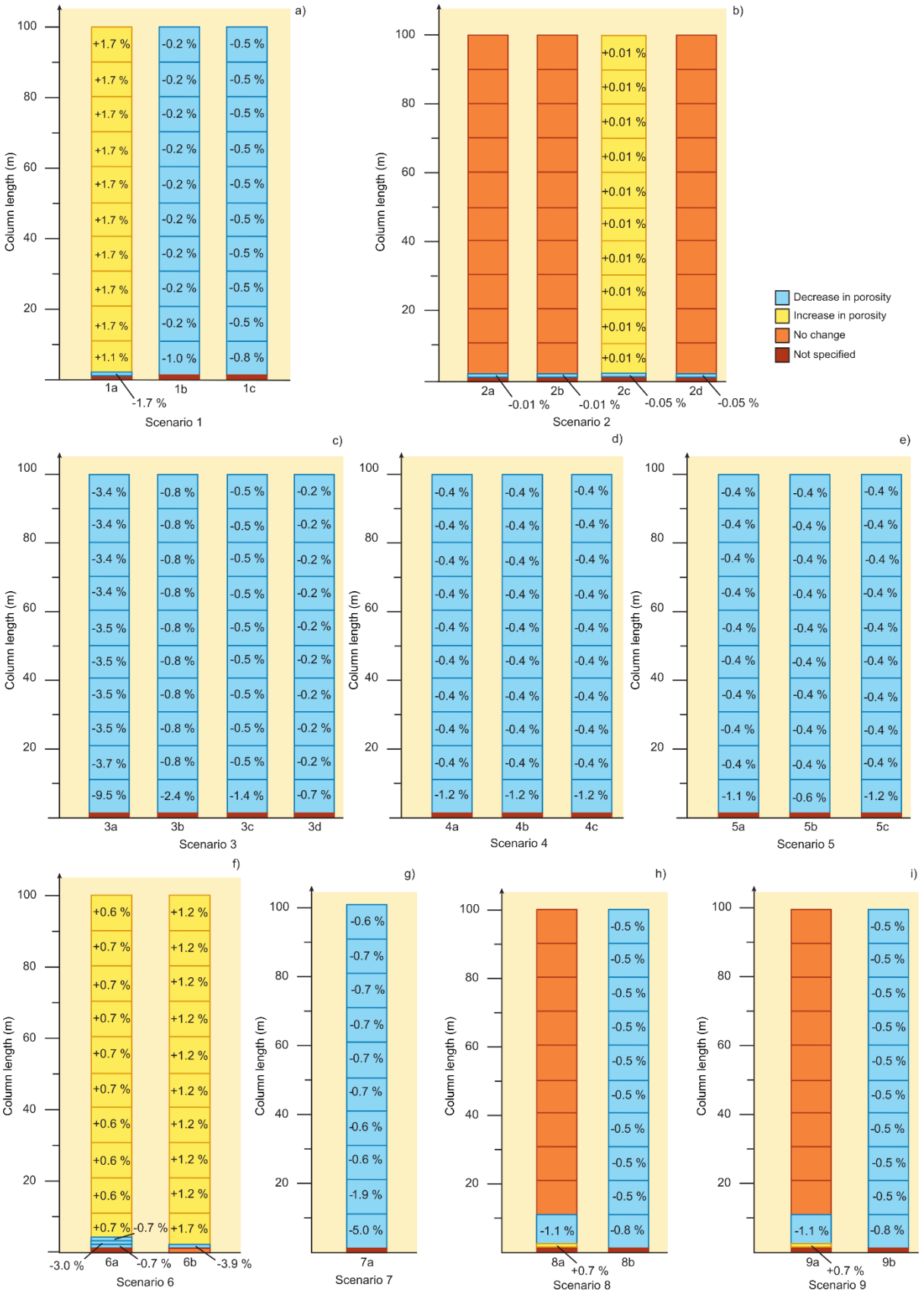

Figure 2.3 Gain or loss of total porosity for scenarios 1 to 9 (a–i) in a column of 101 cells, with a cell length of 1 m. 100 m are located in the cap rock and 1 m in the reservoir rock. The values are given as mean values for every 10 meters.

2.5.2.2 Veins

Cap rock properties like mineralogical compositions rarely show a homogeneous distribution. Quartz veins and calcite veins occur frequently. For this, scenarios 2a−d with mono-mineralogical compositions of quartz and calcite are calculated (Figure 2.3b, Table 2.5). In a quartz vein, a small decrease in porosity is observed in cell 2 (-0.01% from the initial 5.0%), while the porosity change in all other cells is <0.01%. The same results apply for scenario 2b considering a calcite vein and an initial porosity of 5.0%. Calcite veins with a higher initial porosity of 5.5% (scenario 2c) lead to a decrease in porosity in cell 2 (-0.01%) and to a weak increase in all other cells (Δ +0.01%). This trend is measurable up to an initial porosity of 10.0%. Another scenario (2d) considers an initial porosity of 40.0% in the calcite veins, as modeled by Bildstein et al. (2010). Despite such a high initial porosity of 40% in calcite veins, the modeling results show a decrease in porosity of -0.05% in cell 2 but constant porosities in the following cells. In summary, secondary porosity can be created when the initial porosity ranges between ~5.2% and ~10%. The pH in the cap rock brine decreases from 7.9 to 6.8 in all four scenarios (2a–d) and is lower than in the reference scenario (pH 8.4).

2.5.2.3 Initial Cap Rock Porosity

With a scenario series (3a–d) different initial cap rock porosities between 2.0% and 40.0% are calculated to test the effects of this parameter (Figure 2.3c). The high initial cap rock porosity of 40% conceptually represents that open fractures occur in the cap rock. The modeling results with an initial cap rock porosity of 40.0% show a strong decrease in porosity in cell 2 (-16.34%), a decrease of between 8.34% and 31.66% (ø -9.5%) in cells 3–12 and a -3.4 to -3.7% loss in porosity for cells 13–101. This trend is also traceable for initial porosities of 10.0%, 6.0% and 2.0%, as well as for the reference scenario with an initial porosity of 5%. The pH of the cap rock brine lies between 8.4–8.5 in all scenarios (3a–d).

2.5.2.4 Effective Diffusion Coefficient

Scenarios 4a–c aim to unravel the effects of diffusion intensity by varying the effective diffusion coefficients from 1.00×10^{-10} m^2 s^{-1} (Bildstein et al., 2010), 4.50×10^{-11} m^2 s^{-1} (Gaus et al., 2005) to 1.00×10^{-11} m^2 s^{-1} (Bildstein et al., 2010). As in the reference scenario, the pH in the cap rock brine increases in all scenarios (4a–c) to ~8.4. Despite a broad range of diffusion coefficients, similar results indicate that the diffusion intensity has no effect on changes in

porosity (Figure 2.3d). However, this conclusion is only valid for the assumed chemical, physical and mineralogical conditions.

2.5.2.5 Injected Fluid Composition

Based on the study by Mohd Amin et al. (2014), several scenarios consider various compositions of injected fluids, including CH_4 and H_2S mixtures with the main component CO_2. Assuming an ideal gas behavior in the gas mixtures, the fugacity coefficients will be calculated for the gas components. Modeling results of scenario 5a (99.0% CO_2 + 1.0% CH_4) show a strong decrease in porosity in cells 2 and 3 (from the initial 5.0% to 0.0%–3.07%) and a moderate decrease in porosity in the remaining cells (down to ~4.57%). An increase in the concentration of CH_4 in the injected fluids from 1.0% to 50.0% leads to a weaker decrease in the porosity in cells 2 and 3 but similar values in the remaining cells. The addition of 1.0% H_2S in scenario 5c decreases the porosity in cell 2, down to 2.79% in cell 3, whereas the porosity increases slowly up to 4.57% in cell 10 and stays constant in the remaining cells. Summarizing, the main differences in porosity change, when using the various fluid compositions, are identifiable in the first cells (2–10) where the change varies from -0.6% to -1.2%. The porosity changes in cells 11–101 is independent of the injected fluid composition (from pure CO_2 to CH_4 and H_2S mixtures; Figure 2.2 and Figure 2.3e). Similar to the reference scenario, the pH increases in scenarios 5a–c to ~8.4. As mentioned by Mohd Amin et al. (2014), when using CH_4 and H_2S mixtures with the main component CO_2, the porosity in the cap rock decreases and the sealing capacity of the cap rock increases.

2.5.2.6 Initial Conditions According to Published Case Study

In comparison with our reference scenario, Bildstein et al. (2010) used a different mineral assemblage in the cap rock, including illite, anhydrite, kaolinite, quartz, pyrite, ankerite, Ca-montmorillonite and calcite (for percentages see Appendix 2.7). Scenario 6a considers the same mineral assemblage under the pressure and temperature conditions of the reference scenario. In scenario 6a the cap rock porosity decreases in cell 2 (Δ -0.7%), to 2.0% in cell 3 and to 4.3% in cell 4 (Figure 2.4). In the following cells, the porosity increases to 5.9% (cells 5 and 6) and remains constant at ~5.6% (cells 5–101). In cells 5–101 illite, quartz, ankerite, and dawsonite precipitate and anhydrite, kaolinite, calcite, and Ca-montmorillonite dissolve. Another scenario (6b) uses the P−T conditions and the mineral assemblage given by Bildstein et al. (2010). In this scenario, the porosity of the cap rock decreases to 1.11% in cell 2 but

shows a strong increase in cell 2 to 7.46%. The average for the cells 11–101 lies at 6.2% (Figure 2.3f). In scenario 6a the pH in the cap rock brine decreases from 6.54 to ~5.3 and in scenario 6b the pH increases to 10.4.

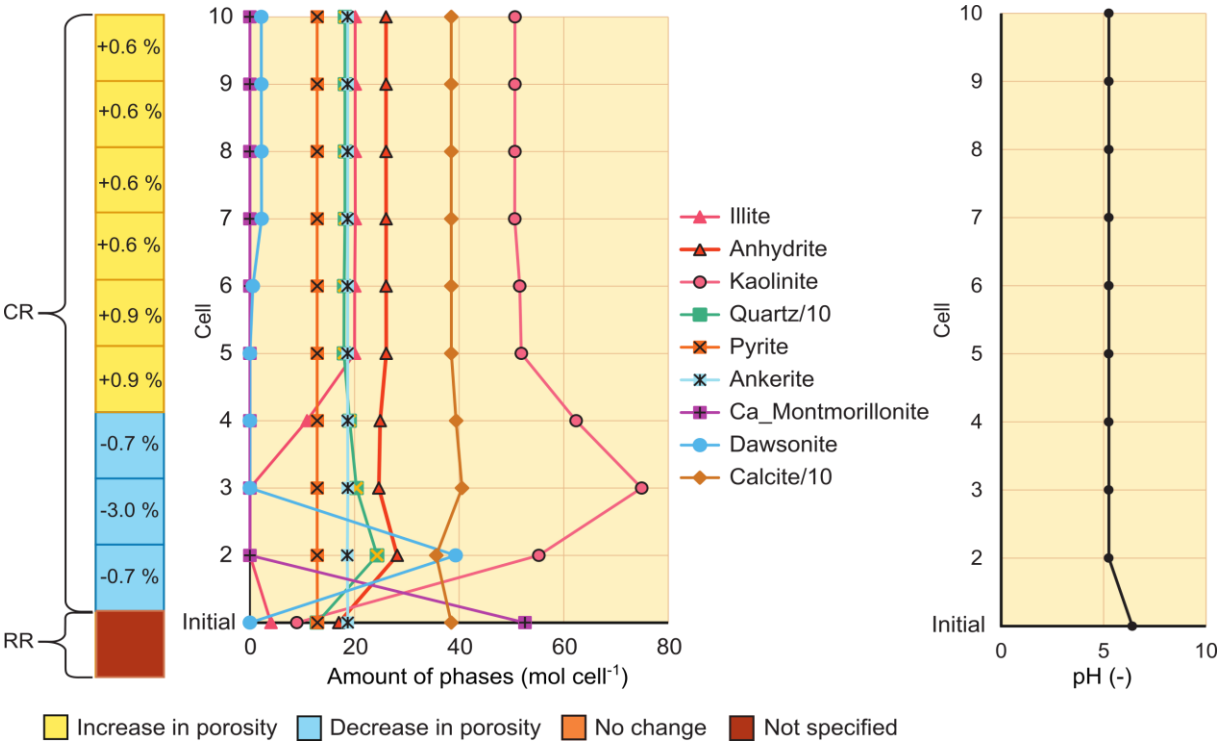

Figure 2.4 Gain or loss of total porosity and mass conversion of the minerals for scenario 6a in the first 10 cells with a cell length of 1 m. 9 m are located in the cap rock (CR) and 1 m in the reservoir rock (RR).

2.5.2.7 Advection as Transport Mechanism

The ability of the cap rock to safely store CO_2 depends, amongst other factors, on the reservoir pressure. If the reservoir pressure becomes too large, new fractures and faults are created (Rutqvist et al., 2007) and pose a high risk of CO_2 leakage. Scenario 7 simulates an intensive CO_2 leakage in fractures and faults by considering advection as the transport mechanism instead of diffusion in the reference scenario (Figure 2.3g). Compared to diffusion, advection enables a faster, stronger and more expansive spread of CO_2. This leads to a lower pH in scenario 7 (to 3.3–5.0 in cells 2–13 and 6.9–7.1 in cells 14–101) compared to 8.4 in all cells of the reference scenario. Such a strong decrease in pH accompanies the complete dissolution of K-feldspar, albite, kaolinite, calcite, chlorite in cells 2–13. However, no secondary porosity is created in these cells because the volume of newly formed quartz and dawsonite

overcompensates the volume resulting from dissolution of K-feldspar, albite, kaolinite, calcite, chlorite.

2.5.2.8 Changing Temperature at a Constant Pressure

Scenarios 1a–c reveal the change in porosity in dependence on temperature and pressure. In contrast, in scenarios 8a+b only the temperature is changed and the pressure is set constant to show the effect of temperature on the porosity change (Figure 2.3h). However, a constant pressure assumed in these scenarios does not comply with a real system. In scenario 8a, change in porosity is limited to cells 2 to 11: increases by 0.7% in cell 2 and decreases by -1.1% on average in cells 3–11. Such calculated changes in porosity are less intensive when compared to scenario 1a. When comparing these results with the results of scenario 1a strong differences are observed in cell 2. In scenario 1a the porosity decreases and in scenario 8a the porosity increases. In cell 3 to 11 the opposite effect is detectable. Whereas the porosity increases in scenario 1a, it decreases in scenario 8a. The pH of the cap rock brine for both scenarios (8a and 1a) decreases from the initial 7.9 to 6.7. In scenario 8b the calculated porosity decreases in all cells, which is similar to scenario 1c. The difference with scenario 1c (in which the temperature and pressure are changed) is detectable in cell 2 only where a difference in the third decimal place is observed. Even the pH of the cap rock brine (8.5–8.6) is the same in scenario 8b and 1c. In summary, scenarios 8a and 8b show that the temperature has a stronger effect on mineral dissolution and precipitation at high pressure and temperature conditions.

2.5.2.9 Changing Pressure at Constant Temperature

Scenarios 9a+b aim to test the influence of pressure on mineral dissolution and precipitation (Figure 2.3i). In scenario 9a, the porosity increases in cell 2 but decreases in cell 3–11, whereas no change in the remaining cells is observable. In contrast, in scenario 1a the porosity decreases in cell 2 only, while all other cells show a porosity increase. As in scenario 1a, the pH of the cap rock brine decreases from the initial 7.9 to 6.7 in scenario 9a.

The modeling results of scenario 9b show that the porosity decreases in all cells. When comparing the results between scenario 9b and scenario 1c (where the temperature and pressure are changed), differences are detectable in the third decimal place in cells 2 and 3 only. The same applies for the pH of the cap rock brine, which increases to 8.5 in scenario 9b

and to 8.5–8.6 in scenario 1c. Like the effect of temperature (scenarios 8a+b), the effect of pressure on the change in total porosity is stronger at higher temperature and pressure conditions. Comparing the effect of temperature with the effect of pressure on porosity change, only small differences are identifiable. The pressure effect is slightly stronger than the temperature effect but there are differences in the second decimal place.

2.5.3 Sensitivity Analysis

The sensitivity analysis aims to show the effect of different solubility constants for $CO_{2(g)}$ on the modeling results. We vary the log *K* values for $CO_{2(g)}$ from initial -1.468 to -1.769 and -1.167 for the reference scenario. These values are chosen by doubling the solubility constant and by reducing the solubility constant by 50%. The modeling results show that the solubility constant of $CO_{2(g)}$ influences the final simulation results. The strongest change in porosity is identifiable in cells 2–4 whereby the change in the following cells (5–10) is at most in the second decimal place (Table 2.6). However, the general trend of decreasing porosity in the reference scenario does not depend on the chosen solubility constant.

Table 2.6 Comparison of solubility constants of $CO_{2(g)}$ based on the change in total porosity in the reference scenario for cells 2–10. log *K* -1.468 is the solubility constant used in the reference scenario.

Solubility constant $CO_{2(g)}$	**log *K* -1.769**	**log *K* -1.468**	**log *K* -1.167**
Cells		Decrease in porosity (%)	
2	-7.2	-5.5	-4.4
3	-1.1	-2.3	-2.0
4	-0.4	-0.6	-1.6
5	-0.5	-0.5	-0.5
6	-0.5	-0.5	-0.5
7	-0.5	-0.5	-0.5
8	-0.5	-0.5	-0.5
9	-0.4	-0.4	-0.4
10	-0.4	-0.4	-0.4

2.5.4 Modeling Limitations

The model presented here uses thermodynamic equilibrium reactions and the local equilibrium assumption for CO_2 storage systems. It does not aim to reflect the complexity of the whole system. However, there is a general agreement that models enable critical analysis of a system and that “model testing and the evaluation of predictive errors lead to improved models and better understanding of the problem” (Konikow and Bredehoeft, 1992).

Our modeling approach is based on assumptions regarding chemical and physical parameters. It excludes kinetic aspects of mineral dissolution/precipitation. The used database phreeqc.dat includes the pressure and temperature dependence of the mass-action law constants for the equilibrium reactions of many aqueous, gaseous and solid species involved but with the exception of the pressure dependence of dawsonite and nahcolite which may be of great relevance for simulating CO_2 storage systems.

For the sake of simplicity, it is neglected that the modeling results of one cell could change the initial parameters for the neighboring cells. Changes in porosity and permeability affect the tortuosity. Such changes should be adapted in every single cell after every time step of the modeling. There is no valid relationship between permeability and porosity because the permeability-porosity correlation is site-specific and depends on many geometric factors (Verma and Pruess, 1988). However, it is shown in laboratory experiments (Vaughan, 1987) as well as in field data (Pape et al., 2000) that even small reductions in porosity, resulting from mineral precipitation, can significantly reduce permeability. Furthermore, newly formed solid phases close pore throats and lead to stronger reductions in permeability (Verma and Pruess, 1988).

Even if the diffusion coefficient is specific to each aqueous species, depending on the species type, pressure, temperature and interaction with other species (Gaus et al., 2005), the used computer code PHREEQC only allows a uniform diffusion coefficient for all aqueous species of 3.33×10^{-10} m^2 s^{-1}. Nevertheless, the modeling results indicate that a change in the diffusion coefficient has no effect on the calculated results. Regarding the diffusion of dissolved CO_2 in cap rock, Fleury et al. (2009) suggest that the diffusion coefficients depend primarily on the porosity. Consequently, in real CO_2 storage systems the effective diffusion coefficient must be calculated not only in dependence on the species and temperature of each cell but also on the newly formed porosity, changed by CO_2−water−rock interactions, in each cell. Furthermore, a homogeneous distribution of relevant cap rock parameters is considered in our study. In contrast, a heterogeneous distribution of relevant cap rock parameters can lead locally to different results. Moreover, tests of different boundary conditions (constant, closed and flux) show no effects on the modeling results.

2.6 Conclusions

The application of the 1DRMT modeling presented in this study provides a good example of how such a modeling approach could (i) identify mineral dissolution and precipitation in the

cap rock triggered by molecular diffusion of CO_2 and (ii) quantify the resulting porosity change, even allowing for several limitations.

Because of hydrogeochemical reactions, the results of the reference scenario show a change in porosity from cell to cell over the length of 101 m after 10^6 years of diffusive mass transport. Quartz and dawsonite precipitate, whereas K-feldspar, albite, kaolinite, calcite, chlorite and barite dissolve. Compared to these dissolved minerals, the more intensive precipitation of quartz and dawsonite causes a decreasing cap rock porosity in the reference scenario. Generally, the main changes in porosity are identifiable close to the cap rock/reservoir rock contact.

Alternative scenarios for selected physical and chemical parameters were performed in this study to identify the key factors controlling the change in porosity. The modeling results show that the creation of porosity depends on different factors. The following conclusions are based on the results of the alternative scenarios.

- Mineral dissolution and precipitation and resulting porosity changes are temperature and pressure dependent, because temperature and pressure affect the mass-action laws of minerals and aqueous species involved in the equilibrium reactions. In the tested range of 30.7–150.0 °C and 50.0–470.0 atm, both temperature and pressure have a stronger effect on mineral dissolution and precipitation at higher P–T conditions. Therefore, it is important to consider that the initial temperature and pressure conditions can differ from location to location in a single system (i.e. in folded structures). Compared to temperature, the effect of pressure on the change of porosity is slightly stronger.
- Regarding temperature and pressure conditions, there is a critical point where the porosity development changes from decrease to increase. For the reference scenario the critical point lies between 135.0 °C and 150.0 °C and 440.0 atm and 470.0 atm. This critical point would vary when the initial conditions change, specifically the initial mineralogical compositions of the cap and reservoir rocks.
- Depending on the initial porosities, calcite, which frequently occurs as veins in cap rocks, can dissolve. Therefore, calcite veins could be a risk for the sealing capacity of the cap rock.
- When using initial cap rock porosities between 2.0% and 10.0%, a decrease in total porosity over the length of one hundred meters of modeled cap rock is identifiable. These results indicate that under the assumed physical, chemical and mineralogical conditions, the sealing capacity of the cap rock is improved.

- Using the mineralogical phase assemblage from Bildstein et al. (2010), an increase in porosity from the fifth meter onwards is identifiable, so the sealing capacity of the cap rock decreases. This result indicates that porosity creation depends strongly on the mineralogical composition of the reservoir and cap rock as well as on the brine compositions.
- Even over a broad range tested, the intensity of diffusive mass transport has negligible effects on mineral precipitation and dissolution as well as on resulting changes in porosity.
- The injected fluid compositions affect the sealing capacity of cap rocks which can increase by mixing CO_2 with CH_4 and H_2S in comparison with pure CO_2 injection.
- An intensive CO_2 leakage in fractures and faults enables a faster and broader spread of CO_2, and consequently, could cause an earlier and stronger sealing risk.
- Compared to nahcolite, dawsonite precipitates in higher amounts and is one reason for the decrease in porosity. However, the potential of dawsonite to trap CO_2 permanently is still a point of discussion (Hellevang et al., 2005).

Therefore, the chemical and physical data of the cap and reservoir rocks and brine must be measured under in situ conditions to develop a numerical model for evaluating a specific CO_2 storage system. Various cap rock mineral phase assemblages should be exposed to different aqueous solutions, partial pressures of carbon dioxide and P–T conditions in long-term laboratory batch experiments to observe mineral dissolution and/or precipitation. These results should be reproduced by batch modeling using identical initial parameters. Such a combination of laboratory experiments and modeling should be performed to test the plausibility of the applied hydrogeochemical equilibrium model.

2.7 Appendix

Table A 2.1 Data from Bildstein et al. (2010).

Temperature = 80 °C, ρCO_2 = 150 bar

Initial mineralogical composition of the cap rock		**Reservoir water**		**Acidified reservoir water**		**Initial cap rock water**	
	Weight percent (wt. %)	pH	6.24	pH	4.75	pH	6.54
Calcite	50	Species	Molality	Species	Molality	Species	Molality
Ankerite	5	Al	5.622×10^{-8}	Al	1.251×10^{-7}	Al	1.531×10^{-7}
Montmorillonite	25	C	4.895×10^{-3}	C	1.141	C	2.180×10^{-3}
Kaolinite	3	Ca	1.612×10^{-2}	Ca	3.204×10^{-2}	Ca	1.528×10^{-2}
Illite	2	Cl	3.014×10^{-1}	Cl	3.015×10^{-1}	Cl	2.601×10^{-1}
Quartz	10	Fe	2.137×10^{-7}	Fe	1.751×10^{-6}	Fe	1.534×10^{-5}
Anhydrite	3	K	2.374×10^{-3}	K	2.375×10^{-3}	K	1.190×10^{-2}
Pyrite	2	Mg	1.282×10^{-2}	Mg	2.424×10^{-2}	Mg	8.937×10^{-4}
		Na	2.594×10^{-1}	Na	2.595×10^{-1}	Na	2.543×10^{-1}
		S	7.642×10^{-3}	S	7.649×10^{-3}	S	1.841×10^{-2}
		Si	8.994×10^{-4}	Si	8.833×10^{-4}	Si	5.371×10^{-4}

Table A 2.2 Additional equilibrium phases, mass-action equations and equilibrium constants used in scenarios 6a–b. Data from phreeqc.dat (Parkhurst and Appelo, 2013), but ankerite is from Bildstein et al. (2010).

Equilibrium phase	**Equilibrium reaction**	**log *K* at 25 °C, 1 bar**
Ankerite	$CaFe_{0.7}Mg_{0.3}(CO_3)_2 + 4H^+ + 0.7Fe^{2+} + 0.3Mg^{2+} + 2H_2O + 2CO_2$	12.14[a]
Montmorillonite	$Ca_{0.165}Al_{2.33}Si_{3.67}O_{10}(OH)_2 + 12H_2O = 0.165Ca^{2+} + 2.33Al(OH)^{4-} + 3.67H_4SiO_4 + 2H^+$	-45.027
Illite	$K_{0.6}Mg_{0.25}Al_{2.3}Si_{3.5}O_{10}(OH)_2 + 11.2H_2O = 0.6K+ + 0.25Mg^{2+} + 2.3Al(OH)^{4-} + 3.5H_4SiO_4 + 1.2H^+$	-40.267
Anhydrite	$CaSO_4 = Ca^{2+} + SO_4^{2-}$	-4.39

[a]: log *K* at 80 °C and 1 bar

2.8 Acknowledgements

We would like to thank the anonymous reviewers for their constructive reviews that considerably improved the manuscript.

2.9 Supplementary Data (on CD)

Input file S1 for the batch model to calculate the cap rock brine and Input file S2 for the transport model to calculate the reference scenario SCGS are available (for PHREEQC Version 3).

3 Salt Cavern Gas Storage (SCGS)

Potential Risk of H_2S Generation and Release in Salt Cavern Gas Storage

Publication II

Authors of the original paper: Christina Hemme, Wolfgang van Berk

Originally published in: Journal of Natural Gas Science & Engineering 47 (2017), 114–123

Summary added for the purpose of this thesis.

Author Contributions:

Conceptual model:	Christina Hemme[1]
Modeling:	Christina Hemme[1] and Wolfgang van Berk[3]
Result evaluation:	Christina Hemme[1] and Wolfgang van Berk[2]
Analysis of results:	Christina Hemme[1] and Wolfgang van Berk[3]
Visualization of results:	Christina Hemme[1]
Writing—original draft preparation:	Christina Hemme[1]
Writing—review and editing:	Christina Hemme[1] and Wolfgang van Berk[3]
Supervision:	Wolfgang van Berk[1]

[1] substantial; [2] medium; [3] minor

Summary

In this part of the study, the gas–water–rock interactions triggered by natural gas storage are considered, and the risks of $H_2S_{(g)}$ generation in salt caverns, which are used for natural gas storage, are analyzed. The focus is on the spatial- and time-dependent $H_2S_{(g)}$ generation processes in salt caverns due to microbial activity (bacterial sulfate reduction) and on technical methods to decrease or inhibit $H_2S_{(g)}$ generation and release.

Storage of natural gas in salt caverns entails risks of hydrogen sulfide ($H_2S_{(g)}$) generation. $H_2S_{(g)}$ is toxic, leads to gas souring and the corrosion of the storage facilities. Therefore, technical regulations prescribe that the $H_2S_{(g)}$ concentration in stored gas is limited to 5 mg m^{-3}.

H_2S is generated by bacterial sulfate reduction (BSR) in the brine and the upper sections of the sump of a salt cavern. Sulfate-S is used by the bacteria as an electron acceptor to oxidize organic compounds and sulfide is generated. In salt caverns, the sulfate source is provided by anhydrite layers within the salt rock. Stored methane (the main component of natural gas) dissolves in the brine until saturation is established and continuously serves as a reductant for BSR. The $H_2S_{(g)}$ generated in brine and sump contaminates the stored gas by outgassing.

These hydrogeochemical processes are quantitatively retraced using a one- and three-dimensional mass-transport model based on chemical equilibrium thermodynamics using PHREEQC and PHAST software with the phreeqc.dat database. Reaction kinetics of BSR are integrated into the model. The modeling approach simulates a semi-generic salt cavern at high pressure and temperature conditions with data from several caverns. The modeling results give basic and quantitative insights into the mechanisms of $H_2S_{(g)}$ generation induced by BSR in salt caverns and lead to a general system- and process-understanding of the hydrogeochemical effects of natural gas storage in salt caverns.

By varying the input parameters, the factors controlling $H_2S_{(g)}$ generation are identified and explain why $H_2S_{(g)}$ is only generated in some salt caverns. An important factor is the availability of anhydrite as a sulfate source. Whereas the occurrence of Fe-bearing minerals like goethite inhibits the release of BSR-generated H_2S into the stored gas. The sulfur (S-II/-I) reacts with Fe+II, and mackinawite or pyrite are formed. To identify early H_2S generation and protect the stored gas from souring, a monitoring system should be installed in the brine of the salt cavern. If the aqueous H_2S concentration increases, the addition of dissolved ferrous iron into the brine and sump is a potential method to reduce H_2S release. The hydrogeochemical model approach can be used and adapted to various salt cavern conditions to answer and solve practically oriented questions and problems (Hemme and van Berk, 2017b).

Abstract

The storage of natural gas in salt caverns can entail the risk of H_2S generation, which in turn leads to gas pollution. H_2S is generated by bacterial sulfate reduction. The bacteria use aqueous $sulfate_{(aq)}$ as an electron acceptor to oxidize the dissolved hydrocarbons and generate sulfide. Anhydrite is available in the rock salt surrounding the cavern and acts as a $sulfate_{(aq)}$ source. The stored natural gas, with its main component, methane, is in solubility equilibrium with the brine and is additionally delivered by diffusion into the brine. The generated H_2S reaches the stored gas by outgassing from the brine. In this study, these processes are simulated by one- and three-dimensional hydrogeochemical diffusive mass transport models, which are based on equilibrium reactions for gas–water–rock interactions and kinetic reactions for sulfate reduction. Modeling results show that the greatest amount of H_2S is generated in the brine. The amount of generated $H_2S_{(g)}$ is mainly controlled by the amount of available $sulfate_{(aq)}$ as well as the rate of diffusion, which is coupled with the maximum operating live time of salt caverns. Additionally, the amount of generated and released $H_2S_{(g)}$ is sensitive to the chosen kinetic rate constant. To ensure constant gas quality over time, the gas and the brine must be analyzed continuously and technical methods must be applied when the $H_2S_{(g)}$ concentration increases. According to the modeling results, $H_2S_{(g)}$ generation is inhibited by addition of dissolved ferrous iron to the brine. Dissolved ferrous iron reacts with sulfide-sulfur to form mackinawite ($FeS_{(s)}$) so that aqueous sulfide is no longer available for $H_2S_{(g)}$ generation. Another method is the addition of NaOH to increase the pH of the brine. Then, higher fractions of generated sulfide-sulfur are transformed to free $S^{2-}{}_{(aq)}$ instead of $H_2S_{(g)}$ and $H_2S_{(aq)}$.

3.1 Introduction

Natural gas is stored in salt caverns to balance the supply and demand of natural gas throughout the year. Salt caverns are highly qualified for hydrocarbon storage because of numerous physical properties and mechanical behaviors of the rock salt halite, like its self-healing forces and its impermeability below 300 m (Evans, 2008; Yang et al., 2013). However, Evans (2008) has stated that “there is a need to assess the safety record of previous and existing underground fuel storage facilities.” One risk is the potential generation and release of gaseous hydrogen sulfide ($H_2S_{(g)}$) in natural gas storage systems. H_2S is toxic if inhaled, is aggressive towards storage facilities (Cord-Ruwisch et al., 1987; Kleinitz and Böhling, 2005), and can pose a threat to the environment (Reitenbach et al., 2015). The presence of H_2S can lead to corrosion of metallic iron under anaerobic conditions and to the precipitation of amorphous ferrous sulfide, which in turn may cause plugging (Cord-Ruwisch et al., 1987).

Even more importantly, H_2S contaminates the stored gas and can affect the gas quality (Cord-Ruwisch et al., 1987). Therefore, in Germany technical regulations determine that the concentration of 5 mg m^{-3} $H_2S_{(g)}$ in stored gas must not be exceeded (DVGW, 2013).

There are considerable indications that $H_2S_{(g)}$ generation could be a potential risk in salt caverns used for gas storage. First, H_2S is observed in hydrocarbon reservoirs where it originates from sulfate reduction (Machel, 2001), either via abiotic reactions or via reactions catalyzed by bacteria. The abiotic reaction, so-called thermochemical sulfate reduction (TSR), is common in geological settings with temperatures ranging from 100 to 180 °C, while the bacterial sulfate reduction (BSR), occurs in low-temperature geological settings ranging from 0 °C to 60–80 °C (Ehrlich, 1990; Machel, 2001; Postgate, 1984). In some cases, BSR has been observed above 80 °C. Hyperthermophilic sulfate-reducing bacteria may live at temperatures up to 110 °C (Jorgensen et al., 1992). However, BSR does not necessarily occur in all hydrocarbon-bearing geosystems with temperatures below 80 or 110 °C. Otherwise, all hydrocarbon reservoirs below this temperature would be sour, meaning H_2S-bearing (Machel, 2001), and would display higher total sulfide concentrations in the aqueous and the gas phase. Therefore, in this study, we focus on salt caverns filled by natural gas and exposed to temperatures ranging from 50 to 80 °C. Our focal point is the formation of sulfide-sulfur (S-II) from sulfate-sulfur (S(+VI)) via BSR and the subsequent release of formed sulfide-sulfur (S-II) as $H_2S_{(g)}$ into the stored natural gas.

An additional indication of H_2S generation by BSR in salt caverns is the possible anaerobic oxidation of methane (AOM), which is observed in marine as well as in non-marine environments (Meulepas et al., 2010). In aqueous anoxic environments, sulfate-reducing bacteria (SRB) use sulfate as an electron acceptor to oxidize organic compounds and generate sulfide (Equation (3.1)). This generated sulfide-S could be available as aqueous H_2S, $HS^-_{(aq)}$, and $S^{2-}_{(aq)}$ and gaseous H_2S. SRB use the produced energy from sulfate reduction to sulfide for cell growth (Cord-Ruwisch et al., 1987). The sulfate for BSR could be derived from the aqueous dissolution of calcium sulfide-sulfur mineral phases like gypsum $(CaSO_4[2H_2O])_{(s)}$ and anhydrite $(CaSO_4)_{(s)}$.

$$SO_4^{2-}{}_{(aq)} + CH_{4(aq)} \xrightarrow{H_2O} H_2S_{(aq)} + CO_3^{2-}{}_{(aq)} + H_2O \quad (3.1)$$

The increasing demand for storage capacity in salt caverns requires the utilization of less favorable salt formations, including inhomogeneous salt structures with larger proportions of insolubles like anhydrite layers (Schneider and Crotogino, 2010). Drilling operations and/or workover operations may lead to bacterial contamination of hydrocarbon reservoirs, or SRB

populations may pre-exist in such reservoirs (Kleinitz and Böhling, 2005). The optimal growth temperature for SRB is 38 °C (Bernardez et al., 2013) at near-neutral pH conditions (Cord-Ruwisch et al., 1987). However, SRB also occur in more acidic environments of pH 3 (Tuttle et al., 1969) and pH 4 (Church et al., 2007).
Furthermore, BSR is observed in saline environments where high rates of sulfate reduction are measured (Kjeldsen et al., 2007). The activity of most SRB decreases if the Na^+/Cl^- concentrations are above 50 to 100 g L^{-1} (Cord-Ruwisch et al., 1987; Postgate, 1984; ZoBell, 1958) but activity of SRB is even found in salt lakes and brines near “salt saturation” (ZoBell, 1958). Even if these conditions are not the optimum for SRB growth, a few SRB tolerate the high salt (NaCl) concentrations and live near salt saturation (Cord-Ruwisch et al., 1987).

Additionally, $H_2S_{(g)}$ is detected in underground storage systems of town gas (Crotogino, 2016) and in underground gas storage in porous media (Kleinitz and Böhling, 2005). Furthermore, the activity of sulfate-reducing bacteria is observed in salt caverns filled by hydrogen gas. There, the SRB live in the sump and in the brine, generating biofilms at the cavern walls (Panfilov, 2016).

This study focuses on H_2S generation by bacterial sulfate reduction in a salt cavern that is described by one- and three-dimensional hydrogeochemical reactive transport models. It is based on thermodynamic equilibrium reactions for gas–water–rock interactions and kinetic reactions for sulfate reduction. The aims of this study are (i) to draw the attention of the possible risk of $H_2S_{(g)}$ pollution in salt caverns, (ii) to clarify and quantify time-dependent $H_2S_{(g)}$ generation processes in salt caverns filled with natural gas, (iii) to analyze the limiting factors for $H_2S_{(g)}$ generation and release in salt caverns, and (iv) to identify technical methods to decrease or inhibit $H_2S_{(g)}$ generation and release.

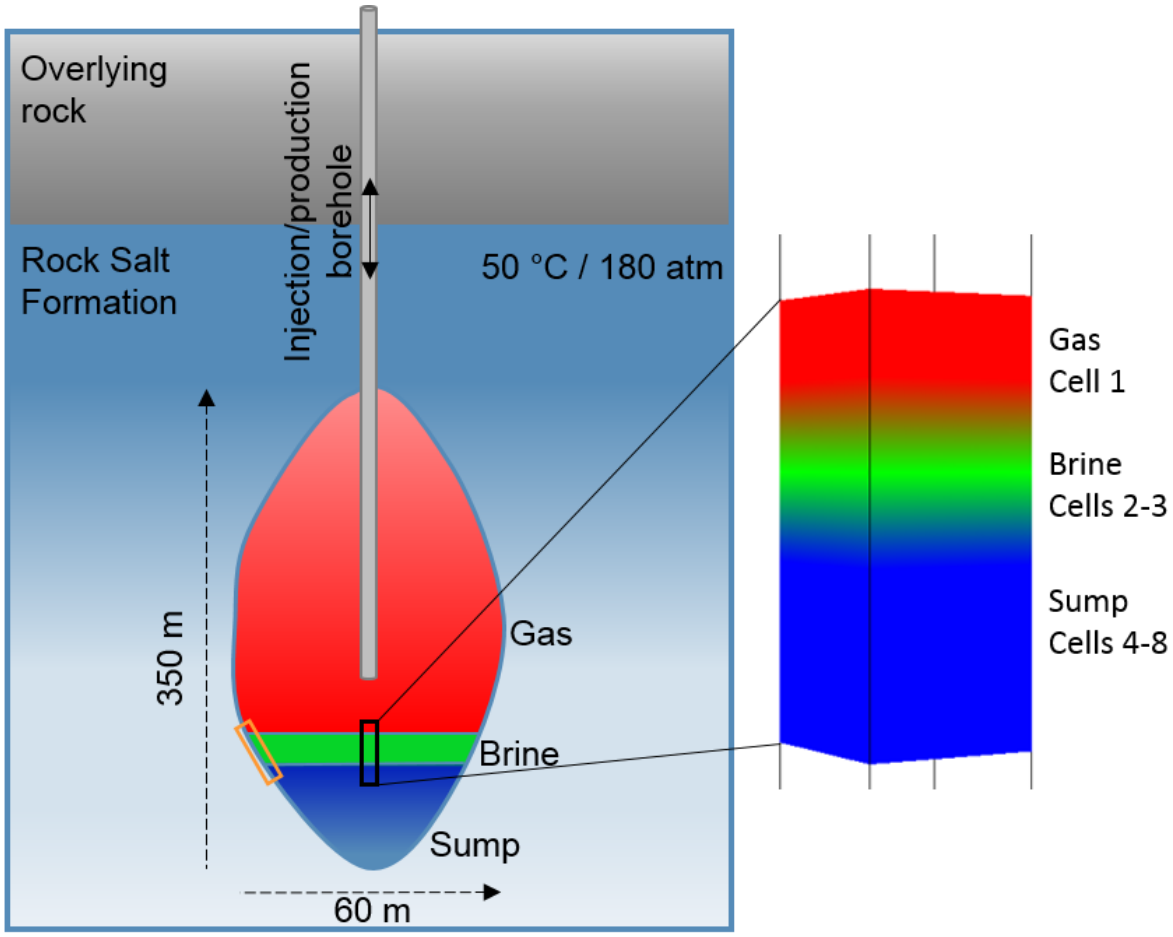

Figure 3.1 System sketch of the model. Black box = reference scenario, orange box = alternative scenario.

3.2 Methodology

3.2.1 Modeling Tools

The one- and three-dimensional reactive mass transport models are based on chemical-thermodynamically principles, the reaction kinetics of BSR and the principles of diffusive mass transport.

The modeling tool for the 1D model in this study is the computer program PHREEQC version 3 provided by the US Geological Survey. PHREEQC is based on an ion-association aqueous model and can simulate batch-reaction, speciation, inverse geochemical and one-dimensional transport calculations (Parkhurst and Appelo, 2013). The calculations are based on mass action laws including all species and their corresponding equilibrium constants. The activity coefficients of species are calculated by the Debye-Hückel equation. The equilibrium phases, mass-action equations, and equilibrium constants used in the model are shown in Table 3.1.

The computer program PHAST (version 3.3.7-11094), provided by the US Geological Survey, is the modeling tool for the 3D model. Using PHAST, multicomponent geochemical reactions, solute transport and groundwater flow can be simulated (Parkhurst et al., 2010). The geochemical reactions in PHAST are simulated with PHREEQC and the flow and transport calculations are based on HST3D; both programs are embedded in PHAST (Parkhurst et al., 2010). The results are visualized using the software Model Viewer (Hsieh and Winston, 2002). The combined application of PHREEQC/PHAST and the Model Viewer software enables the visualization of the temporal and spatial development of H_2S generation in salt cavern gas storages. Detailed information about PHREEQC and PHAST are given in Parkhurst and Appelo (2013) and Parkhurst et al. (2010).

Table 3.1 Equilibrium phases, mass-action equations, and equilibrium constants (log *K*, at 25 °C and 1 bar). Data are from phreeqc.dat, except for $CH_{4(g)}$, $H_2S_{(g)}$, $N_{2(g)}$ which are from llnl.dat (Parkhurst and Appelo, 2013).

Equilibrium phase	Equilibrium reaction	log *K*
Halite	$NaCl = Cl^- + Na^+$	1.570
Anhydrite	$CaSO_4 = Ca^{2+} + SO_4^{2-}$	-4.39
Siderite	$FeCO_3 = Fe^{2+} + CO_3^{2-}$	-10.89
Quartz	$SiO_2 + 2H_2O = H_4SiO_4$	-3.98
Barite	$BaSO_4 = Ba^{2+} + SO_4^{2-}$	-9.97
Pyrite	$FeS_2 + 2H^+ + 2e^- = Fe^{2+} + 2HS^-$	-18.479
Dolomite	$CaMg(CO_3)_2 = Ca^{2+} + Mg^{2+} + 2CO_3^{2-}$	-17.09
Mackinawite	$FeS + H^+ = Fe^{2+} + HS^-$	-4.648
Sulfur[a]	$S + 2H^+ + 2e^- = H_2S$	4.882
Calcite	$CaCO_3 = CO_3^{2-} + Ca^{2+}$	-8.48
$CH_{4(g)}$	$CH_4 = CH_4$	-2.8502
$CO_{2(g)}$	$CO_2 = CO_2$	-1.468
$H_2S_{(g)}$	$H_2S = H^+ + HS^-$	-7.9759
$N_{2(g)}$	$N_2 = N_2$	-3.1864

[a]: Sulfur = elemental sulfur

The thermodynamic database; which includes all elements used in the model with their species (aq, s, g), mass-action equations, and equilibrium constants; is essential for modeling with PHREEQC and PHAST. The database used for 1D and 3D modeling is phreeqc.dat. A more suitable database for the high Na^+ and Cl^- concentrations and the high ionic strength in the model could be the Pitzer database (pitzer.dat), but pitzer.dat does not include Si-containing aqueous species, Al^{3+}, and silicate minerals, which are important factors when modeling H_2S generation in salt caverns. To validate that PHREEQC (using phreeqc.dat) produces correct results, even under high Na^+ and Cl^- concentrations and high ionic strength, the salt solubility in PHREEQC (using phreeqc.dat) is compared with salt solubility data from literature. In Zimmermann et al. (1986), the solubility of Na^+/Cl^- is given in dependence of the temperature. At 40 °C, 36.42 g Na^+/Cl^- (halite) dissolves in 100 g water (= 6.23 mol kgw^{-1} for Na^+ and Cl^-).

This measurement is consistent with the results of Na^+/Cl^- solubility in PHREEQC using phreeqc.dat (= 6.32 mol kgw^{-1} for Na^+ and Cl^-), with the discrepancy that the temperature in the model is 50 °C. $NaCl_{(solid)}$ solubility data in pure water at different temperatures from literature (experimental data) are compared with modeled data (PHREEQC with phreeqc.dat) and are summarized in Table 3.2.

Table 3.2 $NaCl_{(solid)}$ solubility (mol kgw^{-1}) in pure water at different temperatures from literature (experimental data) and modeled data. The database phreeqc.dat is used in the PHREEQC model.

Solubility $NaCl_{(solid)}$ - Data	0 °C	20 °C	40 °C	60 °C
	(mol kgw^{-1})	(mol kgw^{-1})	(mol kgw^{-1})	(mol kgw^{-1})
Zimmermann et al. (1986)	6.09	6.13	6.23	6.34
PHREEQC modeling	6.00	6.10	6.24	6.39

3.2.2 Model Setup

Salt caverns are divided into three parts (Figure 3.1): the stored gas at the top, which takes up the largest volume; the brine in the middle, with a thickness of only a few meters; and the sump at the bottom, which can occupy one third of the total cavern volume (Bérest and Brouard, 2003; Panfilov, 2016). The sump is composed of insoluble residues (Evans, 2008) and a residual pore-filling aqueous solution that is not discharged after leaching (Panfilov, 2016). Due to technical reasons, residual brine is situated above the sump (Haddenhorst, 1989). This brine is in solubility equilibrium with the gas stored above (Fontenot, 1981; Réveillère et al., 2016) and the surrounding mineral phases of the rock salt formation.

The initial gas composition in the model is based on data from DVGW (2013). The main component is $CH_{4(g)}$ (partial pressure of CH_4 (ρCH_4) = 178.128 atm), with minor amounts of $N_{2(g)}$ ($\rho N_{2(g)}$ = 1.548 atm), $CO_{2(g)}$ ($\rho CO_{2(g)}$ = 0.324 atm), and $H_2S_{(g)}$ ($\rho H_2S_{(g)}$ = 0.00018 atm), hereinafter called “initial gas”. For the sake of simplicity, the partial pressure is assumed to be equal to the fugacity f ($\rho = f$). The total gas pressure is 180 atm, and the temperature in the salt cavern is 50 °C.

The mineralogical composition of the sump and the brine are characterized by the composition of the surrounding rock salt formation and the solution used for leaching. The mineralogical composition of the rock salt formation is based on data from Kyle and Posey (1991) and is shown in Table 3.3. For leaching, the chemical composition of groundwater taken from a ca. 20 m depth quaternary aquifer from Lower Saxony, northern Germany (NLWKN, 2015) is used (Table 3.4).

Table 3.3 Initial mineralogical composition of the rock salt formation used for the sump with a porosity of 20%. The data are modified after Kyle and Posey (1991). Mackinawite, elemental sulfur, and calcite are potential secondary phases which may form at saturation.

Primary mineral phases	Weight percent (wt. %)	Amount (mol kgw^{-1})
Halite	97.0	144.62
Anhydrite	2.75	1.76
Siderite	0.05	0.04
Quartz	0.05	0.07
Barite	0.05	0.02
Pyrite	0.05	0.04
Dolomite	0.05	0.02

A salt cavern with a height of 350 m, divided into 300 m stored gas, 2 m brine, and 48 m sump, is assumed. The focal point of the model is the brine-gas interface and the upper meters of the sump (Figure 3.1). Therefore, the model is divided into a column of 8 cells, with a cell height of 1.0 m each (in the *z*-direction). The boundary at the upper end of the column represents a constant amount of stored gas. At the lower end of the column, the boundary condition is defined as diffusive flux. The only mass transport in this model is molecular diffusion of all aqueous species. One diffusion coefficient for all aqueous species of 5.0×10^{-9} m^2 s^{-1} is used. Cell 1 delivers CH_4 (C(-IV)) continuously by diffusion. Cell 2 is located at the brine-gas interface, cell 3 in the brine, and cells 4–8 in the sump. Each cell is defined by specific mineralogical and hydrochemical properties. The brine and residual aqueous solution compositions are calculated in separated batch models with PHREEQC (Table 3.4).

Table 3.4 Groundwater composition used for leaching (NLWKN, 2015), initial composition of the brine, and the aqueous solution in the sump.

	Groundwater	**Solution in the sump**	**Brine**
pH	6.4	8.2	5.7
Temperature (°C)	10.1	50.0	50.0
Elements	Concentration (mol kgw^{-1})	Concentration (mol kgw^{-1})	Concentration (mol kgw^{-1})
Ba	-[a]	8.136×10^{-07}	9.097×10^{-07}
C	-[a]	2.901×10^{-05}	7.077×10^{-03}
Ca	1.622×10^{-03}	5.488×10^{-02}	6.333×10^{-02}
Cl	8.380×10^{-04}	6.306	6.310
Fe	1.522×10^{-06}	2.257×10^{-03}	1.415×10^{-03}
K	1.010×10^{-04}	1.010×10^{-04}	1.010×10^{-04}
Mg	3.150×10^{-04}	1.464×10^{-02}	1.315×10^{-03}
Mn	9.100×10^{-07}	9.100×10^{-07}	9.100×10^{-07}
N_{tot}[b]	1.152×10^{-03}	1.152×10^{-03}	3.008×10^{-04}
Na	7.050×10^{-04}	6.306	6.310
O(0)	6.600×10^{-05}	-[a]	-[a]
P	4.840×10^{-07}	4.840×10^{-07}	4.840×10^{-07}
S_{tot}[c]	8.540×10^{-04}	7.108×10^{-02}[c]	6.262×10^{-02}[c]
Si	2.560×10^{-04}	5.242×10^{-05}	3.368×10^{-02}

[a]: Not present
[b]: summed concentration of aqueous N(-III), N(+III), N(+V) species
[c]: summed concentration of aqueous S(+VI) and S(-II) species

The brine (cell 2) is composed of the solution used for leaching and is equilibrated with the mineralogical composition of the rock salt and the initial gas composition. It has a total volume of 1 L, which is equivalent to 1 kg of pure water (kgw). The gas phase in cell 2 has a total volume of 270,000 L (based on the model height for gas of 300 m, a base area of 0.005 m^2, and a pressure of 180 atm) and represents the stored gas volume at 180 atm under the assumed salt cavern design. For modeling purposes, this gas is a tracer gas with the same chemical properties as $CH_{4(g)}$. It is used instead of $CH_{4(g)}$ because CH_4 is induced and used as reactant in the calculation kinetics. The partial pressure of the tracer gas is equivalent to the total pressure in the cavern so that the generated H_2S is released as gas bubbles. The brine in cell 3 is composed of the solution used for leaching equilibrated with the mineralogical composition of the rock salt but without being in equilibrium with a gas phase. However, the possibility of $H_2S_{(g)}$ outgassing is assumed, and calcite, mackinawite, and elemental sulfur are potential secondary phases that may form at saturation.

The residual aqueous solution in the sump (cells 4–8) is composed of the solution used for leaching equilibrated with the mineralogical composition of the rock salt formation (Table 3.4). An initial porosity of 20% is assumed in the sump. The amount of each mineral phase is calculated in moles per kg of pore water by considering the specific density of each mineral

phase (g cm^{-3}) and is summarized in Table 3.3. Additionally, calcite, mackinawite, and elemental sulfur are potential secondary phases that may form at saturation. No gas phase is available, but the possibility of $H_2S_{(g)}$ outgassing is assumed in all cells.

The oxidation of methane by sulfate in the model system is kinetically controlled. The sulfate reduction rate of 6.46×10^{-10} mol kgw^{-1} s^{-1} at 55 °C is derived from Adams et al. (2013). The initial amount of $CH_{4(aq)}$ in the brine is 0.027 mol kgw^{-1}. That corresponds to the maximum amount of $CH_{4(g)}$ in the brine under assumed solubility–equilibration–conditions at a $pCH_{4(g)}$ of 180 atm and 50 °C. A separate transport model provides the initial amount of $CH_{4(g)}$ in the sump for the kinetic calculation. This amount corresponds to the maximum available amount of $CH_{4(g)}$ that could be delivered to the sump by diffusion in a timeframe of 30 years (because the typically operating lifetime of a salt cavern is 30 years). In 30 years, 0.007 mol kgw^{-1} CH_4 is available in the first meter of the sump, 0.004 mol kgw^{-1} CH_4 in the second meter, 0.003 mol kgw^{-1} CH_4 in the third meter and 0.001 mol kgw^{-1} CH_4 in the fourth meter of the sump.

The diffusive mass fluxes are calculated by multiplying diffusivity with tortuosity. Diffusivity is defined by the coefficient of molecular diffusion of aqueous species in dilute solutions without a porous matrix (Fu et al., 2016). A diffusivity of 10^{-9} m^2 s^{-1} for all aqueous species involved in the model is assumed. Tortuosity describes the relation of effective diffusion mass fluxes in a porous medium to ideal diffusion mass fluxes in dilute solutions without a rock matrix and varies between 0.0 and 1.0. To show the influence of the diffusive mass transport on the modeling results, the values of tortuosity in different modeling scenarios are systematically varied (Section 3.3.2.4).

Alternating operating phases characterize the total gas pressure in a salt cavern, divided into a minimum pressure phase, injection pressure phase, maximum pressure phase, and production pressure phase (Wang et al., 2015). The pressure is varied between a minimum of 60 atm and a maximum of 180 atm in different modeling scenarios (Section 3.3.2.1). Because PHAST is not capable of calculating the pressure dependence of solubility equilibrium constants for minerals, gases and aqueous species, the pressure dependence is simulated in a separate model using the software PHREEQC and the database phreeqc.dat (Parkhurst and Appelo, 2013).

3.3 Results and Discussion

3.3.1 H_2S Generation and Release—Reference Scenario

The results of the modeled reference scenario show that $CH_{4(g)}$ dissolves from the stored gas into the brine (at the brine-gas interface), according to the pressure/temperature conditions. $CH_{4(aq)}$ diffuses through the brine and the sump, where $SO_4^{2-}{}_{(aq)}$-ions are available for BSR. The $SO_4^{2-}{}_{(aq)}$-ions result from anhydrite dissolution and diffuse from the sump to the brine-gas interface, where $CH_{4(aq)}$ is available. The diffusive mass transport is induced by concentration gradients and causes a complex web of hydrogeochemical reactions and processes, including BSR. Modeling results indicate that $H_2S_{(g)}$ generation in salt caverns by bacterial sulfate reduction mainly occurs on the diffusive path where methane and sulfate meet and react with each other. The highest total H_2S concentrations are at this meeting point. Therefore, how much $H_2S_{(g)}$ is generated over time depends on diffusion as well as on the reaction kinetic of BSR, both depending on temperature and/or pressure. Figure 3.2 shows the results of the 3D model and indicates the location of $H_2S_{(g)}$ generation, as well as increasing $H_2S_{(g)}$ concentration with ongoing time and BSR. The maximum amount of generated $H_2S_{(g)}$ is 0.0515 mol kgw^{-1} (= 6.50 mg m^{-3} $H_2S_{(g)}$) after 30 years, in total.

Comparing the results of the reference scenario modeled in 3D in PHAST to the results of the reference scenario modeled in 1D in PHREEQC, slight differences are identifiable. After 30 years, 7.19 mg m^{-3} $H_2S_{(g)}$ are generated in PHREEQC and 6.50 mg m^{-3} $H_2S_{(g)}$ are generated in PHAST. Additionally, the results of the 1D model show that $H_2S_{(g)}$ is released into the stored gas and how much is released after 30 years and the results of the 3D model show the location where $H_2S_{(g)}$ is generated. Furthermore, PHAST includes flow and transport calculations (including parameters like tortuosity and dispersivity). Nevertheless, the differences are small and the chemical processes are the same because the geochemical reactions in PHAST are simulated with PHREEQC. The following results refer to the 1D model to make them comparable with the results of the following scenarios (Section 3.3.2). Another reason to use PHREEQC is the higher interest for industry in $H_2S_{(g)}$ concentration in the stored gas than the point where it is generated.

H_2S is formed as a gas bubble in the brine and released into the stored gas above if the sum of the partial pressure of all dissolved $gases_{(aq)}$ is greater or equal to the total gas pressure in the stored gas. At 50 °C and 180 atm, a total of 7.19 mg m^{-3} $H_2S_{(g)}$ is released into the stored gas after 30 years. The value lies above the allowed limit of 5 mg m^{-3} (defined by DVGW (2013)).

Aqueous sulfate is available in the brine from anhydrite dissolution (during leaching and operation) and is additionally delivered by diffusion from the sump. Furthermore, the dissolution of anhydrite contributes $Ca^{2+}_{(aq)}$ into the brine and, in consequence, calcite precipitates. In 30 years, 0.035 mol kgw^{-1} calcite precipitate at the brine-gas interface and buffers the effects of BSR on the pH of the brine. Therefore, the increase in the pH of the brine over 30 years is small (from 5.7 to 6.1). S(-II), a product of BSR, reacts with the available aqueous Fe(+II) and mackinawite precipitates (0.004 mol kgw^{-1} in 30 years), inhibiting H_2S generation. Another possible reaction is S(-II) with Fe(+II) to form pyrite. Using pyrite instead of mackinawite as a potential secondary phase, the amount of generated $H_2S_{(g)}$ is smaller (5.96 mg m^{-3}). However, the stabilities of pyrite and/or mackinawite at this pressure and temperature conditions are not identified. Furthermore, a small amount of pure water (H_2O) forms as a product of BSR with a maximum of 0.0004 kg kgw^{-1}. Elemental sulfur is included in the model as a potential secondary phase but does not precipitate, even if pyrite and mackinawite are not included as potential secondary phases.

The reference scenario considers the inner part of the cavern and neglects the cavern wall with its equilibrium phases of the rock salt formation which are in contact with the brine (Figure 3.1, orange box). To cover this part of the salt cavern, an alternative scenario is modeled. Modeling results show that $H_2S_{(g)}$ generation at the cavern wall is less intensive (5.15 mg m^{-3}) than in the part of the cavern that is not in contact with the cavern wall (the reference scenario, where no equilibrium phases are available in the brine). This is tested by adding the same equilibrium phases used in the sump to the brine. Conceptually, a water-to-rock ratio equivalent to a theoretical porosity of 80% is assumed. The decrease in $H_2S_{(g)}$ generation can be explained with the occurrence of siderite, which is part of the initial rock salt formation. As long as siderite is available, S(-II) is bound to newly formed mackinawite and inhibits $H_2S_{(g)}$ generation stronger than in the reference scenario. The initial amount of 0.001 mol kgw^{-1} siderite is completely dissolved in less than 3 years. Furthermore, more calcite precipitates (0.06 mol kgw^{-1}), which more strongly buffers the effect of BSR on the pH, so that the pH increase is smaller compared to the $H_2S_{(g)}$ generation in the center of the cavern (from 5.7 to 5.8). After less than 12 years, the available anhydrite at the brine-gas interface (cell 2) is completely dissolved. Furthermore, irreducible water is available in the surrounding rock salt formation so that diffusional transport of $CH_{4(aq)}$ and available $SO_4^{2-}{}_{(aq)}$-ions is possible even at the cavern wall in the part of the cavern where the gas is stored. Consequently, $H_2S_{(g)}$ could be generated even there.

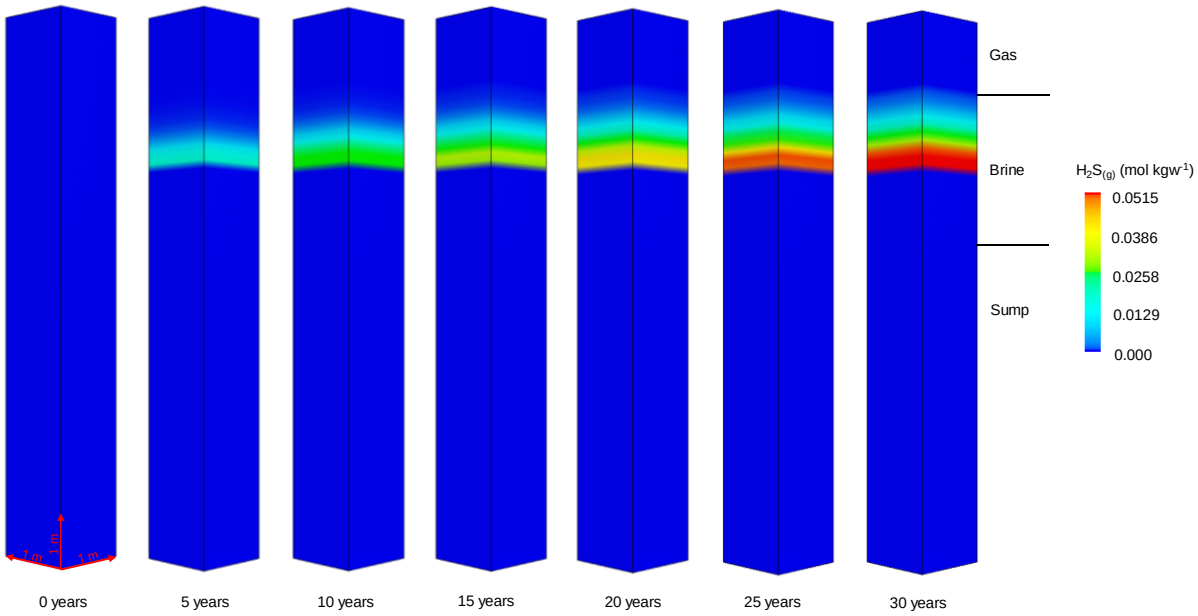

Figure 3.2 $H_2S_{(g)}$ generation and increasing $H_2S_{(g)}$ amount with ongoing time and bacterial sulfate reduction.

3.3.2 Factors Influencing $H_2S_{(g)}$ Generation and Release

Generic model scenarios show the consequences of varying conditions in salt caverns on the H_2S generation and release. In the following Sections, 3.3.2.1–3.3.2.4, the impacts of different factors are analyzed.

3.3.2.1 Gas Pressure Changes in Salt Cavern Gas Storages

Special consideration is given to the effect of pressure changes in the cavern as a consequence of gas injection, storage, and production phases. This scenario is based on Wang et al. (2015) where a 1-year cycle is assumed, divided into 3 months of storage at minimum pressure (60 atm), 3 months of injection (120 atm, as a “mean” between 60 atm and 180 atm), 3 months of storage at maximum pressure (180 atm), and 3 months of production (120 atm). The modeling tool for this scenario is PHREEQC, with the database phreeqc.dat where the pressure-dependent mass-action law constants for the equilibrium reactions of the involved gaseous, aqueous, and solid species are included. Figure 3.3a shows $H_2S_{(g)}$ generation and release versus pressure.

After the first 3 months of storage at maximum pressure, a total of 0.59 mg m^{-3} $H_2S_{(g)}$ is generated and released. During each of the subsequent phases (3 months of production, 3

months of storage at low pressure, and 3 months of injection), 0.3 mg m^{-3} $H_2S_{(g)}$ is generated and released. The cycle starts again with a high-pressure storage phase where only 0.3 mg m^{-3} $H_2S_{(g)}$ is generated and released (Figure 3.3a). The high amount of $H_2S_{(g)}$ (0.59 mg m^{-3}) generated and released in the first maximum pressure phase can be explained with the higher amount of aqueous sulfate in the brine at the beginning of storage, which results from anhydrite dissolution during leaching. The amount of aqueous sulfate available from leaching in the brine decreases with ongoing BSR, but additional aqueous sulfate is delivered by diffusion from the sump, where anhydrite is still available. When the amount of sulfate in the brine is consumed, the sulfate is delivered only by diffusion. Therefore, the change in pressure conditions has minor influence on $H_2S_{(g)}$ generation and release, but diffusion of dissolved sulfate and dissolved methane through the brine is the limiting factor. To confirm these results, additional modeling scenarios were performed with an extended range of pressure conditions. Modeling results show that even under very low-pressure (25 atm) and high-pressure conditions (300 atm) the amount of generated and released $H_2S_{(g)}$ is nearly constant at 0.3 mg m^{-3} (0.2999 mg m^{-3} at 25 atm and 0.30002 mg m^{-3} at 300 atm).

3.3.2.2 Natural Gas Composition

The chemical composition of the stored natural gas can differ. An alternative gas composition, based on data from the DVGW (2013), with 175.032 atm ρCH_4, 1.476 atm ρN_2, 3.492 atm ρCO_2, and 0.000288 atm ρH_2S is used to show the influence of the initial gas composition on $H_2S_{(g)}$ generation and release. The results of the 1D model (in PHREEQC) show a slight increase in $H_2S_{(g)}$ generation and release from 7.19 mg m^{-3} $H_2S_{(g)}$ (reference scenario) to 7.22 mg m^{-3} $H_2S_{(g)}$ using this alternative gas composition (Figure 3.3b). The pH decreases to 5.9 from 6.1 in the reference scenario. The amount of precipitated calcite increases slightly (from 0.035 mol kgw^{-1} in the reference scenario to 0.037 mol kgw^{-1}) but the amount of precipitated mackinawite is nearly constant (0.004 mol kgw^{-1} in 30 years). Generally, the initial gas composition can influence the final $H_2S_{(g)}$ generation and release, but in this case, the effect is minor.

3.3.2.3 Kinetic Rate Constants

The kinetic rate constant of BSR is an important factor controlling $H_2S_{(g)}$ generation and release. The rate constant is varied from an initial 6.46×10^{-10} mol kgw^{-1} s^{-1} (based on Adams et al. (2013)) to 1.04×10^{-09} mol kgw^{-1} s^{-1} (based on Kallmeyer and Boetius (2004)) and

5.95×10^{-08} mol kgw^{-1} s^{-1} (based on Timmers et al. (2016)). All rate constants used apply to temperature and pressure conditions comparable to salt cavern conditions. The presented results are based on the 1D model in PHREEQC. As shown by Figure 3.3c, with increasing rate constant the $H_2S_{(g)}$ generation and release increases. The elevated rate constant of 1.04×10^{-09} mol kgw^{-1} s^{-1} causes an increase from 7.19 to 7.59 mg m^{-3} $H_2S_{(g)}$ and the rate constant of 5.95×10^{-08} mol kgw^{-1} s^{-1} an increase to 8.88 mg m^{-3} $H_2S_{(g)}$ after 30 years. The results show that by varying the rate constant, other interconnected reactions are affected as well. Comparing the results of the reference scenario to the results of the scenario with the rate constant of 5.95×10^{-08} mol kgw^{-1} s^{-1}, the following changes are observable at the brine-gas interface: the amount of the secondary phase calcite decreases slightly from 0.035 mol kgw^{-1} to 0.032 mol kgw^{-1} and mackinawite formation increases from 0.0038 mol kgw^{-1} to 0.0047 mol kgw^{-1} (whereas the pH is constant at 6.1). In consequence, the variations in the amount of generated and released $H_2S_{(g)}$ indicate that it is important to determine the kinetic rate constants at elevated levels of temperature of 50 °C and other relevant site-specific cavern conditions as accurately as possible. However, doubling the rate constant does not double the amount of generated and released $H_2S_{(g)}$ because diffusion is the main limiting factor.

3.3.2.4 Tortuosity

Another influencing factor is the tortuosity, included in the 3D PHAST model. With increasing tortuosity in brine and sump (from 0.001 to 0.01, 0.1 and 1.0), bacterial sulfate reduction increases due to more effective diffusive transport of $CH_{4(aq)}$ and $SO_4^{2-}{}_{(aq)}$. Therefore, the maximum value of generated $H_2S_{(g)}$ increases from 2.17 mg m^{-3} (tortuosity of 0.001) to 7.98 mg m^{-3} (tortuosity of 1.0; Figure 3.3d) after 30 years. The higher the tortuosity, the lower the pH (from pH 9.5 with a tortuosity of 0.001 to pH 8.2 with a tortuosity of 1.0). Furthermore, the amount of precipitated calcite increases with increasing tortuosity (from 0.02 mol kgw^{-1} to 0.05 mol kgw^{-1}) and at higher tortuosity, intensified anhydrite dissolution is identified in the sump. The lower BSR rate at low tortuosity influences the amount of precipitated mackinawite, which is smaller at a tortuosity of 0.001 (0.002 mol kgw^{-1}) than at tortuosity of 1.0 (0.003 mol kgw^{-1}). The most significant difference in the amount of generated $H_2S_{(g)}$ is identifiable from a tortuosity of 0.001 to 0.01 (Figure 3.3d). The differences in $H_2S_{(g)}$ generation from the tortuosity of 0.01 to 0.1 and to 1.0 are minor. These results also indicate that diffusion of dissolved methane and dissolved sulfate through the brine is the major limiting factor.

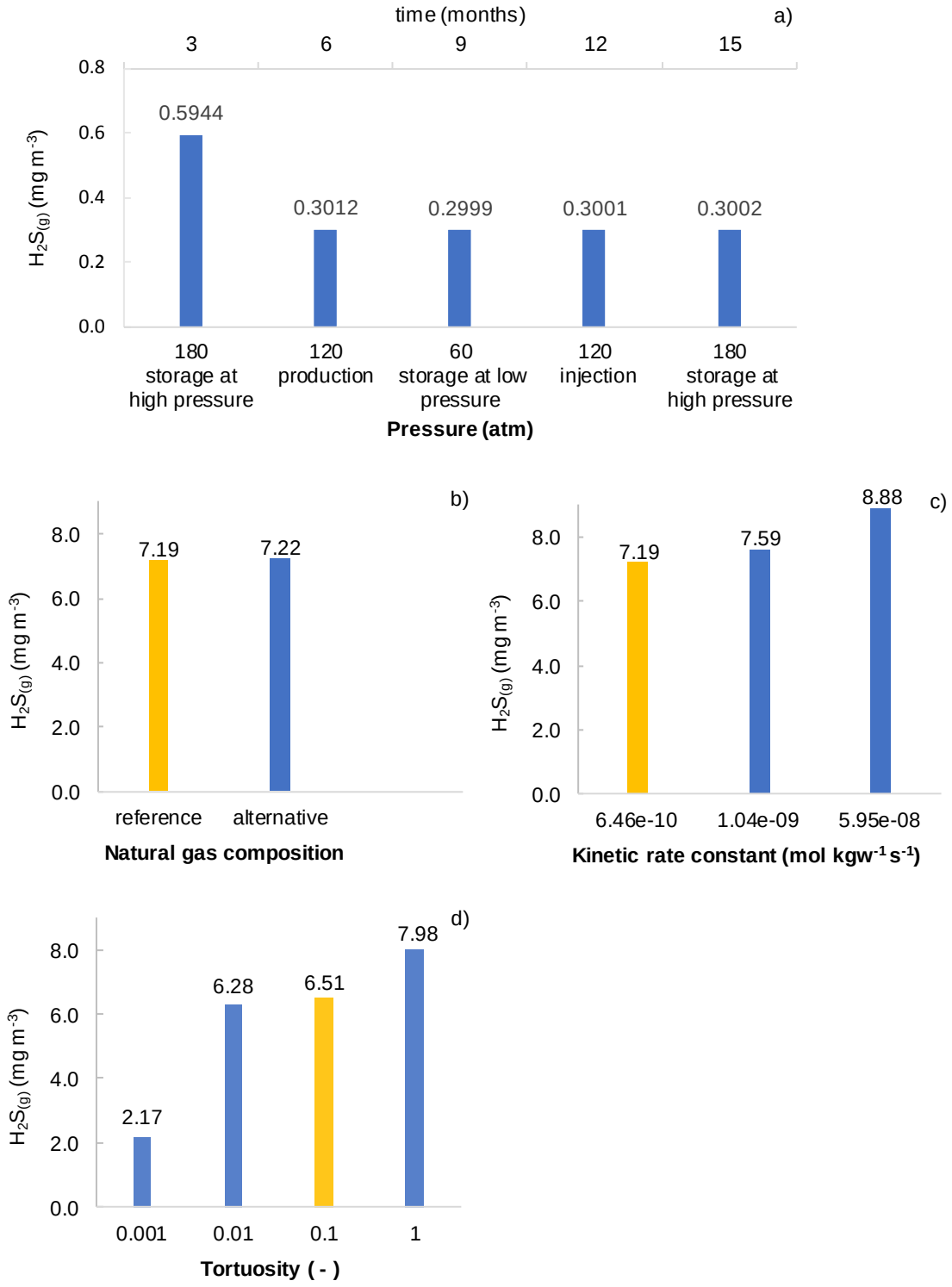

Figure 3.3 $H_2S_{(g)}$ generation influenced by a) pressure changes (after 3 months) b) stored gas composition (reference = typical composition of natural gas from Russia, alternative = typical composition of natural gas from the North Sea (after 30 years) c) kinetic rate constant (after 30 years) d) tortuosity (after 30 years). $H_2S_{(g)}$ in mg m^{-3} in the stored gas. Yellow = reference scenario, blue = modified parameters. a), b), and c) are modeled 1D in PHREEQC, and d) is modeled 3D in PHAST.

3.3.3 Inhibition of $H_2S_{(g)}$ Generation and Release in Salt Caverns

If the $H_2S_{(g)}$ concentration in the stored gas exceeds the limit of 5 mg m^{-3} (DVGW, 2013), the stored gas is polluted and cannot be used anymore. Therefore, additional modeling scenarios show three possible methods to inhibit $H_2S_{(g)}$ generation and release. Generally, salt caverns should be constructed in rock salt formations with low amounts of anhydrite and other sulfate sources (e.g., gypsum). However, with increasing demand for storage capacity in salt structures, this is not always possible. In case the geogenic conditions favor $H_2S_{(g)}$ generation, as a first method a preventative measure should be applied. In this measure, $Fe(+II)_{(aq)}$ (dissolved $FeCl_2$) is added to the brine directly after leaching, before the first gas injection, and inhibits the $H_2S_{(g)}$ generation. The modeling results show a decrease in $H_2S_{(g)}$ generation from 7.19 mg m^{-3} in the reference scenario to 1.52 mg m^{-3}. This can be explained by the higher amount of available Fe(+II), which reacts with aqueous sulfide to form mackinawite so that aqueous sulfide is no longer available for $H_2S_{(g)}$ generation (Figure 3.4a). The amount of precipitated mackinawite increases from 0.004 mol kgw^{-1} (in the reference scenario) to 0.09 mol kgw^{-1} in the operating time of 30 years. The minimum concentration of $FeCl_2$ that must be added before the first gas injection to decrease the amount of generated $H_2S_{(g)}$ below the allowed limit of 5 mg m^{-3} is 0.025 mol kgw^{-1} (assuming a homogeneous distribution of the injected $FeCl_2$).

Two inhibition methods could be used when an increase in $H_2S_{(g)}$ is detected in the stored gas. One method is to add $Fe(+II)_{(aq)}$ (dissolved $FeCl_2$) to the brine after first gas injection. The modeling results show that the available aqueous sulfide reacts with aqueous ferrous iron, and mackinawite precipitates. When adding 0.1 mol kgw^{-1} $FeCl_2$ after 5 years of storage, a total of only 3.47 mg m^{-3} $H_2S_{(g)}$ is released after 30 years (Figure 3.4b). The pH decreases from 6.1 to 5.8, less calcite precipitates (from 0.035 to 0.008 mol kgw^{-1}), and mackinawite precipitation increases strongly from 0.004 to 0.05 mol kgw^{-1}. The addition of 0.05 mol kgw^{-1} $FeCl_2$ after first gas injection is sufficient enough to reduce the $H_2S_{(g)}$ concentration just below the allowed limit of 5 mg m^{-3} (assuming a homogeneous distribution of the added $FeCl_2$).

Another inhibition method is the addition of NaOH to the brine. Modeling results show that this method increases the pH and inhibits $H_2S_{(g)}$ generation. The pH influences the speciation type of the generated sulfide according to the mass action laws (included in the database phreeqc.dat). At neutral pH, most of the sulfide is available as H_2S and HS^-. In higher pH environments, HS^- and S^{2-} predominate, and at low pH, hydrogen sulfide occurs as H_2S. Therefore, when increasing the pH by addition of NaOH, more S^{2-} is generated (at constant S^{2-} in total), and gas pollution by $H_2S_{(g)}$ is inhibited. When 1.0 mol kgw^{-1} NaOH is added after 5 years of storage, the total amount of generated $H_2S_{(g)}$ after 30 years decreases to

0.74 mg m^{-3} (Figure 3.4c). The pH increases from 6.1 (in the reference scenario) to 11.5, calcite precipitation increases from 0.035 to 0.09 mol kgw^{-1}, and less mackinawite precipitates (from 0.004 to 0.002 mol kgw^{-1}). Another possibility is the addition of 0.1 mol kgw^{-1} NaOH after 5 years of storage and repetition of the same input after 10 years of storage. With these conditions, the total amount of generated $H_2S_{(g)}$ decreases to 3.86 mg m^{-3} after 30 years (Figure 3.4c). By addition of only 0.13 mol kgw^{-1} NaOH after 5 years of storage the $H_2S_{(g)}$ concentration is reduced to 4.99 mg m^{-3}. This amount is the minimum amount of NaOH that is needed to reduce the $H_2S_{(g)}$ concentration below the allowed concentration of 5 mg m^{-3} under assumed storage conditions and homogeneous distribution of added NaOH.

To ensure constant gas quality over time, the gas and brine must be analyzed continuously and the inhibition methods must be applied when the $H_2S_{(g)}$ concentration increases. Therefore, $H_2S_{(g)}$ measurements and monitoring in the gas as well as in the brine could be used as an early warning system. The application of sulfide scavengers is widely adopted in the oil and gas industry. Amosa et al. (2010) summarized the different scavenger technologies from copper-base scavengers to zinc-base scavengers and up to iron-base scavengers (among others). Less attention has been paid on the application of scavengers in underground gas storage systems especially in salt cavern gas storages. Some authors suggest to decrease the bacterial activity in the underground gas storage in porous media by “simple substitution” of products like heptamethyl nonane, dioxin, furan (Kleinitz and Böhling, 2005). They focus on procedures which prevent bacterial growth. However, the here presented study focuses on hydrogeochemical methods to decrease the generation and release of $H_2S_{(g)}$ in salt cavern gas storage systems and on the quantitative description of the amount of $FeCl_2$ or NaOH that must be added to decrease the $H_2S_{(g)}$ concentration in the stored gas below the allowed limit of 5 mg m^{-3}.

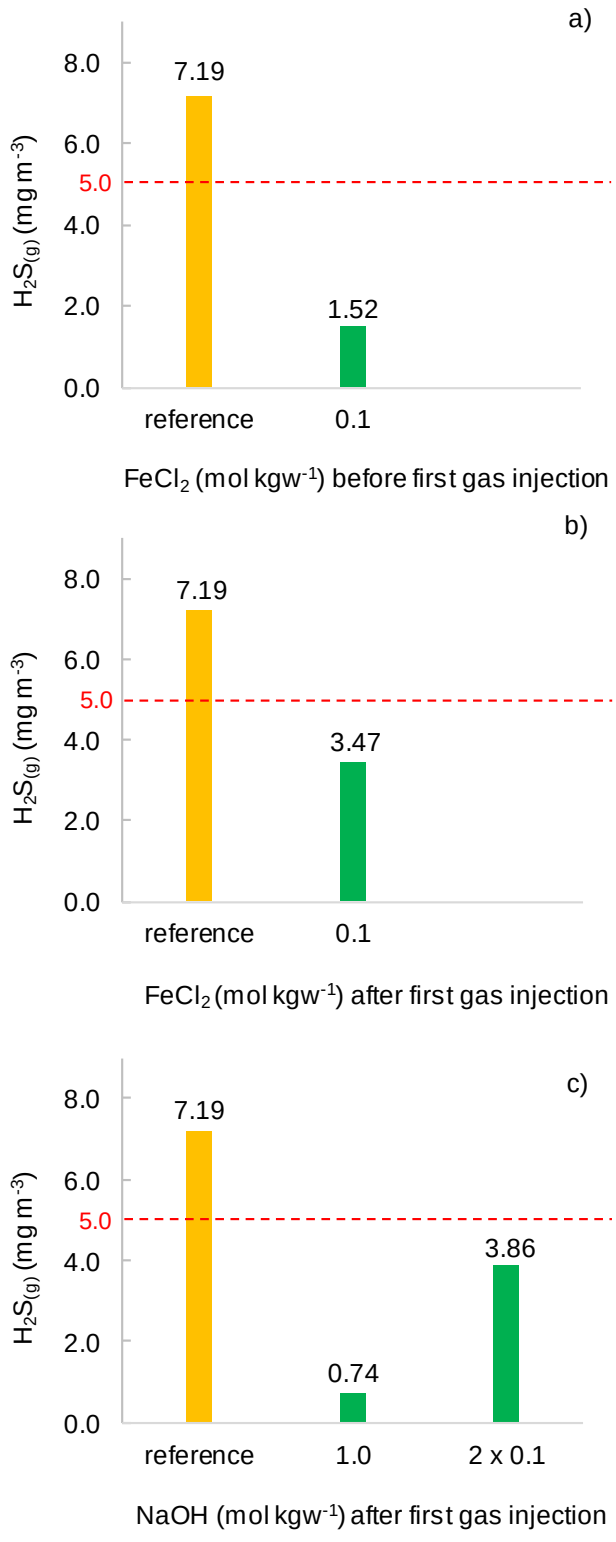

Figure 3.4 $H_2S_{(g)}$, in mg m^{-3}, in the stored gas after 30 years. Inhibition of $H_2S_{(g)}$ generation and release by addition of a) $FeCl_2$ before first gas injection, b) $FeCl_2$ after gas injection c) 1.0 mol kgw^{-1} NaOH after 5 years of storage, and 0.1 mol kgw^{-1} NaOH after 5 years and after 10 years of storage to the brine. Reference is without any inhibition methods. Yellow = reference scenario, green = inhibition factors. Red line = maximum allowed $H_2S_{(g)}$ concentration in stored gas.

3.4 Conclusion

This study indicates that $H_2S_{(g)}$ generation and related pollution of the stored gas are risks in salt caverns. With increasing demand for storage capacity in salt caverns, the use of less favorable salt formations will increase, and the potential risk of $H_2S_{(g)}$ generation and release will rise. $H_2S_{(g)}$ in salt caverns is generated by bacterial sulfate reduction. The amount of available sulfate in the rock salt formation and diffusional transport are the main limiting factors of this process. The kinetic rate constant for bacterial sulfate reduction influences the amount of generated and released $H_2S_{(g)}$. Therefore, determining the kinetic rate constants at elevated levels of temperature and other relevant cavern conditions as accurately as possible is required. Experimental procedures to determine kinetic rate constants under consideration of site-specific conditions are presented e.g. by Adams et al. (2013), Jakobsen and Postma (1994), Timmers et al. (2016), Kallmeyer and Boetius (2004). Changing pressure conditions during injection, storage, and production phases has a minor influence on generated $H_2S_{(g)}$. Furthermore, the composition of the stored natural gas can influence $H_2S_{(g)}$ generation and release. The tortuosity effects the amount of generated $H_2S_{(g)}$, but the diffusion of dissolved methane and dissolved sulfate through the brine dominates this factor. In case of a site-specific model, the tortuosity can be roughly estimated by empirical equations based on petrophysical rock properties. Examples are given by Attia (2005), Shen and Chen (2007), Ewing et al. (2010), Ghassemi and Pak (2011).

Different hydrogeochemical methods inhibit $H_2S_{(g)}$ generation and release in salt caverns. One method is a prevention measure that could be applied before first gas injection if geogenic conditions favor $H_2S_{(g)}$ generation. In that method, $FeCl_2$ is added to the brine directly after leaching. Two further technical methods should be used for the inhibition of $H_2S_{(g)}$ generation, if during the time of storage an increase of $H_2S_{(g)}$ is observed in the gas or brine. The addition of aqueous $FeCl_2$ to the brine after gas injection leads to a reduction of $H_2S_{(g)}$ generation because the available aqueous sulfide reacts with the aqueous ferrous iron and mackinawite precipitates. Alternatively, NaOH could be added to the brine. This method increases the pH and inhibits $H_2S_{(g)}$ generation because the pH influences the speciation type of generated sulfide.

3.5 Acknowledgements

This research did not receive any specific grant from funding agencies in the public, commercial, or not-for-profit sectors.

3.6 Supplementary Data (on CD)

Input file S3 for the transport model to calculate the reference scenario SCGS is available (for PHREEQC Version 3).

4 Underground Hydrogen Storage (UHS)

Hydrogeochemical Modeling to Identify Potential Risks of Underground Hydrogen Storage in Depleted Gas Fields

Publication III

Authors of the original paper: Christina Hemme, Wolfgang van Berk

Originally published in: Applied Sciences 8(11) (2018), 2282

Summary added for the purpose of this thesis.

Author Contributions:

Conceptual model:	Christina Hemme[1]
Modeling:	Christina Hemme[1] and Wolfgang van Berk[3]
Result evaluation:	Christina Hemme[1] and Wolfgang van Berk[2]
Analysis of results:	Christina Hemme[1] and Wolfgang van Berk[3]
Visualization of results:	Christina Hemme[1]
Writing—original draft preparation:	Christina Hemme[1]
Writing—review and editing:	Christina Hemme[1] and Wolfgang van Berk[3]
Supervision:	Wolfgang van Berk[1]

[1] substantial; [2] medium; [3] minor

Summary

In this part of the study, the gas–water–rock interactions triggered by hydrogen storage in depleted hydrocarbon reservoirs are considered. The focus is on the loss of hydrogen by bacterial conversion over storage times at reservoir scale. Furthermore, mineral dissolution and precipitation due to hydrogen storage are qualitatively and quantitatively described and the loss of hydrogen by diffusion along a gradient of decreasing pressure and temperature conditions is analyzed.

The storage of hydrogen in the underground causes hydrogeochemical gas–water–rock interactions. In view of these processes, this study is performed based on the principal laws of chemical-mass conversion and diffusive mass transport through the cap rock. The aim is to obtain an understanding of the spatial- and temporal-dependent hydrogeochemical processes induced by hydrogen storage and to analyze related risks.
Hydrogen is injected into a depleted gas reservoir and dissolves in the brine until saturation is established and continuously serves as a reductant for BSR and methanogenesis. At the interface with the cap rock, the aqueous hydrogen diffuses through the cap rock brine and triggers H_2–water–rock interactions. These processes are retraced using one-dimensional (1D) reactive mass transport models and the modeling tool PHREEQC (phreeqc.dat database). Up to 12 aqueous species and 22 different mineral and gas phases are used to form a semi-generic but well-defined hydrogeochemical modeling approach.
Modeling results show that the total loss of hydrogen gas by aqueous diffusion, gas–water–rock interactions, and bacterial conversion is 76% over 30 years under modeling conditions. Therefore, the loss by aqueous diffusion is minor. Underground hydrogen storage induces a slight decrease of the reservoir rock porosity. A large part of the stored gas is converted by bacterial activity (bacterial sulfate reduction and methanogenesis), limited by the amount of available electron acceptors (sulfate and carbon dioxide), the kinetic rate constants, and maximum storage time.
1D mass transport modeling scenarios help to identify the factors dominating the loss of hydrogen by varying single parameters of the reference model. The modeling approach considers storage times of 30–300 years. Gas–water–rock interactions that may be triggered by the withdrawal or production of hydrogen are considered, as well as different gas compositions and kinetic rate constants. From the modeling results, it seems reasonable to choose depleted gas fields with low temperature and pressure conditions as well as low amounts of carbonate- and sulfate-bearing minerals for hydrogen storage. The hydrogeochemical model approach can be used and adapted to various underground hydrogen storage conditions to answer and solve practically oriented questions and problems.

Abstract

Underground hydrogen storage is a potential way to balance seasonal fluctuations in energy production from renewable energies. The risks of hydrogen storage in depleted gas fields include the conversion of hydrogen to $CH_{4(g)}$ and $H_2S_{(g)}$ due to microbial activity, gas–water–rock interactions in the reservoir and cap rock, which are connected with porosity changes, and the loss of aqueous hydrogen by diffusion through the cap rock brine. These risks lead to loss of hydrogen and thus to a loss of energy. A hydrogeochemical modeling approach is developed to analyze these risks and to understand the basic hydrogeochemical mechanisms of hydrogen storage over storage times at the reservoir scale. The one-dimensional diffusive mass transport model is based on equilibrium reactions for gas–water–rock interactions and kinetic reactions for sulfate reduction and methanogenesis. The modeling code is PHREEQC (**pH**-**RE**dox-**EQ**uilibrium written in the **C** programming language). The parameters that influence the hydrogen loss are identified. Crucial parameters are the amount of available electron acceptors, the storage time, and the kinetic rate constants. Hydrogen storage causes a slight decrease in porosity of the reservoir rock. Loss of aqueous hydrogen by diffusion is minimal. A wide range of conditions for optimized hydrogen storage in depleted gas fields is identified.

4.1 Introduction and Aims

Underground hydrogen storage (UHS) is used to store large amounts of hydrogen generated from renewable energy sources (such as wind and solar) to compensate for seasonal fluctuations in the supply and demand of energy (Ebigbo et al., 2013; Reitenbach et al., 2015). Large amounts of hydrogen can be stored in depleted oil and gas fields, in salt caverns, and in aquifers (Ebigbo et al., 2013; Stone et al., 2009). Nevertheless, practical experience of underground hydrogen storage is still rare. In the US and UK, hydrogen is currently stored in salt caverns (Crotogino et al., 2010; Henkel et al., 2013; Panfilov, 2010; Stone et al., 2009), but hydrogen storage in depleted oil and gas fields is still under research and discussion. Depleted oil and gas fields have a huge storage capacity, are well known from former exploration and production, and qualify therefore for hydrogen storage. However, the existing underground gas storages (UGS) are designed for the storage of natural gas, which does not contain hydrogen (or only very low amounts). Because the chemical and physical properties of hydrogen are different to those of methane (CH_4)—the main component of natural gas—the effects of hydrogen on the reservoir rock, cap rock, and storage facilities must be analyzed before injecting hydrogen into these storages (Reitenbach et al., 2015).

Compared to methane, hydrogen has a higher diffusivity in pure water. The diffusion coefficient for hydrogen is 5.13×10^{-9} m^2 s^{-1} and for CH_4 it is 1.85×10^{-9} m^2 s^{-1}, both in pure water at 25 °C. The data are given in the database phreeqc.dat, that is provided by the US Geological Survey. Generally, the diffusion process of an aqueous species is described by its diffusion coefficient in pure water (m^2 s^{-1}). However, in any porous system, where solids are available, the influence of porosity on the diffusion must be considered by scaling the diffusion coefficient with tortuosity (Shen and Chen, 2007), resulting in an effective diffusion coefficient (Equation (4.1)), where d'_m is the effective diffusion coefficient, d_m is the diffusion coefficient in pure water, and τ is the tortuosity. The tortuosity is the ratio of the effective diffusion mass fluxes in a porous medium to ideal diffusion mass fluxes in solutions without a rock matrix.

$$d'_m = \frac{d_m}{\tau^2} \tag{4.1}$$

Therefore, the effective diffusion coefficient for methane is $2.35{-}2.49 \times 10^{-10}$ m^2 s^{-1} in clayey host rocks at 21 °C (Jacops et al., 2013). The effective diffusion coefficient for hydrogen is 3.0×10^{-11} m^2 s^{-1} in clayey host rocks saturated with water at 25 °C (Krooss, 2008). However, there is a lack of data regarding effective diffusion coefficients of hydrogen at underground storage conditions with higher temperatures and pressures (Panfilov, 2016).

Compared to methane, hydrogen has a lower viscosity. The viscosity of hydrogen at the two-phase boundary at 17 MPa and 350 K is 1.01×10^{-5} kg m^{-1} s^{-1} (McCarty et al., 1981) and methane fluid at 20 MPa and 350 K is 1.81×10^{-5} kg m^{-1} s^{-1} (Friend et al., 1989). Furthermore, hydrogen has a lower density than methane. At normal conditions, the density of hydrogen is eight times smaller than that of methane and the difference increases by 20–30% under storage conditions (Reitenbach et al., 2015). The solubility of $H_{2(g)}$ in pure water is smaller than the solubility of $CH_{4(g)}$. At 25 °C and 1.0 atm, 7.9×10^{-4} mol kgw^{-1} $H_{2(g)}$ and 1.4×10^{-3} mol kgw^{-1} $CH_{4(g)}$ dissolve in pure water (data based on phreeqc.dat).

The properties of hydrogen—being different from those of methane—could lead to risks when storing hydrogen in depleted gas fields, which were constructed for storing methane (underground gas storage). Potential risks include (i) the conversion of hydrogen to CH_4 and H_2S due to microbial activity, (ii) chemical reaction of hydrogen with the minerals of the reservoir rock/cap rock and thus potential resulting porosity changes, and (iii) the loss of aqueous $H_{2(aq)}$ by diffusion through the cap rock.

The first risk (i) arises from microbial activities in the underground. The two processes relevant here are bacterial sulfate reduction (Equation (4.2)) and methanogenesis (Equation (4.3)), where hydrogen is microbially catalyzed by bacteria and is converted to $H_2S_{(aq)}$ or $CH_{4(aq)}$. The activity of the different bacteria depends on the availability of the different electron acceptors such as sulfate or carbon dioxide (Ebigbo et al., 2013). Other possible microbial processes are acetogenesis and iron(III)-reduction, summarized by Hagemann et al. (2016).

Bacterial sulfate reduction (BSR): $SO_4^{2-}{}_{(aq)} + 5H_{2(aq)} \rightarrow H_2S_{(aq)} + 4H_2O$ (4.2)

Methanogenesis: $CO_{2(aq)} + 4H_{2(aq)} \rightarrow CH_{4(aq)} + 2H_2O$ (4.3)

In aqueous anoxic environments, the sulfate-reducing bacteria (SRB) use sulfate as an electron acceptor to oxidize hydrogen and generate sulfide-S which could be available as aqueous $S^{2-}{}_{(aq)}$, $HS^{-}{}_{(aq)}$, and $H_2S_{(aq)}$ and as gaseous $H_2S_{(g)}$ as well. The sulfate is derived from the aqueous dissolution of mineral phases like anhydrite ($CaSO_{4(s)}$). The energy gained from sulfate reduction is used by the SRB for cell growth (Cord-Ruwisch et al., 1987). SRB prefer temperatures around 38 °C (Bernardez et al., 2013) and near-neutral pH conditions (Cord-Ruwisch et al., 1987), but are active even at extreme habitat conditions such as at great depths and temperatures, ranging from 0 °C to 60–80 °C (Ehrlich, 1990; Machel, 2001; Postgate, 1984) and in some cases up to 110 °C (Jorgensen et al., 1992). SRB activity was observed, for example, in hydrocarbon reservoirs (Machel, 2001) and in the underground storage of town gas (Postgate, 1979). The risk arising from bacterial sulfate reduction lies in the produced H_2S, which is corrosive towards the storage facilities, toxic if inhaled, and can pose a risk to the environment.

Typical environments for methanogenic bacteria are, for example, anoxic sediments and flooded soils (Whitman et al., 2006). However, the existence of methanogenic bacteria was also observed in town gas storages (Šmigáň et al., 1990). Methanogenic bacteria prefer temperatures of 30–40 °C for growth (Panfilov, 2016), but they also have been found at higher temperatures of 80 °C (Davydova-Charakhch`yan et al., 1992; Magot et al., 2000) and up to 97 °C (Gusev and Mineeva, 1992; Panfilov, 2016). With these bacteria, $H_{2(aq)}$ is the electron donor and $CO_{2(aq)}$ is the electron acceptor, which is reduced to form $CH_{4(aq)}$. The methanogenic bacteria obtain their energy for cell growth from this conversion (Šmigáň et al., 1990; Whitman et al., 2006). The problem associated with methanogenesis lies in the loss of hydrogen and the related energy loss (Reitenbach et al., 2015). This phenomenon has already been observed in the underground storage of town gas. A well-known example is the Czech town gas storage at Lobodice, where the 54 vol. % injected $H_{2(g)}$ diminished to 37 vol. % $H_{2(g)}$.

Concurrently, $CH_{4(g)}$ increased from 21.9 vol. % to 40.0 vol. % within a time span of 7 months (Šmigáň et al., 1990).

Another risk of underground hydrogen storage (ii) is the reaction of $H_{2(g/aq)}$ with the minerals of the reservoir rock and the cap rock, which can lead to mineral dissolution and precipitation and resulting porosity changes as known from carbon capture and storage (e.g. Bildstein et al., 2010; Gaus et al., 2005; Hemme and van Berk, 2017a; Mohd Amin et al., 2014). Changes in the porosity of the cap rock can either improve or deteriorate its sealing capacity. Furthermore, precipitation of minerals at the well equipment may cause scaling (Reitenbach et al., 2015).

In depleted gas fields, the high diffusivity of hydrogen could be the reason for hydrogen loss (iii). The hydrogen is dissolved in the formation water of the cap rock and diffuses through the cap rock (Reitenbach et al., 2015). Reitenbach et al. (2015) stated that a significant loss of hydrogen can be expected. The high diffusivity, low viscosity, and low density of hydrogen leads to a high mobility and therefore the potential loss due to leakage should be considered (Ebigbo et al., 2013).

A natural analog for an unintended and unpredictable leakage of hydrogen can be found in hydrogen anomalies associated with faults. These so called natural hydrogen seeps have been described by Larin et al. (2015), Sato et al. (1986), Wakita et al. (1980), Ware et al. (1985), and Zgonnik et al. (2015). In these cases, faults act as “fluid conduits” (Larin et al., 2015). An increased CH_4 concentration is also observed within these anomalies because of the increased microbial activity stimulated by the increased amount of hydrogen (Larin et al., 2015). If hydrogen reaches the surface, it could inhibit the growth of trees, underbrush, and grass (Larin et al., 2015).

There are experimental studies concerning kinetics of pyrite and pyrrhotite reduction by hydrogen at high temperatures (Truche et al., 2010), the reactivity of hydrogen in sandstones (Yekta et al., 2018), and the petrographic and petrophysical variation in reservoir sandstones due to hydrogen storage (Flesch et al., 2018). However, modeling studies of hydrogen storage to predict “long-term” behaviors are still rare. Therefore, this study is performed to model the loss of hydrogen (and related energy loss) as a combination of (i) the conversion by bacteria, (ii) gas–water–rock interactions in the reservoir and cap rock, which are connected with porosity changes, and (iii) loss by aqueous diffusion along a gradient of decreasing pressure and temperature conditions.

These processes are retraced by a one-dimensional reactive mass transport model to simulate gas–water–rock interactions resulting from hydrogen storage in depleted gas fields. The aim of this study is to investigate the basic mechanisms of BSR and methanogenesis in an

integrated way over storage times at the reservoir scale and to describe qualitatively and quantitatively which reservoir rock and cap rock minerals dissolve or precipitate because of hydrogen storage as well as the related porosity changes. Furthermore, the parameters that influence the loss of hydrogen are determined.

Therefore, a model is presented, in which the hydrogeochemical mechanisms of underground hydrogen storage are simulated in a reference scenario (Sections 4.3.1–4.3.3). In further scenarios, single parameters will be changed in the model to show their effects on the modeling results and to identify the parameters that are most sensitive for underground hydrogen storage (Section 4.3.4).

4.2 Methodology

4.2.1 Modeling Tools

The modeling program for the one-dimensional reactive mass transport (1DRMT) model is PHREEQC version 3 (PHREEQC = **pH**-**RE**dox-**EQ**uilibrium written in the **C** programming language), provided by the US Geological Survey (Parkhurst and Appelo, 2013). PHREEQC has capabilities to simulate (i) speciation and saturation-index calculations, (ii) batch-reaction and 1D transport calculations, and (iii) inverse modeling (Parkhurst and Appelo, 2013). The used database is phreeqc.dat extended by dawsonite, nahcolite, $CH_{4(g)}$, $H_2S_{(g)}$, $N_{2(g)}$, which are taken from llnl.dat. The 1DRMT model considers equilibrium reactions for gas–water–rock interactions, and kinetic reactions for sulfate reduction and methanogenesis. The equilibrium calculations are based on the mass action law including all species used in this study (Al, Ba, C, Ca, Cl, Fe, K, Mg, N, Na, S, Si) and their corresponding equilibrium constants. The equilibrium phases, mass action equations, and equilibrium constants used in the model are summarized in Table 4.1. For detailed information about PHREEQC, see Parkhurst and Appelo (2013).

Table 4.1 Equilibrium phases, mass action equations, and equilibrium constants used in the model. Data from phreeqc.dat, except for dawsonite, nahcolite, $CH_{4(g)}$, $H_2S_{(g)}$, $N_{2(g)}$, which are from llnl.dat (Parkhurst and Appelo, 2013).

Equilibrium Phase	Equilibrium Reaction	log *K* at 25 °C, 1 bar
K-feldspar	$KAlSi_3O_8 + 8H_2O = K^+ + Al(OH)_4^- + 3H_4SiO_4$	−20.573
Albite	$NaAlSi_3O_8 + 8H_2O = Na^+ + Al(OH)_4^- + 3H_4SiO_4$	−18.002
Kaolinite	$Al_2Si_2O_5(OH)_4 + 6H^+ = H_2O + 2H_4SiO_4 + 2Al^{3+}$	7.435
Quartz	$SiO_2 + 2H_2O = H_4SiO_4$	3.98
Calcite	$CaCO_3 = CO_3^{2-} + Ca^{2+}$	8.48
Pyrite	$FeS_2 + 2H^+ + 2e^- = Fe^{2+} + 2HS^-$	−18.479
Illite	$K_{0.6}Mg_{0.25}Al_{2.3}Si_{3.5}O_{10}(OH)_2 + 11.2H_2O = 0.6K^+ + 0.25Mg^{2+} + 2.3Al(OH)^{4-} + 3.5H_4SiO_4 + 1.2H^+$	−40.267
Dawsonite	$NaAlCO_3(OH)_2 + 3H^+ = Al^{3+} + HCO_3^- + Na^+ + 2H_2O$	4.35
Mackinawite	$FeS + H^+ = Fe^{2+} + HS^-$	−4.648
Dolomite	$CaMg(CO_3)_2 = Ca^{2+} + Mg^{2+} + 2CO_3^{2-}$	−17.09
Nahcolite	$NaHCO_3 = HCO_3^- + Na^+$	−0.11
Anhydrite	$CaSO_4 = Ca^{2+} + SO_4^{2-}$	−4.39
Halite	$NaCl = Cl^- + Na^+$	1.570
Gypsum	$CaSO_4{\cdot}2H_2O = Ca^{2+} + SO_4^{2-} + 2H_2O$	−4.58
Sulfur[a]	$S + 2H^+ + 2e^- = H_2S$	4.882
Barite	$BaSO_4 = Ba^{2+} + SO_4^{2-}$	−9.97
Goethite	$FeOOH + 3H^+ = Fe^{3+} + 2H_2O$	−1.0
$H_{2(g)}$	$H_2 = H_2$	−3.1050
$CO_{2(g)}$	$CO_2 = CO_2$	−1.468
$CH_{4(g)}$	$CH_4 = CH_4$	−2.8502
$H_2S_{(g)}$	$H_2S = H^+ + HS^-$	−7.9759
$N_{2(g)}$	$N_2 = N_2$	−3.1864

[a]: Sulfur = elemental sulfur

4.2.2 Model Setup

Gaseous hydrogen ($H_{2(g)}$) is injected into the reservoir rock where residual gas from the previous natural gas reservoir is still available and the reservoir brine is in equilibrium with these gases and the reservoir rock. When $H_{2(g)}$ is injected, the available brine is saturated with H_2. With ongoing injection of $H_{2(g)}$, the initial reservoir brine is displaced and $H_{2(g)}$ builds up a plume. The only available water in the reservoir rock is then the irreducible water. On contact with the cap rock, $H_{2(g)}$ dissolves into the cap rock brine and diffuses through the cap rock brine. These processes are retraced with a hydrogeochemical, 1D reactive mass transport modeling approach, which is of semi-generic nature. The conditions assumed in the model are based on conditions of a depleted gas field with a temperature of 40 °C and a reservoir pressure of 40 atm. The model is divided into a column of 1488 cells, with a cell height of 1.0 m each (in the *z*-direction). The cap rock is assumed to have a height of 182 m (cells 1–182), the reservoir rock consists of 667 m (cells 183–850), and the underlying rock of 637 m (cells 851–1488; Figure 4.1). For the sake of simplicity, a constant partial pressure in the $H_{2(g)}$ plume is

assumed and the partial pressure is set to be equal to the hydrostatic pressure. Even during production, an amount of hydrogen remains in the reservoir.

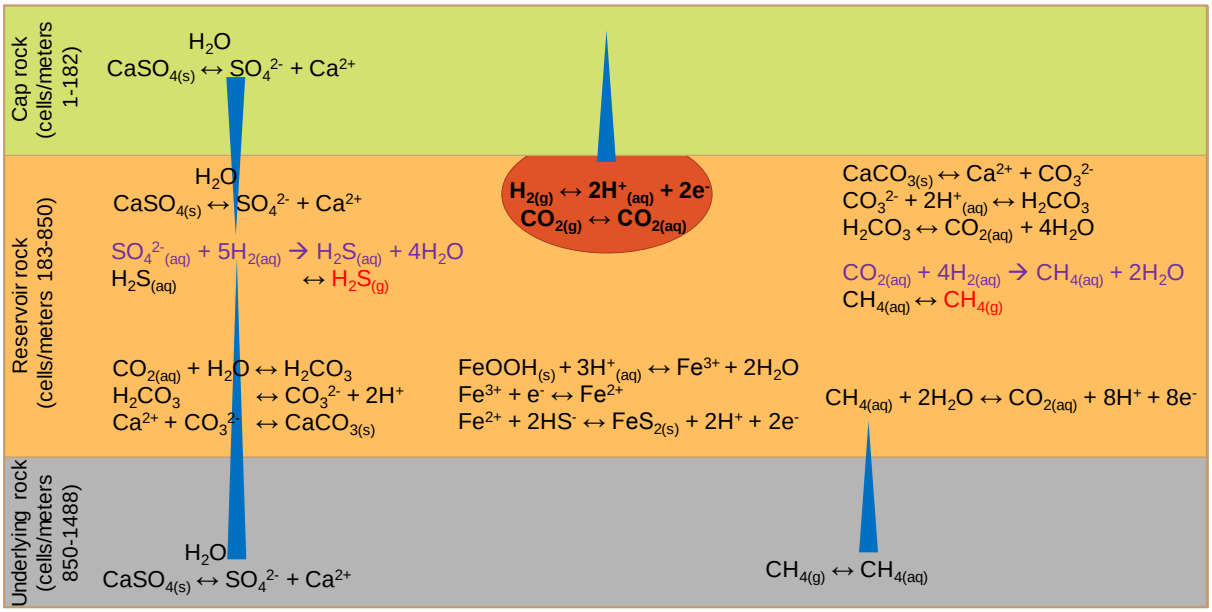

Figure 4.1 Selected reactions and processes associated with bacterial sulfate reduction and methanogenesis (purple). Single arrow = kinetic-controlled reactions; double arrow = equilibrium reactions; blue triangles = time-dependent diffusive transport of aqueous components; bold = injected gas for storage.

The mineralogical compositions of the cap rock, the reservoir rock, and the underlying rock are based on data of the Röt Formation (Dersch-Hansmann et al., 2010; Feist-Burkhardt et al., 2008), Buntsandstein Formation (Soyk, 2015), and Zechstein Formation (Biehl et al., 2016; Schreiber and Bąbel, 2007) and are summarized in Table 4.2. The reactive amount of each mineral phase is calculated in moles per kg of pore water (mol kgw^{-1}) with the consideration of the specific density of each mineral phase (g cm^{-3}). Dawsonite, mackinawite, elemental sulfur, albite (and pyrite) are considered as potential secondary phases, which may form at saturation. The clay minerals are considered as follows: illite is defined as a primary mineral phase, and the cation exchange capacity of chlorite, illite, montmorillonite, and kaolinite are estimated based on the data given by Appelo and Postma (1999). An initial small amount of CO_2 (pCO_2 = partial pressure of CO_2 = 1.0 atm) is assumed to be available in the cap rock, reservoir rock, and underlying rock from burial. The possible outgassing of $CH_{4(g)}$, $N_{2(g)}$, $CO_{2(g)}$, $H_2S_{(g)}$, and $H_{2(g)}$ is assumed in all cells.

The reservoir rock (cells 183–850) has an initial porosity of 10% (n = 0.1), 2.5% (n = 0.025) of the pore space is filled with irreducible water, which is equal to 1 L H_2O, and 7.5% (n = 0.075) of the pore space is filled with gas. The total volume is 40 L (1 L/0.025) and therefore, 3 L are

filled with gas (40 L × 0.075). The porosity is filled with 3 L gas and 1 L H_2O, so 36 L are occupied by solids in each cell of the reservoir rock. The gas consists of 10% residual gas (that was not extracted during natural gas production) and 90% stored hydrogen gas. The composition of the residual gas in the reservoir rock is based on data from Bischoff and Gocht (1984) with $pCH_{4(g)}$ = 3.56 atm, $pN_{2(g)}$ = 0.4 atm, and $pCO_{2(g)}$ = 0.04 atm. The stored hydrogen gas is composed of 96% $H_{2(g)}$ ($pH_{2(g)}$ = 34.56 atm) and 4% $CO_{2(g)}$ ($pCO_{2(g)}$ = 1.44 atm), these values are modified from data presented by Panfilov (2010). For modeling purposes, the stored hydrogen gas is additionally induced as a tracer gas with the same chemical properties as $H_{2(g)}$. It is used instead of $H_{2(g)}$ because $H_{2(g/aq)}$ is induced and used as the reactant in the calculation kinetics. The amount of tracer gas corresponds to 4.3 mol L^{-1} of gas in each cell of the reservoir. The summed volume of all gases in the reservoir rock is 3 L per cell and represents the stored gas volume at 40 atm under the assumed reservoir conditions. The sum of the partial pressure of all available gases (including tracer gas) is equivalent to the total pressure (40 atm) in the reservoir so that the generated gases ($H_2S_{(g)}$, $CH_{4(g)}$) are released as gas bubbles.

Table 4.2 Mineralogical composition of the reservoir rock, cap rock, and underlying rock. Dawsonite, nahcolite, mackinawite, sulfur, albite (and pyrite) are potential secondary phases.

Primary Minerals	Weight Percent (wt. %)	Amount (mol kgw^{-1})
Cap rock		
Halite	5.0	76.74
Quartz	50.0	746.42
Illite	20.0	46.73
Dolomite	5.0	24.32
Anhydrite	15.0	131.77
Reservoir rock		
K-feldspar	30.0	103.90
Kaolinite	1.0	3.73
Quartz	55.0	882.43
Calcite	0.5	4.82
Dolomite	0.5	0.03
Anhydrite	0.5	0.132[a]
Illite	11.5	28.88
Barite	0.5	0.0009
Goethite	0.5	0.002
Underlying rock		
Halite	50.0	758.46
Quartz	8.0	118.04
Calcite	6.0	53.14
Dolomite	10.0	0.03
Pyrite	1.0	7.39
Anhydrite	25.0	66.11

[a]: Reactive amount of anhydrite

The cap rock (cells 1–182) is defined by an initial porosity of 5.0% (n = 0.05), with 1 L irreducible water and 19 L solid. The underlying rock (cells 851–1488) is defined by an initial porosity of 10% (n = 0.1), divided into 2.5% (n = 0.025) irreducible water, which is equal to 1 L H_2O, and 7.5% (n = 0.075) gas. The porosity is filled with 3 L gas and 1 L H_2O, so 36 L are occupied by solids in each cell of the underlying rock. The assumed natural gas composition in the underlying rock is $pCH_{4(g)}$ = 81.1 atm, $pN_{2(g)}$ = 4.3 atm, $pH_2S_{(g)}$ = 10.7 atm, and $pCO_{2(g)}$ = 10.7 atm (Bischoff and Gocht, 1984).

The initial brine compositions of the cap rock, reservoir rock, and underlying rock are pre-calculated in a separate transport model to simulate the million-years-long interaction of the different brines with each other. The cap rock brine is composed of a 0.5 M Na^+/Cl^--dominated solution equilibrated with the mineral phases of the cap rock under cap rock pressure and temperature conditions. The temperature and pressure conditions change along the diffusive pathway of the aqueous species through the cap rock, starting with 40 °C and 40 atm at the reservoir depth (data from Pudlo et al. (2010)). A gradient of decreasing temperature and pressure conditions according to the geothermal gradient (33.3 °C km^{-1} depth) and a pressure gradient of 100 atm km^{-1} depth under hydrostatic conditions is assumed. Therefore, each cell is defined by a specific temperature and pressure condition (e.g., cell 182: 39.967 °C and 39.9 atm; cell 181: 39.934 °C and 39.8 atm; and so on). The initial reservoir rock brine composition is a 0.5 M Na^+/Cl^--dominated solution, which is in equilibrium with the reservoir rock and the initial gas composition at 40 atm and 40 °C. The underlying rock is dominated by a 6.7 M Na^+/Cl^--dominated solution equilibrated with the underlying rock and gas composition under underlying rock pressure and temperature conditions (106.7 atm and 60 °C). To simulate the million-years-long interaction, molecular diffusion of all aqueous species through the cap rock brine, reservoir rock brine, and underlying rock brine is simulated over one million years. The brine compositions are summarized in Table 4.3.

The high Na^+ and Cl^- concentrations and high ionic strength in the brines require the use of the Pitzer database. However, the Pitzer database does not include Al^{3+}, which is important when modeling hydrogen storage in depleted gas fields. Therefore, the database phreeqc.dat is used. The validation that PHREEQC using phreeqc.dat simulates correct results with high Na^+ and Cl^- concentrations and high ionic strength is shown by Hemme and van Berk (2017a). Furthermore, Parkhurst and Appelo (1999) stated that models are reliable at higher ionic strength if the system is sodium chloride dominated.

Table 4.3 Composition of the initial irreducible water in the reservoir rock, the cap rock brine, and the underlying rock brine.

Parameter	Cap Rock Brine	Irreducible Water in the Reservoir Rock	Underlying Rock Brine
pH	6.4	6.4	5.9
Temperature (°C)	37.0	40.0	60.0
Elements	Concentration (mol kgw^{-1})	Concentration (mol kgw^{-1})	Concentration (mol kgw^{-1})
Al	1.31×10^{-7}	2.209×10^{-8}	1.776×10^{-8}
Ba	5.85×10^{-7}	3.922×10^{-7}	2.206×10^{-5}
C_{tot}[a]	3.11×10^{-2}	1.762×10^{-2}	7.405×10^{-3}
Ca	3.63×10^{-2}	1.186×10^{-2}	1.562×10^{-2}
Cl	1.27	1.123	5.396
Fe	5.69×10^{-2}	6.572×10^{-2}	4.263×10^{-11}
K	5.28×10^{-1}	6.151×10^{-1}	4.604×10^{-1}
Mg	8.73×10^{-4}	2.579×10^{-3}	1.142×10^{-2}
N	5.61×10^{-2}	6.485×10^{-2}	5.081×10^{-2}
Na	1.27	1.123	5.396
S_{tot}[b]	1.01	1.143	7.540×10^{-1}
Si	8.73×10^{-5}	9.878×10^{-5}	1.509×10^{-4}

[a]: Summed concentration of aqueous CH_4 and C(+IV) species

[b]: Summed concentration of aqueous S(+VI) and S(−II) species

Molecular diffusion of all aqueous species is the only mass transport accounted for by the model. Multicomponent diffusion is calculated where each “solute can be given its own diffusion coefficient, allowing it to diffuse at its own rate, but with the constraint that overall charge balance is maintained” (Appelo and Wersin, 2007; Parkhurst and Appelo, 2013; Vinograd and McBain, 1941). Fluid flow is not considered in the model due to the lack of total hydraulic head differences in depleted gas reservoirs. A homogeneous distribution of the relevant parameters in the reservoir and cap rock such as mineralogical composition is assumed. Furthermore, no fractures or natural faults are considered. Because of the lack of data, the storage time of hydrogen in depleted oil and gas fields is based on the equipment lifetime of 30 years (Lord et al., 2014), but is varied in an additional scenario (Section 4.3.4.1).

The oxidation of hydrogen by SO_4^{2-} and/or CO_2 in the model is kinetically controlled. The reaction kinetics describe the time-dependent changes of reaction products and educts of a chemical reaction. To calculate the irreversible reactions, catalyzed by microorganisms like sulfate-reducing bacteria and methanogenic bacteria, the Monod equation (Equation (4.4)) is used. Bacterial concentrations are kept constant in the model with the aim to model the “worst-case” scenario.

$$\psi^{\text{growth}} = \psi_{\max}^{\text{growth}} \left(\frac{c^{\text{s}}}{\alpha + c^{\text{s}}} \right) \tag{4.4}$$

where $\psi_{\max}^{\text{growth}}$ is the maximum specific growth rate (mol L^{-1} s^{-1}), c^{s} is the concentration of the limiting substrates (mol L^{-1}), and α is the half-velocity constant. The maximum specific growth rate that is assumed in the model is 2.30×10^{-9} mol kgw^{-1} s^{-1} for methanogenesis (at 37 °C) (Šmigáň et al., 1990) and 9.26×10^{-8} mol kgw^{-1} s^{-1} for BSR (at 30 °C) (Herrera et al., 1997). For bacterial sulfate reduction, the limiting substrate is sulfate and for methanogenesis it is carbon dioxide.

Panfilov (2010) defined a new model to describe the substrate-limited growth models (Equation (4.5)), where t_e is the "individual time of eating" (s) and n_{max} is the maximum population size (m^{-3}). Due to the lack of data regarding the characteristic time of eating and the maximum population size, the Panfilov model is not considered.

$$\psi^{growth} = \frac{1}{t_e} \frac{n}{1 + \frac{n^2}{n_{max}^2}} \left(\frac{c^s}{\alpha + c^s} \right) \tag{4.5}$$

The lower boundary of the column (in the underlying rock) and the upper boundary of the column (in the cap rock) are defined as diffusive flux. To check the numerical accuracy of the results, discretization studies for one scenario are performed, in which the number of shifts and the number of cells are refined. The model calculation for one scenario is rerun and results are compared (Parkhurst and Appelo, 2013).

4.3 Results and Discussion

4.3.1 Loss of $H_{2(g/aq)}$ by Bacterial Conversion to $CH_{4(g)}$ and $H_2S_{(g)}$

The modeling results of the reference scenario (defined in Section 4.2.2; input file S4) show that the maximum amount of bacterial-converted $H_{2(g/aq)}$ to $CH_{4(g)}$ and $H_2S_{(g)}$ depends on the amount of available (and reactive) electron acceptors, carbon dioxide and sulfate, and on the amount of available $H_{2(g/aq)}$. Figure 4.1 shows selected reactions and processes that are coupled to bacterial sulfate reduction and methanogenesis.

When CO_2 and SO_4^{2-} are fully consumed, methanogenesis and BSR will not proceed. The stored gas is composed of 96% hydrogen and 4% carbon dioxide (residual gas is still available). Therefore, CO_2 is available as electron acceptor for the methanogenesis and $CH_{4(g)}$

is generated. After less than 3 years of storage, the injected $CO_{2(g)}$ is completely consumed, but an ongoing supply of CO_2 is provided by the dissolution of carbonate-bearing minerals (such as calcite, for example). Consequently, the amount of generated $CH_{4(g)}$ is limited by the assumed storage time of 30 years and the time-dependent kinetics of methanogenesis.

The available sulfate for BSR in the reservoir rock results from anhydrite dissolution. If anhydrite is still present in a depleted natural gas reservoir, it is not reactive (e.g., it is coated by other minerals). Otherwise, the sulfate would have been catalyzed by bacterial sulfate reduction, with methane—the main component of natural gas—as electron donor. The same applies to hydrogen storage in depleted natural gas reservoirs. However, the creation of new fractures and natural faults or the dissolution of carbonate cements (pore-filling cements) leads to contact of reactive anhydrite with the stored hydrogen. To simulate this “worst-case” scenario, a small amount of reactive anhydrite is assumed in this model. The dissolution of anhydrite provides $SO_4^{2-}{}_{(aq)}$ for $H_2S_{(g)}$ generation and $Ca^{2+}{}_{(aq)}$ for calcite precipitation. Additionally, the dissolution of anhydrite creates porosity, which in turn can be superseded by the precipitation of other minerals (see Section 4.3.2). The reactive anhydrite is in solution equilibrium with the brine. The consumption of $sulfate_{(aq)}$ by BSR is accompanied by ongoing anhydrite dissolution and more sulfate becomes available for BSR until the reactive anhydrite is completely dissolved.

As a product of BSR and methanogenesis, small amounts of water (0.007 kg) are formed (Equations (4.2) and (4.3)). This increases the water content in the reservoir rock (1.0 kg initial water + 0.007 kg generated water = 1.007 kg total water mass per cell after 30 years). The water will probably be suppressed by the gas along the reservoir/cap rock boundary. However, the small increase in the mass of water could increase the anhydrite dissolution, resulting in a higher amount of sulfate ions that are available for BSR. Additional sulfate is delivered by diffusion from the cap rock and the underlying rock, where the dissolution of anhydrite acts as a sulfate source. The amount of generated $H_2S_{(g)}$ depends on the storage time, the amount of available and reactive anhydrite, the diffusion, and the time-dependent kinetic rate constant. However, the last three mentioned factors depend on pressure and/or temperature.

Two hotspot regions with higher amounts of generated $H_2S_{(g)}$ (related to a higher loss of hydrogen) are identified: the contact area of the reservoir rock and the cap rock and the contact area of the reservoir rock and the underlying rock. These are the regions where additional sulfate is delivered into the reservoir rock by diffusion. However, the highest $CH_{4(g)}$ concentrations can be found at the contact area of the reservoir rock and the underlying rock, where additional CO_2 is delivered by diffusion of the gas in the underlying rock into the reservoir rock.

The 1DRMT modeling results show an average loss of 3.3 mol $H_{2(g/aq)}$ after 30 years in each cell of the reservoir rock (cells 183–850). Over the same period, on average, 0.2 mol L^{-1} of gas $CH_{4(g)}$ and 0.005 mol L^{-1} of gas $H_2S_{(g)}$ are generated and 0.06 mol L^{-1} of gas $CO_{2(g)}$ is consumed, which corresponds to the total amount of $CO_{2(g)}$ that was available as injected and residual gas. The changes in gas composition in the reservoir rock in cell 183, located at the contact with the cap rock, with ongoing time are shown in Figure 4.2a. The mass of lost $H_{2(g/aq)}$ that is not converted to $CH_{4(g)}$ or $H_2S_{(g)}$ is bound in aqueous species (OH^-, CH_4, HCO_3^-, $Al(OH)_4^-$, $CaOH^+$, $CaHCO_3^+$, $MgOH^+$, $MgHCO_3^+$, H_2, NH_4^+, NH_3, H_2S, HS^-, H_4SiO_4, and $H_3SiO_4^-$) or in mineral phases (see Section 4.3.2).

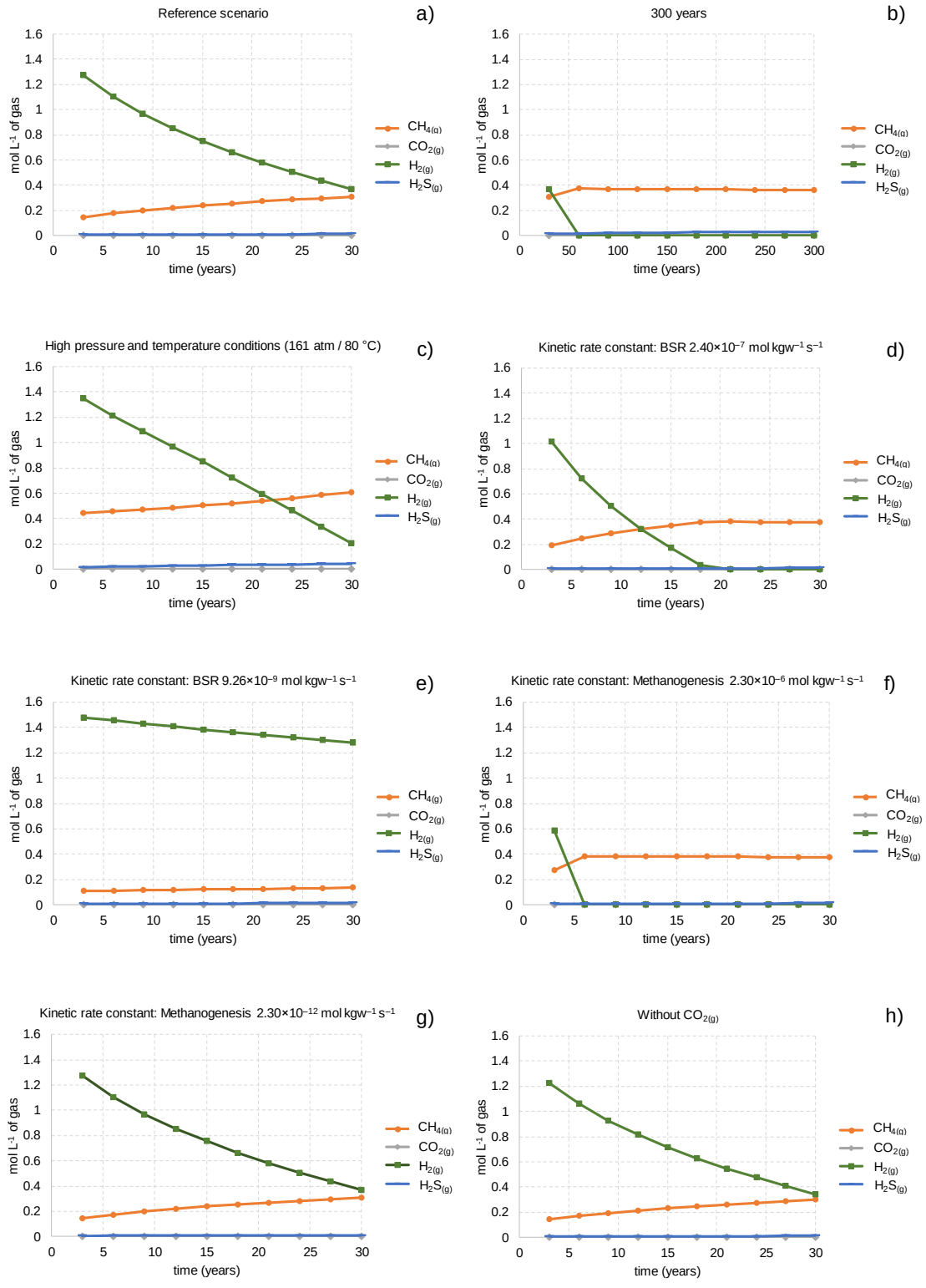

Figure 4.2 Changes in gas composition in the reservoir rock with ongoing time in (a) reference scenario and influenced by (b) increased storage time of 300 years, (c) higher pressure and temperature conditions, (d) higher kinetic rate constant for BSR of 2.40×10^{-7} mol kgw^{-1} s^{-1}, (e) lower kinetic rate constant for BSR of 9.26×10^{-9} mol kgw^{-1} s^{-1}, (f) higher kinetic rate constant for methanogenesis of 2.30×10^{-6} mol kgw^{-1} s^{-1}, (g) lower kinetic rate constant for methanogenesis of 2.30×10^{-12} mol kgw^{-1} s^{-1}, (h) varied stored gas composition (without $CO_{2(g)}$).

The competition between methanogenic microorganisms and sulfate-reducing bacteria is widely discussed in the literature (Adler et al., 2011; Kalyuzhnyi and Fedorovich, 1998; Robinson and Tiedje, 1984; Timmers et al., 2015) and is not the object of this study. However, in PHREEQC, BSR occurs prior to methanogenesis. This reaction order of $H_{2(g/aq)}$ with $SO_4^{2-}{}_{(aq)}$ (BSR) and $CO_{2(aq)}$ (methanogenesis) is tested in a separate batch model. It includes $H_2O_{(aq)}$, $CO_{2(aq)}$, and $SO_4^{2-}{}_{(aq)}$ (in equal amounts) and a sufficient amount of hydrogen. $H_{2(g/aq)}$ reacts primarily with $SO_4^{2-}{}_{(aq)}$ to form $S^{2-}{}_{(aq)}$ until the total amount of the initial $SO_4^{2-}{}_{(aq)}$ is consumed. This is followed by the reaction of $H_{2(g/aq)}$ with $CO_{2(aq)}$ to $CH_{4(aq)}$. Thereby, the equilibrium constant (log *K*) is the crucial value. In a separate model, the log *K* value for SO_4^{2-} (33.65; Equation (4.6)) is reduced to below the log *K* value of CO_2 (16.861; Equation (4.7); data from phreeqc.dat). In this case, the methanogenesis takes place before BSR.

$$SO_4^{2-}{}_{(aq)} + 9H^+{}_{(aq)} + 8e^- = HS^-{}_{(aq)} + 4H_2O \quad (4.6)$$

$$CO_3^{2-}{}_{(aq)} + 2H^+{}_{(aq)} = CO_{2(aq)} + H_2O \quad (4.7)$$

4.3.2 Hydrogeochemical Effects of Hydrogen Storage on Reservoir Rock and Cap Rock

Storage of hydrogen in depleted gas fields can lead to dissolution and precipitation of minerals, which in turn could change the porosity of the reservoir rock and cap rock. An increase in the cap rock porosity would decrease the sealing capacity and increase the risk of pathways for the stored hydrogen to reach, for example, overlying aquifers. On the contrary, a decrease of the cap rock porosity would increase its sealing capacity.

Truche et al. (2013) argued that the influence of hydrogen on sulfur-bearing minerals like framboidal pyrite is high but the effect on other minerals available in claystones like clay minerals, quartz and calcite is minor at “low temperatures”. By contrast, Reitenbach et al. (2015) stated that the addition of hydrogen causes abiotic reactions of hydrogen with minerals of the reservoir and cap rocks which leads to dissolution of sulfate and carbonate-bearing minerals, clay minerals of the chlorite group and feldspars and to precipitation of iron-sulfide bearing minerals, illite, and pyrrhotite. However, both studies agree that pyrite is a potential oxidant for hydrogen and is reduced to pyrrhotite ($FeS_1 + x$) (Reitenbach et al., 2015; Truche et al., 2013). The 1DRMT modeling results of the reference scenario of this study show that at 40 °C and 40 atm the storage of hydrogen induces K-feldspar, kaolinite, and dolomite precipitation in the reservoir rock. Quartz, calcite, and illite are dissolved. The reactive amounts of barite, goethite, and anhydrite are completely consumed during the storage time of 30 years.

After the complete consumption of reactive anhydrite, the only sulfate source comes from the cap rock and the underlying rock by diffusion and consequently this limits the loss of hydrogen by bacterial sulfate reduction. High concentrations of $S(-II)_{(aq)}$ species in the reservoir brine can be observed from the modeling results. The assumed reactive amount of goethite is completely consumed in less than 3 years. The goethite dissolution buffers the effect of $H_2S_{(g)}$ generation because the amount of Fe(+II), which has been reduced from Fe(+III), reacts with the aqueous sulfide to form pyrite (a potential secondary phase in the model) so that aqueous sulfide is no longer available for $H_2S_{(g)}$ generation. The modeling results show also that the higher pH conditions (pH increases from initial 6.4 to 8.2–8.7) and the high sodium concentrations in the brine induce weak albitization in the hotspot areas (the contact area of the reservoir rock and the cap rock and the contact area of the reservoir rock and the underlying rock). Except for pyrite and albite, the other potential secondary phases, dawsonite, mackinawite, nahcolite, and sulfur, are not formed under reservoir conditions. Elemental sulfur does not form, even if mackinawite and pyrite are not considered as potential secondary phases. Small amounts of calcite are precipitated because the dissolution of anhydrite contributes $Ca^{2+}_{(aq)}$ into the reservoir brine. However, at the same time, calcite is dissolved and delivers CO_2 for methanogenesis so that the total amount of calcite decreases. The volume changes of the mineral phases are shown in Figure 4.3. The changes in porosity are calculated from the PHREEQC modeling results. The porosity in the reservoir rock decreases from initially 10% to 9.79–9.95%. This means that the available pore space for hydrogen storage decreases over 30 years such that (i) the same amount of hydrogen is moved to greater distances from the bore hole or (ii) less hydrogen can be stored in future injection phases (max. 0.2%).

The mineralogical changes in the cap rock, induced by diffusion of aqueous $H_{2(aq)}$ from the reservoir rock, are minimal and cause no changes to the initial porosity. The reasons for that are the short storage time of 30 years and the slow diffusion process. Furthermore, the hydrogen reacts with the mineralogical assemblage of the reservoir rock and brine and it is converted by BSR and methanogenesis.

The used modeling program, PHREEQC, has no capabilities to simulate gas transport between the different cells (multiphase flow). To overcome this limitation, a separate transport model provides an initial amount of $H_{2(g)}$ in the cap rock for the kinetic calculation to simulate the influence of $H_{2(g)}$ on the cap rock properties in the case of a gas loss from the reservoir rock by, for example, new fractures or natural faults. The initial amount corresponds to the maximum available amount of $H_{2(g)}$ that could be available per cell in the cap rock and represents a worst-case scenario. Modeling results indicate an increase in pH from 6.4 to 7.8 in the cap rock brine after 30 years of storage. The intense contact of hydrogen with the cap

rock results in a total loss in porosity, which increases the sealing capacity of the cap rock. This decrease in porosity is caused mainly by albitization, whereas the dissolution of halite, quartz, illite, and anhydrite counteracts a stronger porosity decrease. Precipitation of dolomite is negligible. The potential secondary phase pyrite is precipitated whereas dawsonite, mackinawite, and sulfur are not formed.

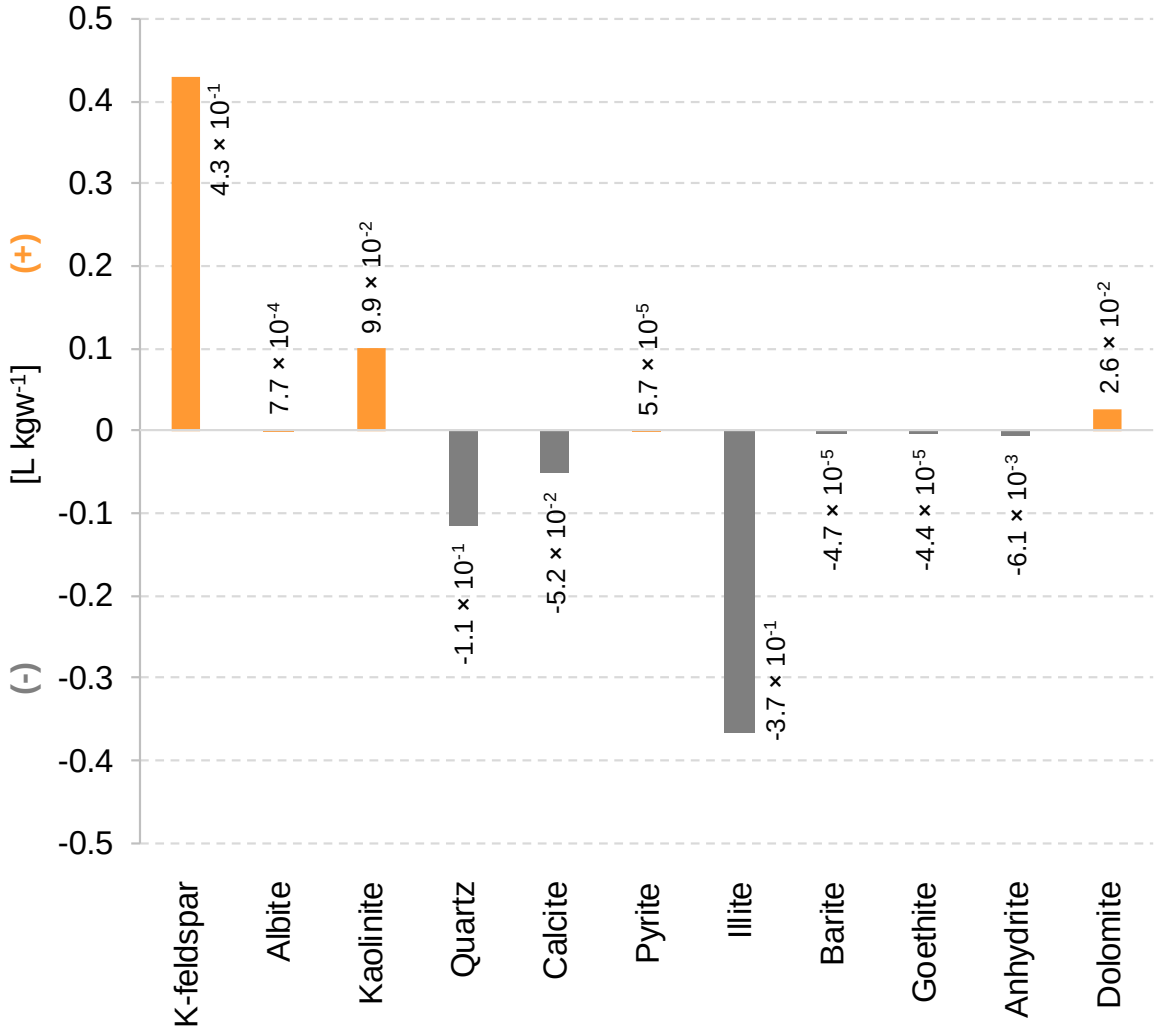

Figure 4.3 Volume changes of mineral phases (L kgw^{-1}) in the reservoir rock after 30 years of hydrogen storage (reference scenario).

4.3.3 Loss of Aqueous $H_{2(aq)}$ by Diffusion through the Cap Rock

By assuming specific diffusion coefficients for the different aqueous species, the diffusion of hydrogen and related products is modeled. A non-reactive tracer, with the same diffusion coefficient as hydrogen of 5.13×10^{-9} m^2 s^{-1}, shows that significant amounts of hydrogen (greater than 4.0×10^{-7} mol kgw^{-1}) were calculated only for distances less than 4 m through

the cap rock (in the *z*-direction) over 30 years, assuming an initial cap rock porosity of 5%, no faults, and non-reactive hydrogen (Figure 4.4a). However, hydrogen reacts with the mineralogical assemblage of the reservoir rock and brine and is converted by BSR and methanogenesis. The loss of aqueous hydrogen by diffusion is minor. Dissolved hydrogen and corresponding aqueous species concentrations (OH^-, CH_4, HCO_3^-, $Al(OH)_4^-$, $CaOH^+$, $CaHCO_3^+$, $MgOH^+$, $MgHCO_3^+$, H_2, NH_4^+, NH_3, H_2S, HS^-, H_4SiO_4, and $H_3SiO_4^-$) in the cap rock brine show no significant changes. The most significant difference has been calculated for the NH_4^+ concentration, which rises to around 4×10^{-4} mol kgw^{-1} in the first meter of the cap rock (cell 182). Therefore, the effect of hydrogen storage on the cap rock is only visible in the first meter of the cap rock, which is in contact with the reservoir rock (cell 182), after 30 years. Even though each aqueous species migrates with a different rate along its concentration gradient, as described by Buzek et al. (1994), the difference in migration is too small to see deviations in the model over the modeled time of 30 years. The loss of the non-reactive hydrogen tracer by diffusion into the cap rock is 25% and represents the maximal loss of aqueous hydrogen by diffusion over 30 years.

In summary (Sections 4.3.1–4.3.3), the loss of hydrogen gas by bacterial conversion, gas–water–rock interactions, and aqueous diffusion is 76% over 30 years.

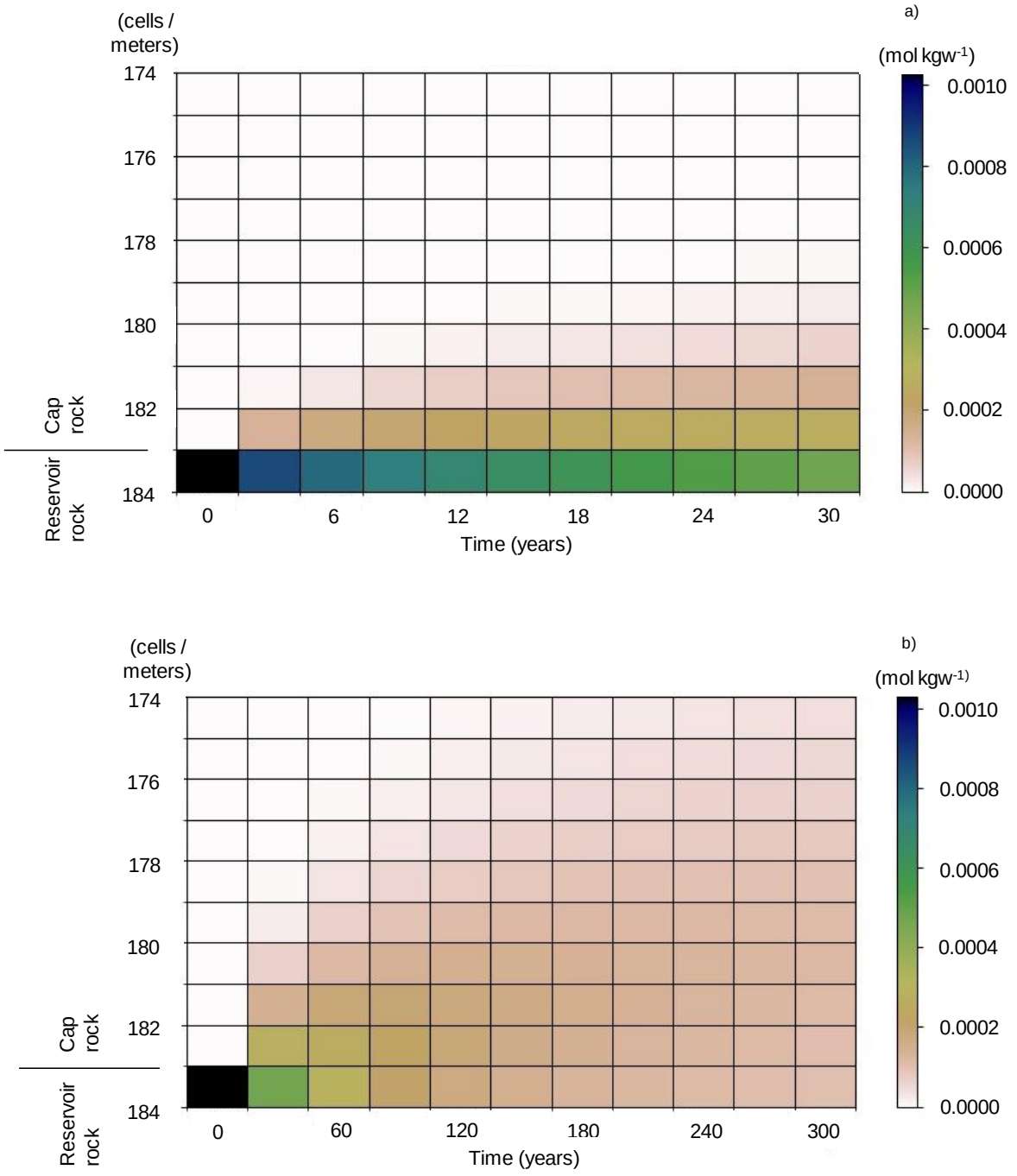

Figure 4.4 Diffusion of a non-reactive hydrogen tracer through the cap rock over (a) 30 years and (b) 300 years.

4.3.4 Influencing Factors

To identify the controlling factors of hydrogen loss and the parameters that affect the modeling results, simulation of generic model scenarios was performed.

4.3.4.1 Storage Time

Because of the lack of data, the storage time has been chosen based on the equipment lifetime of 30 years (Lord et al., 2014). To show the influence of longer storage times on the system environment, in this scenario a longer storage time of 300 years is modeled. With increasing storage time, the dissolved hydrogen has more time to diffuse into higher regions of the cap rock. After 300 years, the non-reactive tracer diffuses 10 m through the cap rock (Figure 4.4b), whereas the reactive hydrogen affects just the first 5 m of the cap rock.

When considering longer storage times, it becomes clear that the mass of generated water is increased to 1.03 kg (1 kg + 0.3 kg = 1.03 kg water in total) in the reservoir rock because the water-producing processes, BSR and methanogenesis (Equations (4.2) and (4.3)), are time-dependent. In the reservoir rock, the pH is increased to 8.7. The porosity loss from 10% to 9.19–9.99% is greater than that after 30 years of storage. The reason for the greater decrease is the intensified dissolution of quartz and illite. Calcite is completely consumed in the hotspot areas, the contact areas of the cap rock to the reservoir rock and of the underlying rock to the reservoir rock. In all other cells, calcite is still available, but it is only partly dissolved. On the other hand, the albitization process is intensified in the hotspot areas and more kaolinite is formed. The reactive amounts of anhydrite and goethite are completely consumed. The only sulfate source for BSR is delivered by diffusion from the underlying rock and the cap rock into the reservoir rock. The mineralogical changes in the cap rock are minimal and show that even after 300 years of hydrogen storage, the effects of diffusion of aqueous hydrogen are small.

When the storage time is increased to 300 years (under the assumption that no new gas mixture of $H_{2(g)}$ and $CO_{2(g)}$ is injected), the total amount of newly generated $CH_{4(g)}$ is increased to an average of 0.25 mol L^{-1} of gas and the $H_2S_{(g)}$ concentration is increased to an average of 0.006 mol L^{-1} of gas (Figure 4.2b). After 300 years, the total amount of stored $H_{2(g)}$ is consumed.

In the case of storage cycles, including gas injection, storage, and production phases, the newly injected hydrogen gas is again accompanied by a new amount of $CO_{2(g)}$, which is available as an electron acceptor for methanogenic bacteria. This aspect is modeled in a separate transport model. The total loss of hydrogen by conversion to $CH_{4(g)}$ is higher if the storage cycle has a higher frequency, because $CO_{2(g)}$ is co-injected and is available for methanogenesis. With a total storage time of 30 years and a dwelling time of 6 months, a maximum of 60 injections of “fresh gas” (composed of $H_{2(g)}$ and $CO_{2(g)}$) can be stored in the reservoir. This leads to a total generation of 6.72 mol L^{-1} of gas $CH_{4(g)}$ after 30 years. However, the loss of hydrogen after 6 months, the shorter storage period, is of course smaller

(0.112 mol L^{-1} of gas in 6 months) than after 30 years of storage. Consequently, a shorter storage period leads to a lower amount of generated $CH_{4(g)}$ (and a lower loss of hydrogen) because methanogenesis is a time-dependent process. However, over the total time, the loss of hydrogen sums to a higher amount. This holds true only for methanogenesis. For bacterial sulfate reduction, the amount of generated $H_2S_{(g)}$ depends not only on the amount of available sulfate but also on the time-dependent kinetic rate constant.

To summarize, it is clear that longer storage times increase the risk of loss of hydrogen. On the other hand, the reactive anhydrite and calcite will be consumed after a few years of storage and safer storage conditions arise because BSR and methanogenesis will be limited by the amount of sulfate and carbon dioxide delivered by diffusion (and diffusion is a slow process). In this case, the hotspot areas gain in importance. However, assuming shorter storage periods of 6 months, the $CH_{4(g)}$ concentration in the stored gas will be lower than after a storage time of 30 years, but the total loss of hydrogen sums to higher amounts regarding shorter storage periods (60 injections in 30 years).

4.3.4.2 Pressure and Temperature Conditions in Gas Reservoirs

Each depleted gas field has specific pressure and temperature conditions. To analyze the influence of pressure and temperature on the modeling results of hydrogen storage, the pressure and temperature conditions are varied.

The higher pressure and temperature conditions chosen are 161 atm and 80 °C. At even higher temperature conditions, the sulfate-reducing bacteria and methanogenic bacteria are mostly no longer active. The maximum temperature for SRB and methanogenic bacteria is 80 °C (Jorgensen et al., 1992; Magot et al., 2000). At higher pressure and temperature conditions, thermochemical sulfate reduction, as known from deeply buried hydrocarbon reservoirs, must be considered.

At 161 atm and 80 °C (at invariable kinetic rate constants for BSR and methanogenesis), the amount of consumed $H_{2(g/aq)}$ is slightly lower (75%) than that in the reference scenario (76%; modeled at 40 atm and 40 °C). The increased pressure results in a decreased gas volume and in higher gas concentrations. The $H_2S_{(g)}$ concentration is increased to an average of 0.009 mol L^{-1} of gas and the $CH_{4(g)}$ concentration is increased to an average 0.54 mol L^{-1} of gas after 30 years (Figure 4.2c).

The porosity loss (from initial 10% to 9.52–9.86%) in the reservoir rock is, on average, higher than in the reference scenario. This can be explained by the stronger albitization at this higher pressure and temperature conditions and the pyrite formation increases as well. On the other hand, the dissolution of quartz, calcite, and illite is higher. However, the amount of precipitated minerals is higher than the amount of dissolved minerals and this causes the decrease in porosity. The pH in the reservoir rock brine is 7.5–8.4, which is lower than in the reference scenario. In addition, the amount of the aqueous sulfide sulfur (S(–II)) in the reservoir brine is decreased at these conditions. The mass of generated water is, despite BSR and methanogenesis, decreased from 1 kg to 0.96 kg. A reason for this could be the stronger albitization process, binding the water.

The changed pressure and temperature conditions affect the equilibrium constants of the mass action laws of gases, minerals, and aqueous species. Here, a modeling limitation is achieved because the phreeqc.dat database does not contain pressure dependencies for the equilibrium constants for all mineral phases that are used in the model. The pressure dependency of the following mineral phases in the model are included: calcite, dolomite, anhydrite, barite, quartz, and halite.

As in the reference scenario, the temperature and pressure conditions change along the diffusive pathway of the aqueous species through the cap rock according to the geothermal gradient of 33.3 °C km^{-1} depth and 100 atm km^{-1} depth under hydrostatic conditions, starting with 80 °C and 161 atm at the reservoir depth. Each cell is defined by a specific temperature and pressure condition. The influence of these changing pressure and temperature conditions on the cap rock is minor. The concentration of aqueous sulfate sulfur S(+VI) is higher and aqueous sulfide sulfur (S(–II)) is lower than in the reference scenario. Different from the reference scenario, albitization occurs at these higher pressure and temperature conditions even in the cap rock, and dawsonite precipitation and halite dissolution are slightly increased.

To summarize, at higher pressure and temperature conditions (while the kinetic rate constants are not changed), the concentration of $CH_{4(g)}$ and $H_2S_{(g)}$ is increased due to a lower gas volume. Furthermore, the loss in porosity in the reservoir rock is increased. However, the kinetic rate constant is pressure- and temperature-dependent; therefore, this influence is tested in a further scenario (Section 4.3.4.3).

4.3.4.3 Kinetic Rate Constant

Special consideration is given to the influence of the kinetic rate constants of bacterial sulfate reduction and methanogenesis on the loss of hydrogen during storage. Therefore, the rate constants are varied. As a reminder, the initial kinetic rate constant in the reference scenario for BSR is 9.26×10^{-8} mol kgw^{-1} s^{-1} and 2.30×10^{-9} mol kgw^{-1} s^{-1} for methanogenesis.

By increasing the kinetic rate constant for BSR slightly to 2.40×10^{-7} mol kgw^{-1} s^{-1}, based on data from Herrera et al. (1997), the total amount of stored hydrogen is lost in less than 20 years. The amount of generated $H_2S_{(g)}$ does not change because the reactive amount of anhydrite in the reservoir rock is completely consumed and the only sulfate source comes from the cap rock and underlying rock by diffusion and diffusion is a slow process. By increasing the storage time to 300 years (with a kinetic rate constant of 2.40×10^{-7} mol kgw^{-1} s^{-1} for BSR), the effect of diffusion is recognizable and the $H_2S_{(g)}$ generation increases in the hotspot areas. The amount of generated $CH_{4(g)}$ increases from 0.2 mol L^{-1} of gas to an average of 0.25 mol L^{-1} of gas in each cell of the reservoir rock after 30 years (Figure 4.2d). The reason for this could be that methanogenesis starts as soon as all the sulfate for BSR is consumed. Because sulfate is consumed faster, due to the increased kinetic rate constant, the timeframe in which the methanogenesis can take place is expanded. On decreasing the kinetic rate constant for BSR to 9.26×10^{-9} mol kgw^{-1} s^{-1}, the amount of generated $H_2S_{(g)}$ does not change because the reactive amount of anhydrite in the reservoir rock is completely consumed. Less $H_{2(g/aq)}$ is consumed (14% loss) and a smaller amount of $CH_{4(g)}$ (on average 0.013 mol L^{-1} of gas) is generated (Figure 4.2e).

At a higher kinetic rate constant for methanogenesis of 2.30×10^{-6} mol kgw^{-1} s^{-1}, the total amount of stored hydrogen is lost in less than 6 years (Figure 4.2f). $CH_{4(g)}$ production increases to an average of 0.25 mol L^{-1} of gas and the mass of water rises to 1.03 kg per cell in the reservoir rock after 30 years of storage. The amount of $CO_{2(g)}$ from the injected gas mixture and the residual gas is completely consumed in less than 3 years of storage and is not the limiting factor for methanogenesis. If no $CO_{2(g)}$ is available anymore from the injected gas mixture and residual gas, the dissolution of carbonate-bearing minerals begins and delivers CO_2 for methanogenesis. With a smaller kinetic rate constant for methanogenesis of 2.30×10^{-12} mol kgw^{-1} s^{-1}, the loss of $H_{2(g/aq)}$ is slightly lower (75.7%). Less $CH_{4(g)}$ is generated (but the differences are in the third decimal place, only from 0.192 mol L^{-1} of gas in the reference scenario to 0.191 mol L^{-1} of gas) and the $H_2S_{(g)}$ generation is constant (Figure 4.2g). The produced mass of water and the pH conditions show no changes compared to the reference scenario.

It can be concluded that the kinetic rate constants are important factors controlling the loss of hydrogen storage. Knowledge of the kinetic rate constants for BSR and methanogenesis at elevated temperature and pressure are required. Nevertheless, the maximal amount of generated $H_2S_{(g)}$ is, if all reactive sulfate-bearing minerals (e.g., anhydrite) are consumed, limited by diffusion. On the other hand, the maximal amount of generated $CH_{4(g)}$ depends on the kinetic rate constant and the storage time.

4.3.4.4 Stored Gas Composition

In the "POWER-to-GAS-to-POWER" concept for the storage and usage of hydrogen, the hydrogen is stored purely in underground storage systems (Hagemann et al., 2016). As a consequence of pure $H_{2(g)}$ injection and storage (no $CO_{2(g)}$ is co-injected), the amount of generated $CH_{4(g)}$ decreases to an average of 0.32 mol L^{-1} of gas after 30 years. $H_2S_{(g)}$ generation is constant with an average of 0.005 mol L^{-1} of gas after 30 years (Figure 4.2h). The loss of stored $H_{2(g/aq)}$ is slightly increased to 77% after 30 years of storage.

An alternative CO_2 source for methanogenesis is the residual gas that was not removed during natural gas production. Only if the residual gas is consumed or not reactive, does carbonate-bearing mineral dissolution increase and delivers CO_2 for methanogenesis, which is even more pronounced at a longer storage time of 300 years. Finally, the amount of available and reactive carbonate-bearing minerals (here calcite and dolomite) limits the process of methanogenesis if no $CO_{2(g)}$ is stored with $H_{2(g/aq)}$. On the other hand, a separate test model shows that a higher amount of co-injected $CO_{2(g)}$ (14.8 atm; 10 times higher than in the reference scenario) increases the amount of generated $CH_{4(g)}$ to an average of 1.0 mol L^{-1} of gas. If the amount of available $CO_{2(g)}$ would be infinitely large, the time-dependent kinetic rate constant and the storage time limit the loss of hydrogen by conversion to $CH_{4(g)}$.

Without $CO_{2(g)}$ co-injection, the porosity in the reservoir rock decreases from 10% to 9.82–9.98%. This loss in porosity is slightly smaller than in the reference scenario in which 4% $CO_{2(g)}$ is co-injected. The changes in mineral dissolution and precipitation are minor in comparison to the reference scenario. The amounts of precipitated kaolinite, K-feldspar, and dolomite are slightly smaller than in the reference scenario and less calcite and illite are dissolved. No changes in the pH are observable. The smaller amount of precipitated K-feldspar and kaolinite leads to a smaller amount of bound water in these minerals. Consequently, the mass of water increases to 1.025 kg in the reservoir rock and is higher than the increase in the reference scenario (1.007 kg). The changes in the mineralogical composition of the cap rock are minor.

4.4 Conclusions

The simulation results show that the underground storage of hydrogen in depleted gas fields entails the risk of hydrogen loss (and related energy loss) by bacterial conversion to $CH_{4(g)}$ and $H_2S_{(g)}$ and gas–water–rock interactions, which in turn lead to changes in the porosity of the reservoir rock. The modeling results of the one-dimensional reactive mass transport model identify the factors that control the loss of hydrogen:

- The loss of hydrogen by bacterial conversion to $CH_{4(g)}$ via methanogenesis is limited mainly by the amount of co-injected $CO_{2(g)}$, the reaction kinetics, and the connected maximal storage time of 30 years. Less co-injected $CO_{2(g)}$ will reduce $H_{2(g)}$ loss but cannot inhibit the conversion to $CH_{4(g)}$ if further CO_2 sources are available in the form of residual gas and carbonate-bearing minerals. The generation of $CH_{4(g)}$ by methanogenesis where CO_2 is only delivered by the dissolution of carbonate-bearing minerals is slower because the dissolution process limits the conversion to $CH_{4(g)}$.
- The loss of hydrogen by bacterial conversion to $H_2S_{(g)}$ via bacterial sulfate reduction is limited mainly by the amount of available sulfate in the reservoir. After complete consumption of reactive anhydrite, the only sulfate source comes from the cap rock and the underlying rock by diffusion and consequently limits the loss of hydrogen by bacterial sulfate reduction because the process of diffusion is slow.
- The mass of generated water, as a product of BSR and methanogenesis, increases the pressure in the system and diffusion can be intensified.
- The mineralogical changes in the reservoir rock result in a small decrease in porosity. As a consequence, the available pore space for hydrogen storage decreases over 30 years such that (i) the same amount of hydrogen is moved to greater distances from the bore hole or (ii) less hydrogen can be stored in future injection phases.
- The loss of aqueous hydrogen by diffusion and related effects on the cap rock mineralogy is negligibly small, with a storage time of 30 years, because hydrogen storage causes gas–water–rock interactions in the reservoir rock and brine and is converted by BSR and methanogenesis to a greater extent. Furthermore, the process of diffusion is slow.
- A longer storage period increases the loss of the stored hydrogen. Shorter storage periods lead to less hydrogen loss for each period, but over the total time the summed loss of hydrogen is higher because new $CO_{2(g)}$ is available for methanogenesis after each gas injection.

- At higher pressure and temperature conditions, the concentrations of $CH_{4(g)}$ and $H_2S_{(g)}$ increase due to a lower gas volume. Furthermore, the loss in porosity in the reservoir rock increases as well.
- Knowledge of kinetic rate constants for bacterial sulfate reduction and methanogenesis at elevated levels of pressure and temperature are required as accurately as possible.

It is recommended to choose depleted gas fields for hydrogen storage where the residual gas has low $CO_{2(g)}$ concentrations. The mineralogical composition of the reservoir rocks should contain low amounts of sulfate- and carbonate-bearing minerals but high amounts of reactive iron-bearing minerals. Reservoirs with low pressure and temperature conditions are recommended as well as storage gas compositions with low amounts of $CO_{2(g)}$. From the modeling results, it seems reasonable to implement a multicomponent transport model and to conduct a joint variation of several parameters as a next step.

4.5 Acknowledgements

We thank Leo Fuhrmann for technical assistance. We would like to thank three anonymous reviewers for their constructive reviews.

4.6 Supplementary Data (on CD)

Input file S4 for the transport model to calculate the reference scenario UHS is available (for PHREEQC Version 3).

5 Final Discussion

When addressing the increasing carbon dioxide emissions and related climate changes, it is necessary to draw attention to a shift in energy production (Henkel et al., 2016). This also comprises the research about safe underground gas storage, including carbon capture and storage, natural gas storage in salt caverns, and underground hydrogen storage.

These underground gas storage options are important for the so-called German “Energiewende”. CCS is of relevance for the reduction of greenhouse gas emissions, SCGS is relevant to being more independent from gas suppliers and to compensate seasonal fluctuations in the supply and demand of energy, and UHS is relevant for storing energy generated from renewable energy sources like wind and solar but also, like SCGS, to compensate for seasonal fluctuations.

This study aims at analyzing the hydrogeochemical processes that are induced by underground gas storage. The chemical reactions between the available gases, aqueous solutions, and mineral phases (gas–water–rock interactions) in the considered systems are modeled. The tools for modeling the reactive mass transport are PHREEQC (1D) and PHAST (3D), both are provided by the US Geological Survey. The semi-generic, hydrogeochemical models are based on chemical equilibrium thermodynamics and kinetic reactions for sulfate reduction in SCGS and UHS, as well as kinetic reactions for methanogenesis in UHS.

In the field of CCS, many studies focus on CO_2–water–rock interactions in reservoir rocks in depleted hydrocarbon reservoirs but much less attention has been paid to interactions in the cap rocks. However, this is of great importance for risk assessment. To fill this gap, the first part of this study (Section 2) focuses on the long-term change in the sealing capacity of the cap rock in CO_2 storage systems triggered by mineral dissolution and precipitation. The main difference to other studies is the consideration of the diffusive mass transport of CO_2 along a gradient of decreasing pressure and temperature conditions. The results of this model are discussed and allow the identification and quantification of the loss or gain of total porosity affected by hydrogeochemical reactions driven by diffusive mass transport.

In the second part of this study (Section 3), modeling-based evidence is presented that $H_2S_{(g)}$ generation in salt cavern gas storage is possible in terms of chemical thermodynamics, reaction kinetics, and coupled diffusive mass transport. It is a potential risk for the gas quality of the stored gas. Several studies on $H_2S_{(g)}$ generation in hydrocarbon reservoirs and hydrocarbon storage environments exist. However, this one is the first that clarifies and quantifies $H_2S_{(g)}$ generation processes in salt caverns filled with natural gas. Because of the

increasing demand for storage capacity in salt caverns, the use of less favorable and sulfate-bearing salt formations will increase, and the potential risk of $H_2S_{(g)}$ generation will rise in the future. Therefore, the interpretation of the modeling results allows the analysis of the limiting factors for $H_2S_{(g)}$ generation in salt caverns and the identification of technical approaches to decrease or inhibit $H_2S_{(g)}$ generation and release into the stored gas.

The third part of this study (Section 4) deals with the loss of hydrogen during underground storage in terms of chemical thermodynamics, reaction kinetics, and coupled diffusive mass transport. This study is the first one that clarifies and quantifies the loss of hydrogen (and related energy loss) as a combination of (i) the conversion by bacteria, (ii) gas–water–rock interactions in the reservoir and cap rock, which relate to porosity changes, and (iii) loss by aqueous diffusion along a gradient of decreasing pressure and temperature conditions. The interpretation of the modeling results allows analysis of the limiting factors of the loss of hydrogen and the identification of storage conditions optimized for hydrogen storage in depleted gas fields.

5.1 General Model Similarities and Differences

In all three subtopics of this study, numerical models are developed to simulate the hydrogeochemical processes induced by underground gas storage in space and time. In each, the gas–water–rock interactions that could lead to risks when storing gases in deep geological formations are analyzed, followed by the description of possible consequences and potential inhibitions methods. This study also shows new dependencies (like the pressure and temperature changes along the diffusional transport) that were not considered in previous studies and opens new applicability (like inhibitions methods for $H_2S_{(g)}$ generation in salt caverns). All discussed models are set up so that they can be adapted and applied to other underground gas storage systems.

Panfilov (2010) stated that the hydrodynamic and chemical behavior of hydrogen stored in the underground has little in common with the storage of natural gas or carbon dioxide. Underground storage of hydrogen comes with more leakage problems than natural gas storage due to its chemical and physical properties, such as high diffusivity, low viscosity, and low density, resulting in a higher mobility (Ebigbo et al., 2013). Nevertheless, the principal hydrogeochemical modeling approaches and general basics, such as induced gas–water–rock interactions, the pressure and temperature dependence, dissolution and precipitation of minerals, gas solubilities, diffusional transport, and so on, are the same in all three gas storage

systems (see Table 1.2 and Figure 5.1). The differences between the systems are e.g. the dimension (CCS and UHS: 1D, SCGS: 1D and 3D), the kind of modeling (CCS thermodynamic equilibrium modeling, SCGS and UHS thermodynamic equilibrium and kinetic modeling), the transport mechanisms (SCGS and UHS diffusion only, in CCS diffusion and advection in an alternative model scenario), and the modeling time (CCS is constructed for long-term storage, SCGS and UHS are designed for seasonal storage).

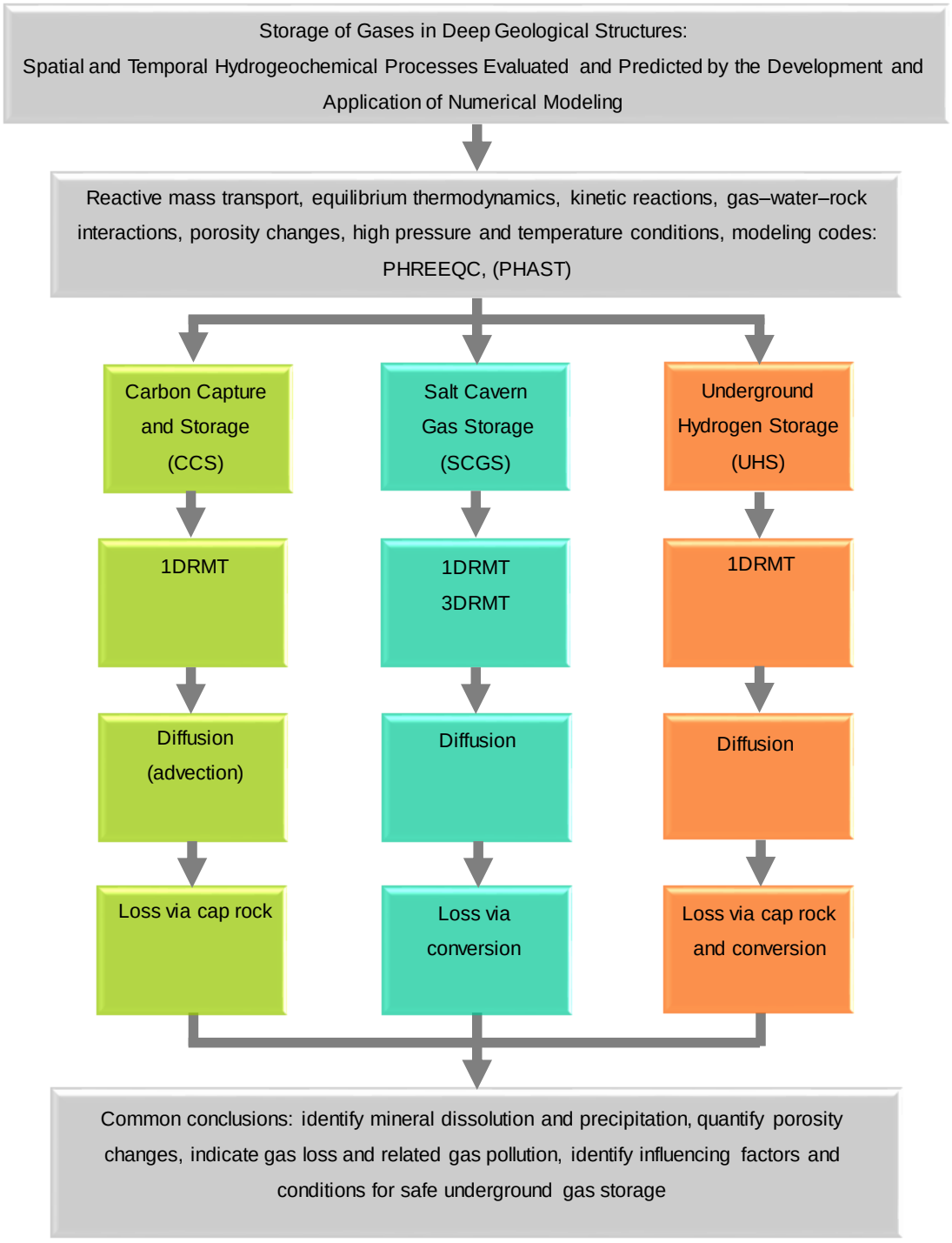

Figure 5.1 Overview of the three subtopics CCS, SCGS, and UHS.

Furthermore, the analyzed gases are the same that occur in natural oil and gas fields (like $CH_{4(g)}$, $CO_{2(g)}$, and in small amounts $H_{2(g)}$), in which, under same reservoir conditions, similar problems occur. For example, the problem of $H_2S_{(g)}$ generation in natural gas fields is already known but has not been analyzed in salt caverns when storing natural gas.

Additionally, in all three underground gas storage systems “hotspot” areas are identified and the factors that could influence the modeling results are compared. These hotspot areas are regions where intensified gas–water–rock interactions occur. In CCS the main changes in porosity are identifiable close to the cap rock/reservoir rock contact. The hotspot area for SCGS, in which the highest total H_2S concentrations occur, is identified in the brine on the diffusive path where methane and sulfate meet and react with each other. In UHS, two hotspot regions with higher amounts of generated $H_2S_{(g)}$ are identified. The contact area of the reservoir rock and the cap rock and the contact area of the reservoir rock and the underlying rock. The highest $CH_{4(g)}$ concentrations can be found at the contact area of the reservoir rock and the underlying rock. In summary, hotspot areas in all three underground gas storage systems are identified at the interface of two units with different mineralogical compositions and/or brine compositions.

5.2 Influencing Factors

In all three subtopics, the influencing factors that affect the modeling results are analyzed and identified. Table 5.1 shows the comparison of the considered parameters for each underground gas storage system. Tortuosity, initial cap rock porosities, and the advection transport mechanism are only considered in a single study and are not compared.

Table 5.1 Effect of the different influencing factors on the modeling results in comparison of the three underground gas storage systems. Red = high influence, green = low influence, grey = not considered.

	CCS	SCGS	UHS
Pressure/temperature			
Kinetic rate constant			
Tortuosity			
Gas composition			
Mineralogical compositions			
Initial cap rock porosities			
Effective diffusion coefficient			
Advection			
Storage time			

The influence of pressure and temperature conditions when storing gases in deep geological structures is of great interest. When storing carbon dioxide in depleted hydrocarbon reservoirs, mineral dissolution and precipitation and resulting porosity changes are pressure and temperature dependent. Higher pressure and temperature conditions have a stronger effect on mineral dissolution and precipitation. Compared to temperature, the effect of pressure on the change of porosity is slightly stronger in CCS systems. When storing natural gas in salt caverns, the changing pressure conditions during the injection, storage, and production phases have a minor influence on generated $H_2S_{(g)}$. However, the pressure and temperature dependent kinetic rate constant for bacterial sulfate reduction influences the amount of generated and released $H_2S_{(g)}$. The pressure and temperature conditions are also of interest when storing hydrogen in depleted gas reservoirs because at higher pressure and temperature conditions, the concentrations of $CH_{4(g)}$ and $H_2S_{(g)}$ increase due to a lower gas volume and the loss in porosity of the reservoir rock increases. Similar to SCGS, the kinetic rate constant influences the loss of the stored hydrogen. Therefore, accurate knowledge of the kinetic rate constants at elevated pressure and temperature conditions is required.

In CCS systems, the injected gas composition affects the sealing capacity of the cap rock, which can increase by mixing CO_2 with CH_4 and H_2S in comparison to pure CO_2 injection. In SCGS systems, the composition of the stored natural gas can influence the amount of generated and released $H_2S_{(g)}$. In UHS systems, less co-injected $CO_{2(g)}$ will reduce $H_{2(g)}$ loss, and the initial residual gas in the reservoir should have low $CO_{2(g)}$ concentrations as well.

The results of the CCS model indicate that porosity creation depends strongly on the mineralogical composition of the reservoir and cap rock as well as on the corresponding brine composition. This is also shown in SCGS where the amount of available sulfate in the rock salt formation is one of the main limiting factors of the $H_2S_{(g)}$ generation process. This is comparable with the results of the UHS study in which the loss of hydrogen by bacterial conversion to $H_2S_{(g)}$ is limited mainly by the amount of the available sulfate in the reservoir rock, the cap rock, and the underlying rock.

The effective diffusion coefficient is only varied in the study of CCS, but the influence of diffusion is analyzed in SCGS and UHS as well. In CCS, even over the broad range of effective diffusion coefficients tested, the intensity of the diffusive mass transport has negligible effects on mineral precipitation and dissolution and on resulting porosity changes. In SCGS, the tortuosity affects the amount of generated $H_2S_{(g)}$, but the diffusion of dissolved methane and dissolved sulfate through the brine have a stronger effect on the generation of $H_2S_{(g)}$. In UHS, the loss of $H_{2(aq)}$ induced by BSR and methanogenesis predominates, assuming a storage time of 30 years. Whereas the loss of aqueous hydrogen by diffusion is negligible. Furthermore, the

loss of hydrogen by BSR is limited mainly by the amount of anhydrite (the sulfate source in the reservoir rock). After complete consumption of reactive anhydrite, the only sulfate supply into the reservoir is via diffusion from the cap rock and the underlying rock. This consequently limits the loss of hydrogen by bacterial sulfate reduction because the process of diffusion is slow.

In CCS, a storage time of one million years is simulated because it is considered as final disposal and the long-term effects must be analyzed. In SCGS and UHS the typical 30 years lifetime of the salt caverns or the equipment is modeled. Additionally, in UHS a longer storage time of 300 years is modeled which increases the loss of the stored hydrogen.

5.3 Optimal Storage Conditions

With the increasing demand for underground storage capacities and the related conflict of interest, it is of rising importance to figure out which storage option is optimal for which kind of gas. With the results of the hydrogeochemical modeling in this study, safe conditions for each considered gas can be defined.

For the storage of natural gas in salt caverns, salt structures with low amounts of anhydrite and high amounts of iron-bearing minerals should be chosen. The pressure conditions have a minor influence on the loss of the stored natural gas by conversion to $H_2S_{(g)}$.

For the storage of hydrogen in depleted gas reservoirs, similar problems as for SCGS in salt caverns arise. Therefore, the conditions in the depleted gas reservoirs must be similar to those for SCGS in salt caverns. The mineralogical composition of the reservoir rocks should contain low amounts of sulfate- and carbonate-bearing minerals but high amounts of reactive iron-bearing minerals. Depleted gas reservoirs with low pressure and temperature conditions are recommended. The stored hydrogen gas, as well as the initial gas in the reservoir, should have low amounts of $CO_{2(g)}$.

When storing carbon dioxide in depleted hydrocarbon reservoirs, the cap rock should contain low amounts of calcite. Furthermore, low initial cap rock porosities are recommended as well as low pressure and temperature conditions in the reservoir.

5.4 Model Limitations

All models have their limitations. Modeling is always an attempt to reproduce reality but the interlocking of all the parameters that must be considered are too complex and only single

parts of a system can be displayed. Nevertheless, models enable a critical analysis and lead to a better understanding of the analyzed system (Konikow and Bredehoeft, 1992).

Even if PHREEQC is a general hydrogeochemical program, which is applicable to various hydrogeochemical environments, some limitations occur (Parkhurst and Appelo, 2013).

- High-salinity waters can be calculated with the pitzer.dat database when the Debye-Hückel equation is no longer applicable. The Pitzer approach calculates ion activity coefficients at high ionic strength but the pitzer.dat database includes only a limited number of elements and is therefore limited in application.
- Mass transport modeling does not consider gas-transport between different cells (multi-phase flow). To overcome this limitation, separate transport models can be simulated that provide initial amounts of the gases in the appropriate cells.
- The changes in porosity must be calculated manually from PHREEQC results. The effects of porosity and permeability changes during modeling on diffusion are, therefore, not considered.
- PHREEQC cannot calculate in 3D.
- The database phreeqc.dat used includes the pressure and temperature dependence of the mass-action law constants for the equilibrium reactions of many but not all aqueous, gaseous, and solid species involved in the models.

The reactive amount of each mineral in the rock assemblages are precalculated based on the respective porosity and is included in the input file. PHREEQC and PHAST allow mineral precipitation until the available water is no longer oversaturated with any mineral (Fu, 2014). That could result in a higher amount of newly formed minerals than the available pore space allows. This effect should be considered at the evaluation and re-calculation phase of the PHREEQC and PHAST modeling results when dealing with porosity changes. Furthermore, PHAST is not capable of calculating the pressure dependence of solubility equilibrium constants for minerals, gases, and aqueous species.

The data required for kinetic models (like kinetic rate constants, activation energies, and experimental rate laws) are learned from experiment and are still rare. The corresponding information required for equilibrium models (equilibrium constants, enthalpies, entropies, Gibbs free energies, and heat capacities) are more abundant (Stumm and Morgan, 1981). Kinetically-based models are limited by the rare rate constants for the modeling conditions.

6 Final Conclusion and Outlook

The hydrogeochemical one-dimensional reactive mass transport modeling approaches presented in this study link the sciences of hydrogeology, petroleum geology, and engineering, including safety and geochemical aspects related to underground gas storage systems. This study contributes to the process-understanding of underground gas storage systems. The application of the reactive mass transport modeling presented provides a good example of how such modeling approaches could (i) identify mineral dissolution and precipitation in the cap and reservoir rocks triggered by gas storage and molecular diffusion of stored gases, (ii) quantify the resulting porosity changes, (iii) indicate gas loss and related gas pollution by bacterial conversion via BSR and methanogenesis, (iv) identify hydrogeochemical methods to inhibit $H_2S_{(g)}$ generation and release, and (v) identify conditions for safe underground gas storage.

With the results of this study, the discussion of CO_2–water–rock interactions in the cap rocks of carbon capture and storage systems may be stimulated, attention may be drawn to the risk of $H_2S_{(g)}$ generation in salt caverns, and the hydrogeochemical risks of underground hydrogen storage may be highlighted, concluding that hydrogeochemical modeling provides an effective tool for efficient underground gas storage management.

In future studies, the focal point could be on specific modeling approaches considering propane-butane liquid storage in relation to the $H_2S_{(g)}$ generation in salt caverns. The existing model can be adapted to different cavern conditions, various hydrocarbons, and is able to consider—besides anhydrite—further sulfur minerals. For upcoming studies, it seems reasonable to implement a multicomponent transport model and to conduct a joint (probabilistic) variation of several parameters as a next step. The software platform RESUS (Bojanowski, 2017; Ghofrani, 2016; Li, 2015)—originally developed for the final disposal of radioactive waste from the Clausthal University of Technology—could be applied. For the evaluation of a specific gas storage system with the development of a numerical model, the physical and chemical data of the underground gas storage system must be measured under in situ conditions. In a next step, the mineral phase assemblages of the reservoir should be exposed to different partial pressures of the stored gases, aqueous solutions, and pressure and temperature conditions in long-term laboratory batch experiments. The mineral dissolution and precipitation, as well as gas compositions, should be observed and the results retraced by batch modeling using identical initial parameters. Such a combination of laboratory experiments and modeling is recommended to test the plausibility of the applied hydrogeochemical equilibrium models.

List of Figures

List of Tables

Abbreviations

aq	Aqueous
BSR	Bacterial sulfate reduction
CCS	Carbon capture and storage
CR	Cap rock
d_m	Diffusion coefficient in pure water
$d´_m$	Effective diffusion coefficient
f	Fugacity
g	Gaseous
IAP	Ion activity product
K	Equilibrium constant
kgw	Kilogram water
M	Molal
P	Pressure
ρ	Partial pressure
pε	Negative log of the activity of the electron (-)
pH	Negative logarithm of the activity of aqueous H^+ ions (-)
RR	Reservoir rock
s	Solid
SCGS	Salt cavern gas storage
SI	Saturation index, (-) (ion activity product/solubility constant)
SRB	Sulfate-reducing bacteria
T	Temperature
TSR	Thermochemical sulfate reduction
UHS	Underground hydrogen storage
wt %	Weight percent
1D	One-dimensional
3D	Three-dimensional
1DRMT	One-dimensional reactive mass transport
3DRMT	Three-dimensional reactive mass transport

References

Adams, M.M., Hoarfrost, A.L., Bose, A., Joye, S.B., Girguis, P.R., 2013. Anaerobic oxidation of short-chain alkanes in hydrothermal sediments: potential influences on sulfur cycling and microbial diversity. Front. Microbiol. 4 (110). doi:10.3389/fmicb.2013.00110.

Adler, M., Eckert, W., Sivan, O., 2011. Quantifying rates of methanogenesis and methanotrophy in Lake Kinneret sediments (Israel) using pore-water profiles. Limnol. Oceanogr. 56 (4), 1525–1535. doi:10.4319/lo.2011.56.4.1525.

Alemu, B.L., Aagaard, P., Munz, I.A., Skurtveit, E., 2011. Caprock interaction with CO_2: A laboratory study of reactivity of shale with supercritical CO_2 and brine. Appl. Geochem. 26 (12), 1975–1989. doi:10.1016/j.apgeochem.2011.06.028.

Allison, J.D., Brown, D.S., Novo-Gradac, K.J., 1991. MINTEQA2/PRODEFA2, a geochemical assessment model for environmental systems: Version 3.0 user's manual. Environmental Research Laboratory, Office of Research and Development, Athens, Georgia, 107 pp.

Amid, A., Mignard, D., Wilkinson, M., 2016. Seasonal storage of hydrogen in a depleted natural gas reservoir. Int. J. Hydrogen Energy 41 (12), 5549–5558. doi:10.1016/j.iJhydene.2016.02.036.

Amosa, M.K., Mohammed, I.A., Yaro, S.A., 2010. Sulphide scavengers in oil and gas industry: A review. NAFTA 61 (2), 85–92.

Angus, S., Armstrong, B., De Reuck, K.M., 1976. Carbon Dioxide – International thermodynamic tables of the fluid state. Pergamon Press Ltd, Oxford–New York, 385 pp.

Appelo, C.A.J., Postma, D., 1999. Geochemistry, groundwater and pollution, 4th ed. Balkema, Rotterdam, 536 pp.

Appelo, C.A.J., Postma, D., 2005. Geochemistry, groundwater and pollution, 2nd ed. CRC Press, Leiden, 649 pp.

Appelo, C.A.J., Wersin, P., 2007. Multicomponent diffusion modeling in clay systems with application to the diffusion of tritium, iodide, and sodium in opalinus clay. Environ. Sci. Technol. 41 (14), 5002–5007. doi:10.1021/es0629256.

Araújo, O.d.Q.F., de Medeiros, J.L., 2017. Carbon capture and storage technologies: Present scenario and drivers of innovation. Curr. Opin. Chem. Eng. 17, 22–34. doi:10.1016/j.coche.2017.05.004.

Arning, E.T., Fu, Y., van Berk, W., Schulz, H.-M., 2011. Organic carbon remineralisation and complex, early diagenetic solid–aqueous solution–gas interactions: Case study ODP Leg 204, Site 1246 (Hydrate Ridge). Mar. Chem. 126 (1–4), 120–131. doi:10.1016/j.marchem.2011.04.006.

Arts, R., Eiken, O., Chadwick, A., Zweigel, P., van der Meer, L., Zinszner, B., 2004. Monitoring of CO_2 injected at Sleipner using time-lapse seismic data. Energy 29 (9–10), 1383–1392. doi:10.1016/j.energy.2004.03.072.

Attia, A.M., 2005. Effects of petrophysical rock properties on tortuosity factor. J. Petrol. Sci. Eng. 48 (3–4), 185–198. doi:10.1016/j.petrol.2005.06.012.

Ball, J.W., Nordstrom, D.K., 1991. User's manual for WATEQ4F, with revised thermodynamic data base and text cases for calculating speciation of major, trace, and redox elements in natural waters: U.S. Geological Survey Open-File Report 91–183, 189 pp.

Barajas, P., Faruk, C., 2014. Effective modeling and analysis of salt-cavern natural-gas storage. SPE Prodcution and Operations 29 (01), 51–60.

Barnes, H.L. (Ed.), 1979. Geochemistry of hydrothermal ore deposits, 2nd ed. Wiley, New York, 816 pp.

Bear, J., 1972. Dynamics of fluids in porous media. American Elsevier, New York, 764 pp.

Bérest, P., Brouard, B., 2003. Safety of salt caverns used for underground storage: Blow out, mechanical instability, seepage, cavern abandonment. Oil Gas Sci. Technol. 58 (3), 361–384.

Bernardez, L.A., de Andrade Lima, L.R., de Jesus, E.B., Ramos, C.L.S., Almeida, P.F., 2013. A kinetic study on bacterial sulfate reduction. Bioprocess. Biosyst. Eng. 36 (12), 1861–1869. doi:10.1007/s00449-013-0960-0.

Bethke, C.M., Yeakel, S., 2009. The Geochemist´s Workbench release 8.0 hydrogeology program. University of Illinois, Urbana, 110 pp.

Beutel, T., Black, S., 2005. Salt deposits and gas cavern gas storage in the UK with a case study of salt exploration from Cheshire. Oil Gas Eur. Mag. 1, 31–35.

Biehl, B.C., Reuning, L., Schoenherr, J., Lewin, A., Leupold, M., Kukla, P.A., 2016. Do CO_2-charged fluids contribute to secondary porosity creation in deeply buried carbonates? Mar. Pet. Geol. 76, 176–186. doi:10.1016/j.marpetgeo.2016.05.005.

Bildstein, O., Kervévan, C., Lagneau, V., Delaplace, P., Crédoz, A., Audigane, P., Perfetti, E., Jacquemet, N., Jullien, M., 2010. Integrative modeling of caprock integrity in the context of CO_2 storage: Evolution of transport and geochemical properties and impact on performance and safety assessment. Oil Gas Sci. Technol. – Rev. IFP 65 (3), 485–502. doi:10.2516/ogst/2010006.

Bischoff, G., Gocht, W., 1984. Energietaschenbuch, 2nd ed. Vieweg+Teubner Verlag, Wiesbaden, 454 pp.

Black, J.R., Carroll, S.A., Haese, R.R., 2015. Rates of mineral dissolution under CO_2 storage conditions. Chem. Geol. 399, 134–144. doi:10.1016/j.chemgeo.2014.09.020.

Blackford, J., Bull, J.M., Cevatoglu, M., Connelly, D., Hauton, C., James, R.H., Lichtschlag, A., Stahl, H., Widdicombe, S., Wright, I.C., 2015. Marine baseline and monitoring strategies for carbon dioxide capture and storage (CCS). Int. J. Greenh. Gas Con. 38, 221–229. doi:10.1016/j.ijggc.2014.10.004.

Blanc, P., Lassin, A., Piantone, P., Azaroual, M., Jacquemet, N., Fabbri, A., Gaucher, E.C., 2012. Thermoddem: A geochemical database focused on low temperature water/rock interactions and waste materials. Appl. Geochem. 27 (10), 2107–2116. doi:10.1016/j.apgeochem.2012.06.002.

BMU, 2010. Sicherheitsanforderungen an die Endlagerung wärmeentwickelnder radioaktiver Abfälle: Bundesministerium für Umwelt, Naturschutz und Reaktorsicherheit, 22 pp.

Bojanowski, R., 2017. Probabilistische Modellierung hydrogeochemischer Prozesse mit dem Code PHAST und der Softwareplattform RESUS. Bachelor Thesis TU Clausthal.

Bolourinejad, P., Herber, R., 2015. Chemical effects of sulfur dioxide co-injection with carbon dioxide on the reservoir and caprock mineralogy and permeability in depleted gas fields. Appl. Geochem. 59, 11–22. doi:10.1016/j.apgeochem.2015.03.003.

Bowden, A.R., Rigg, A., 2005. Assessing reservoir performance risks in CO_2 storage projects, in: Greenhouse gas control technologies. Elsevier, pp. 683–691.

Bozau, E., 2013. Prozessmodellierung hochsalinarer Wässer mit einem erweiterten PHREEQC-Datensatz. Grundwasser 18 (2), 93–98. doi:10.1007/s00767-013-0222-8.

Buzek, F., Onderka, V., Vančura, P., Wolf, I., 1994. Carbon isotope study of methane production in a town gas storage reservoir. Fuel 73 (5), 747–752.

Church, C.D., Wilkin, R.T., Alpers, C.N., Rye, R.O., McCleskey, R.B., 2007. Microbial sulfate reduction and metal attenuation in pH 4 acid mine water. Geochem. T. 8 (10). doi:10.1186/1467-4866-8-10.

Cord-Ruwisch, R., Kleinitz, W., Widdel, F., 1987. Sulfate-reducing bacteria and their activities in oil production. J. Pet. Technol. 39 (01), 97–106.

Cornot-Gandolphe, S., 2017. Underground Gas Storage in the World - 2017 Status. Cedigaz Insights 22, 13 pp.

Credoz, A., Bildstein, O., Jullien, M., Raynal, J., Pétronin, J.-C., Lillo, M., Pozo, C., Geniaut, G., 2009. Experimental and modeling study of geochemical reactivity between clayey caprocks and CO_2 in geological storage conditions. Energy Proced. 1 (1), 3445–3452. doi:10.1016/j.egypro.2009.02.135.

Crotogino, F., 2011. Wasserstoffspeicherung im geologischen Untergrund: Stand der Technik und Potential. KBB Underground Technologies GmbH Hannover. Fachkonferenz Energiespeicher für Deutschland, 2011, Köln.

Crotogino, F., 2016. Larger scale hydrogen storage, in: Letcher, T.M. (Ed.), Storing energy. With special reference to renewable energy sources, 1 ed. Elsevier, Amsterdam, Oxford, Cambridge, pp. 411–429.

Crotogino, F., Donadei, S., Bünger, U., Landinger, H., 2010. Large-scale hydrogen underground storage for securing future energy supplies, in: Stolten, D., Grube, T. (Eds.), 18th World Hydrogen Energy Conference 2010 - WHEC 2010. Proceedings. Forschungszentrum IEF-3, Jülich.

Crotogino, F., Köckritz, V., Reinhold, S., 2006. Conceptual design of storage caverns for an LNG receiving terminal in Europe. SMRI Spring Meeting Brussels (Technical conference paper).

Cussler, E.L., 2009. Diffusion: Mass transfer in fluid systems, 3rd ed. Cambridge Univ. Press, Cambridge, 631 pp.

Davydova-Charakhch`yan, I.A., Kuznetsova, V.G., Mityushina, L.L., Belyaev, S.S., 1992. Methane-forming bacilli from oil fields of Tataria and western Siberia. Microbiology 61, 299–305.

De Windt, L., Burnol, A., Montarnal, P., van der Lee, J., 2003. Intercomparison of reactive transport models applied to UO_2 oxidative dissolution and uranium migration. J. Contam. Hydrol. (61), 303–312.

Dersch-Hansmann, M., Hug-Diegel, N., Wonik, T., 2010. Ein vollständiges Röt-Profil (Oberer Buntsandstein) in Nordhessen - Lithostratigraphie, Sedimentfazies, Geochemie und Geophysik der Kernbohrung Fürstenwald. Geol. Jahrb. Hessen 136, 65–107.

DeVries, K.L., Mellegard, K.D., Callahan, G.D., 2002. Salt damage criterion: Proof-of-concept research. Prepared for the United States Department of Energy and National Energy Technology Laboratory, Rapid City, 90 pp.

DVGW, 2013. Technische Regel-Arbeitsblatt DVGW G 260 (A), Gasbeschaffenheit. Deutscher Verein des Gas und Wasserfaches.

Ebigbo, A., Golfier, F., Quintard, M., 2013. A coupled, pore-scale model for methanogenic microbial activity in underground hydrogen storage. Adv. Water Res. 61, 74–85. doi:10.1016/j.advwatres.2013.09.004.

Ehrlich, H.L., 1990. Geomicrobiology, 2nd ed. Dekker, New York, 646 pp.

Emberley, S., Hutcheon, I., Shevalier, M., Durocher, K., Mayer, B., Gunter, W.D., Perkins, E.H., 2005. Monitoring of fluid–rock interaction and CO_2 storage through produced fluid sampling at the Weyburn CO_2-injection enhanced oil recovery site, Saskatchewan, Canada. Appl. Geochem. 20 (6), 1131–1157. doi:10.1016/j.apgeochem.2005.02.007.

Evans, D.J., 2008. An appraisal of underground gas storage technologies and incidents, for the development of risk assessment methodology. British Geological Survey for the Health and Safety Executive, HSE Books, 264 pp.

Ewing, R.P., Hu, Q., Liu, C., 2010. Scale dependence of intragranular porosity, tortuosity, and diffusivity. Water Resour. Res. 46 (6). doi:10.1029/2009WR008183.

Farahani, A.F., Rahimi, G., Hosseini, S.E., 2015. Economical evaluation of different methods of underground storage of natural gas. Res. J. Rec. Sci. 4(2), 114–119.

Federal Ministry for Education and Research, 2011. Förderinitative Energiespeicher. https://www.bmbf.de/foerderungen/bekanntmachung.php?B=639. Accessed 12 September 2018.

Feist-Burkhardt, S., Götz, A.E., Szulc, J., Borkhataria, R., Geluk, M., Haas, J., Hormung, J., Jordan, P., Kempf, O., Michalik, J., Nawrocki, J., Reinhardt, L., Ricken, W., Röhling, H.-G., Rüffer, T., Török, A., Zühlke, R., 2008. Triassic, in: McCann, T. (Ed.), The geology of Central Europe. Geological Society, London, pp. 749–822.

Flesch, S., Pudlo, D., Albrecht, D., Jacob, A., Enzmann, F., 2018. Hydrogen underground storage—Petrographic and petrophysical variations in reservoir sandstones from laboratory experiments under simulated reservoir conditions. Int. J. Hydrogen Energy 43 (45), 20822–20835. doi:10.1016/j.ijhydene.2018.09.112.

Fleury, M., Berne, P., Bachaud, P., 2009. Diffusion of dissolved CO_2 in caprock. Energy Proced. 1 (1), 3461–3468. doi:10.1016/j.egypro.2009.02.137.

Fleury, M., Pironon, J., Le Nindre, Y.M., Bildstein, O., Berne, P., Lagneau, V., Broseta, D., Pichery, T., Fillacier, S., Lescanne, M., Vidal, O., 2011. Evaluating sealing efficiency of caprocks for CO_2 storage: An overview of the Geocarbone Integrity Program and results. Energy Proced. 4, 5227–5234. doi:10.1016/j.egypro.2011.02.501.

Fontenot, D.J., 1981. Degassing method and apparatus, US4417907 A.

Foster Associates Inc., 1995. Profile of underground natural gas storage facilities and market hubs, Washington, DC, 256 pp.

Friend, D.G., Ely, J.F., Ingham, H., 1989. Thermophysical properties of methane. J. Phys. Chem. Ref. Data 18 (2), 583–638. doi:10.1063/1.555828.

Fu, Y., 2014. Development and application of numerical modeling for evaluating and predicting hydrogeochemical processes temporally and spatially evolving in petroleum reservoirs. Ph.D. Thesis, TU Clausthal, Clausthal-Zellerfeld.

Fu, Y., van Berk, W., Schulz, H.-M., 2016. Hydrogen sulfide formation, fate, and behavior in anhydrite-sealed carbonate gas reservoirs: A three-dimensional reactive mass transport modeling approach. AAPG Bull. 100 (05), 843–865. doi:10.1306/12111514206.

Gaus, I., Audigane, P., André, L., Lions, J., Jacquemet, N., Durst, P., Czernichowski-Lauriol, I., Azaroual, M., 2008. Geochemical and solute transport modelling for CO_2 storage, what to expect from it? Int. J. Greenh. Gas Con. 2 (4), 605–625. doi:10.1016/j.ijggc.2008.02.011.

Gaus, I., Azaroual, M., Czernichowski-Lauriol, I., 2005. Reactive transport modelling of the impact of CO_2 injection on the clayey cap rock at Sleipner (North Sea). Chem. Geol. 217 (3–4), 319–337. doi:10.1016/j.chemgeo.2004.12.016.

Ghassemi, A., Pak, A., 2011. Pore scale study of permeability and tortuosity for flow through particulate media using Lattice Boltzmann method. Int. J. Numer. Anal. Met. Geomech. 35 (8), 886–901. doi:10.1002/nag.932.

Gherardi, F., Xu, T., Pruess, K., 2007. Numerical modeling of self-limiting and self-enhancing caprock alteration induced by CO_2 storage in a depleted gas reservoir. Chem. Geol. 244 (1–2), 103–129. doi:10.1016/j.chemgeo.2007.06.009.

Ghofrani, J., 2016. Conceptualisation and software development of a simulation environment for probabilistic safety assessments of radioactive waste repositories. Ph.D. Thesis, TU Clausthal, Clausthal-Zellerfeld.

Grenthe, I., Plyasunov, A.V., Spahiu, K., 1997. Estimations of medium effects on thermodynamic data, in: Grenthe, I., Allard, B. (Eds.), Modelling in aquatic chemistry. OECD, Paris, pp. 325–426.

Gundogan, O., Mackay, E., Todd, A., 2011. Comparison of numerical codes for geochemical modelling of CO_2 storage in target sandstone reservoirs. Chem. Eng. Res. Des. (89), 1805–1816.

Gusev, M.V., Mineeva, L.A., 1992. Microbiology, Moscow Lomonosov University, Moscow, 464 pp.

Haase, C., Dethlefsen, F., Ebert, M., Dahmke, A., 2013. Uncertainty in geochemical modelling of CO_2 and calcite dissolution in NaCl solutions due to different modelling codes and thermodynamic databases. Appl. Geochem. 33, 306–317. doi:10.1016/j.apgeochem.2013.03.001.

Haddenhorst, H.-G., 1989. Storage of natural gas in salt caverns, in: Tek, M.R. (Ed.), Underground storage of natural gas. Kluwer Academic Publishers, pp. 177–195.

Hagemann, B., Rasoulzadeh, M., Panfilov, M., Ganzer, L., Reitenbach, V., 2016. Hydrogenization of underground storage of natural gas. Comput. Geosci. 20 (3), 595–606. doi:10.1007/s10596-015-9515-6.

Helgeson, H.C., 1967. Solution chemistry and metamorphism. Res. Geochem. 2, 362–404.

Helgeson, H.C., 1968. Evaluation of irreversible reactions in geochemical processes involving minerals and aqueous solutions–I. Thermodynamic relations. Geochim. Cosmochim. Ac. 32 (8), 853–877.

Helgeson, H.C., 1979. Mass transfer among minerals and hydrothermal solutions, in: Barnes, H.L. (Ed.), Geochemistry of hydrothermal ore deposits, 2nd ed. Wiley, New York, pp. 568–610.

Helgeson, H.C., Brown, T.H., Nigrini, A., Jones, T.A., 1970. Calculation of mass transfer in geochemical processes involving aqueous solutions. Geochim. Cosmochim. Ac. 34, 569–592.

Helgeson, H.C., Garrels, R.M., Mackenzie, F.T., 1969. Evaluation of irreversible reactions in geochemical processes involving minerals and aqueous solutions–II. Applications. Geochim. Cosmochim. Ac. 33, 455–481.

Hellevang, H., Aagaard, P., Oelkers, E.H., Kvamme, B., 2005. Can dawsonite permanently trap CO_2? Environ. Sci. Technol. 39 (21), 8281–8287. doi:10.1021/es0504791.

Hemme, C., van Berk, W., 2015. One-dimensional reactive transport modeling of CO_2 storage systems - change in cap rock porosity triggered by pressure and temperature dependent CO_2-water-rock interactions. AGU Fall Meeting, San Francisco.

Hemme, C., van Berk, W., 2017a. Change in cap rock porosity triggered by pressure and temperature dependent CO_2–water–rock interactions in CO_2 storage systems. Petroleum 3 (1), 96–108. doi:10.1016/j.petlm.2016.11.010.

Hemme, C., van Berk, W., 2017b. H_2S generation and release in salt cavern gas storage. AAPG 2017 Annual Convention & Exhibition in Houston, Texas.

Henkel, S., Pudlo, D., Enzmann, F., Reitenbach, V., Albrecht, D., Ganzer, L., Gaupp, R., 2016. X-ray CT analyses, models and numerical simulations: A comparison with petrophysical analyses in an experimental CO_2 study. Solid Earth 7 (3), 917–927. doi:10.5194/se-7-917-2016.

Henkel, S., Pudlo, D., Gaupp, R., 2013. Research sites of the H2STORE project and the relevance of lithological variations for hydrogen storage at depths. Energy Proced. 40, 25–33. doi:10.1016/j.egypro.2013.08.004.

Henkel, S., Pudlo, D., Werner, L., Enzmann, F., Reitenbach, V., Albrecht, D., Würdemann, H., Heister, K., Ganzer, L., Gaupp, R., 2014. Mineral reactions in the geological underground induced by H_2 and CO_2 injections. Energy Proced. 63, 8026–8035. doi:10.1016/j.egypro.2014.11.839.

Herrera, L., Hernández, J., Bravo, L., Romo, L., Vera, L., 1997. Biological process for sulfate and metals abatement from mine effluents. Environ. Toxicol. Water Qual. 12 (2), 101–107.

Holloway, S., 1997. An overview of the underground disposal of carbon dioxide. Energ. Convers. Manage. 38, 193–198.

Hsieh, P.A., Winston, R.B., 2002. User´s guide to Model Viewer, a program for three-dimensional visualization of groundwater model results. U.S. Geological Survey Open-File Report 02–106, 18 pp.

IPCC, 2005. Special report on carbon dioxide capture and storage. Prepared by Working Group III of the International Panel of Climate Change. Cambridge University Press, Cambridge, United Kingdom/New York, NY, USA.

Jacops, E., Volckaert, G., Maes, N., Weetjens, E., Govaerts, J., 2013. Determination of gas diffusion coefficients in saturated porous media: He and CH_4 diffusion in Boom Clay. Appl. Clay Sci. 83–84, 217–223. doi:10.1016/j.clay.2013.08.047.

Jakobsen, R., Postma, D., 1994. In situ rates of sulfate reduction in an aquifer (Rømø, Denmark) and implications for the reactivity of organic matter. Geology 22 (12), 1101–1106. doi:10.1130/0091-7613(1994)022<1103:ISROSR>2.3.CO;2.

Jorgensen, B.B., Isaksen, M.F., Jannasch, H.W., 1992. Bacterial sulfate reduction above 100 °C in deep-sea hydrothermal vent sediments. Science 258 (5089), 1756–1757. doi:10.1126/science.258.5089.1756.

Kallmeyer, J., Boetius, A., 2004. Effects of temperature and pressure on sulfate reduction and anaerobic oxidation of methane in hydrothermal sediments of Guaymas Basin. Appl. Environ. Microbiol. 70 (2), 1231–1233. doi:10.1128/AEM.70.2.1231-1233.2004.

Kalyuzhnyi, S.V., Fedorovich, V.V., 1998. Mathematical modelling of competition between sulphate reduction and methanogenesis in anaerobic reactors. Biores. Technol. 65 (3), 227–242. doi:10.1016/S0960-8524(98)00019-4.

Kemp, S.J., Bouch, J., Murphy, H.A., 2001. Mineralogical characterisation of the Nordland Shale, UK Quadrant 16, northern North Sea, 52 pp.

Kirkner, D.J., Reeves, H., 1988. Multicomponent mass transport with homogeneous and heterogeneous chemical reactions: Effect of the chemistry on the choice of numerical algorithm: 1. Theory. Water Resour. Res. 24 (10), 1719–1729. doi:10.1029/WR024i010p01719.

Kjeldsen, K.U., Loy, A., Jakobsen, T.F., Thomsen, T.R., Wagner, M., Ingvorsen, K., 2007. Diversity of sulfate-reducing bacteria from an extreme hypersaline sediment, Great Salt Lake (Utah). FEMS Microbiol. Ecol. 60 (2), 287–298. doi:10.1111/j.1574-6941.2007.00288.x.

Kleinitz, W., Böhling, E., 2005. Underground gas storage in porous media - operating experience with bacteria on gas quality. Society of Petroleum Engineers SPE 94248 (SPE Europe/EAGE Annual Conference Madrid 13-16 June 2005).

Konikow, L.F., Bredehoeft, J.D., 1992. Ground-water models cannot be validated. Adv. Water Res. 15 (1), 75–83. doi:10.1016/0309-1708(92)90033-X.

Krooss, B., 2008. Evaluation of database on gas migration through clayey host rocks. Belgian National Agency for Radioactive Waste and Enriched Fissile Material (ONDRAF-NIRAS), RWTH Aachen.

Krumbein, W.C., Graybill, F.A., 1965. An introduction to statistical models in geology. McGraw-Hill, New York, 475 pp.

Kyle, J.R., Posey, H.H., 1991. Chapter 5 Halokinesis, cap rock development, and salt dome mineral resources, in: Melvin, J.L. (Ed.), Evaporites, petroleum and mineral resources, vol. 50. Elsevier, Amsterdam, Oxford, New York, Tokyo, pp. 413–474.

Laesecke, A., Muzny, C.D., 2017. Reference correlation for the viscosity of carbon dioxide. J. Phys. Chem. Ref. Data 46. doi:10.1063/1.4977429.

Larin, N., Zgonnik, V., Rodina, S., Deville, E., Prinzhofer, A., Larin, V.N., 2015. Natural molecular hydrogen seepage associated with surficial, rounded depressions on the European Craton in Russia. Nat. Resour. Res. 24 (3), 369–383. doi:10.1007/s11053-014-9257-5.

LBEG, 2016. Untertage-Gasspeicherung in Deutschland, Landesamt für Bergbau, Energie und Geologie. Erdöl Erdgas Kohle 132 (11), 409–417.

Leung, D.Y.C., Caramanna, G., Maroto-Valer, M.M., 2014. An overview of current status of carbon dioxide capture and storage technologies. Renew. Sust. Energ. Rev. 39, 426–443. doi:10.1016/j.rser.2014.07.093.

Li, X., 2015. Entwicklung der Softwareplattform RESUS: Repository Simulation, Uncertainty Propagation and Sensitivity Analysis. Ph.D. Thesis, TU Clausthal, Clausthal-Zellerfeld.

Lindenberg, E., Wessel-Berg, D., 1997. Vertical convection in an aquifer column under a gas cap of CO_2. Energ. Convers. Manage. (38), 229–234.

Liu, H., Hou, Z., Were, P., Gou, Y., Xiong, L., Sun, X., 2015. Modelling CO_2-brine-rock interactions in the Upper Paleozoic formations of Ordos Basin used for CO_2 sequestration. Environ. Earth Sci. 73 (5), 2205–2222. doi:10.1007/s12665-014-3571-4.

Lord, A.S., Kobos, P.H., Borns, D.J., 2014. Geologic storage of hydrogen: Scaling up to meet city transportation demands. Int. J. Hydrogen Energy 39 (28), 15570–15582. doi:10.1016/j.iJhydene.2014.07.121.

Machel, H.G., 2001. Bacterial and thermochemical sulfate reduction in diagenetic settings — old and new insights. Sedimentary Geol. 140 (1–2), 143–175. doi:10.1016/S0037-0738(00)00176-7.

Magot, M., Ollivier, B., Patel, B.K.C., 2000. Microbiology of petroleum reservoirs. Antonie van Leeuwenhoek 77 (2), 103–116. doi:10.1023/A:1002434330514.

Marini, L., 2007. Geological sequestration of carbon dioxide: Thermodynamics, kinetics, and reaction path modeling. Elsevier, Amsterdam, 453 pp.

McCarty, R.D., Hord, J., Roder, H.M., 1981. Selected properties of hydrogen (engineering design data). National Bureau of Standards Monograph 168 - U.S. Department of Commerce, Boulder, CO, 523 pp.

Merkel, B.J., Planer-Friedrich, B., 2002. Grundwasserchemie: Praxisorientierter Leitfaden zur numerischen Modellierung von Beschaffenheit, Kontamination und Sanierung aquatischer Systeme. Springer, Berlin, 219 pp.

Meulepas, R.J.W., Stams, A.J.M., Lens, P.N.L., 2010. Biotechnological aspects of sulfate reduction with methane as electron donor. Rev. Environ. Sci. Bio./Techn. 9 (1), 59–78. doi:10.1007/s11157-010-9193-8.

Mohd Amin, S., Weiss, D.J., Blunt, M.J., 2014. Reactive transport modelling of geologic CO_2 sequestration in saline aquifers: The influence of pure CO_2 and of mixtures of CO_2 with CH_4

on the sealing capacity of cap rock at 37°C and 100bar. Chem. Geol. 367, 39–50. doi:10.1016/j.chemgeo.2014.01.002.

NLWKN, 2015. Grundwassermessstelle Brauel I Stade. Niedersächsiches Ministerium für Umwelt, Energie und Klimaschutz. www.umweltkarten-niedersachsen.de. Accessed 5 January 2017.

Nowack, B., Mayer, K.U., Oswald, S.E., van Beinum, W., Appelo, C.A.J., Jacques, D., Seuntjens, P., Gérard, F., Jaillard, B., Schnepf, A., Roose, T., 2006. Verification and intercomparison of reactive transport codes to describe root-uptake. Plant Soil (285), 305–321.

Palandri, J.L., Kharaka, Y.K., 2004. A compilation of rate parameters of water-mineral interaction kinetics for application to geochemical modeling, Menlo Park, California, 64 pp.

Panfilov, M., 2010. Underground storage of hydrogen: In situ self-organisation and methane generation. Transp. Porous Med. 85 (3), 841–865. doi:10.1007/s11242-010-9595-7.

Panfilov, M., 2016. Underground and pipeline hydrogen storage, in: Gupta, R.B., Basile, A., Veziroğlu, T.N. (Eds.), Compendium of hydrogen energy. Volume 2: Hydrogen storage, distribution and infrastructure. Elsevier, Cambridge, Waltham, Kidlington, pp. 91–115.

Panfilov, M., Gravier, G., Fillacier, S., 2006. Underground storage of H_2 and H_2-CO_2-CH_4 mixtures, in: ECMOR X - 10th European Conference on the Mathematics of Oil Recovery, Amsterdam, Netherlands. 04.09.2006 - 07.09.2006. EAGE Publications.

Pape, H., Clauser, C., Iffland, J., 2000. Variation of permeability with porosity in sandstone diagenesis interpreted with a fractal pore space model. Pure Appl. Geophys. 157 (4), 603–619.

Parkhurst, D.L., Appelo, C.A.J., 1999. Users guide to PHREEQC Version 2— A computer program for speciation, batch-reaction, one-dimensional transport and inverse geochemical calculations.: U.S. Geological Survey, Denver, Colorado, 326 pp.

Parkhurst, D.L., Appelo, C.A.J., 2013. Description of input for PHREEQC Version 3—A computer program for speciation, batch-reaction, one-dimensional transport, and inverse geochemical calculations: U.S. Geological Survey Techniques and Methods 6-A43, 519 pp.

Parkhurst, D.L., Kipp, K.L., Charlton, S.R., 2010. PHAST Version 2—A program for simulating groundwater flow, solute transport, and multicomponent geochemical reactions: U.S. Geological Survey Techniques and Methods 6-A35, 235 pp.

Parkhurst, D.L., Thorstenson, D.C., Plummer, N., 1980. PHREEQE—A computer program for geochemical calculations: U.S. Geological Survey Water-Resources Investigations Report 80–96, 195 pp.

Pietzner, K., 2012. Folgeprojekt CCS-Kommunikation - Multivariate Analysen der Einflussfaktoren auf die Akzeptanz von CCS. Wuppertal Institut für Klima, Umwelt, Energie GmbH, 70 pp.

Pitzer, K.S., 1973. Thermodynamics of electrolytes. I. Theoretical basis and general equations. J. Phys. Chem. 77 (2), 268–277. doi:10.1021/j100621a026.

Ponomarev-Stepnoi, N.N., 2004. Nuclear-hydrogen power. Atomic Energy 96 (6), 375–385.

Postgate, J.R., 1979. The sulphate-reducing bacteria. Cambridge University Press, Cambridge, 151 pp.

Postgate, J.R., 1984. The sulphate-reducing bacteria, 2nd ed. Cambridge University Press, Cambridge, 208 pp.

Pruess, K., 2013. Numerical simulation of CO_2 leakage from a geologic disposal reservoir, including transitions from super- to subcritical conditions, and boiling of liquid CO_2. SPE Journal 9 (02), 237–248. doi:10.2118/86098-PA.

Pudlo, D., Ganzer, L., Henkel, S., Kühn, M., Liebscher, A., De Lucia, M., Panfilov, M., Pilz, P., Reitenbach, V., Albrecht, D., Würdemann, H., Gaupp, R., 2010. The H2STORE Project: Hydrogen underground storage – A feasible way in storing electrical power in geological media?, in: Hou, M.Z., Xie, H., Yoon, J.S. (Eds.), Underground storage of CO_2 and energy. CRC Press, Taylor & Francis Group, Boca Raton, Fla., pp. 395–412.

Reichl, A., Schneider, G., Schliepdiek, T., Reimuth, O., 2015. Carbon capture and storage for enhanced oil recovery: integration and optimization of a post-combustion CO_2-capture facility at a power plant in Abu Dhabi. Oil Gas Facili. 05 (4), 37–46. doi:10.2118/171692-PA.

Reitenbach, V., Ganzer, L., Albrecht, D., Hagemann, B., 2015. Influence of added hydrogen on underground gas storage: A review of key issues. Environ. Earth Sci. 73 (11), 6927–6937. doi:10.1007/s12665-015-4176-2.

Réveillère, B., Azimi, B., Arnold, C., 2016. Prevention of stored gas humidification: lessons learnt and review of possibilities. Solution Mining Research Institute Spring 2016 Technical Conference, Galveston, Texas, USA.

Robinson, J.A., Tiedje, J.M., 1984. Competition between sulfate-reducing and methanogenic bacteria for H_2 under resting and growing conditions. Arch. Microbiol. 137 (1), 26–32. doi:10.1007/BF00425803.

Rochelle, C.A., Moore, Y.A., 2002. The solubility of supercritical CO_2 into pure water and synthetic Utsira pore water: British Geological Survey report CR/02/052N, 28 pp.

Rutqvist, J., Birkholzer, J., Cappa, F., Tsang, C.-F., 2007. Estimating maximum sustainable injection pressure during geological sequestration of CO_2 using coupled fluid flow and geomechanical fault-slip analysis. Energ. Convers. Manage. 48 (6), 1798–1807. doi:10.1016/j.enconman.2007.01.021.

Salimi, H., Wolf, K.-H., Bruining, J., 2012. The influence of capillary pressure on the phase equilibrium of the CO_2–water system: Application to carbon sequestration combined with geothermal energy. Int. J. Greenh. Gas Con. 11, 47–66. doi:10.1016/j.ijggc.2012.09.015.

Sato, M., Sutton, A.J., McGee, K.A., Russell-Robinson, S., 1986. Monitoring of hydrogen along the San Andreas and Calaveras faults in central California in 1980-1984. J. Geophys. Res. Solid Earth 91 (B12), 12315–12326. doi:10.1029/JB091iB12p12315.

Schäfer, D., 2004. Numerische Modellierung reaktiver Prozesse organischer Kontaminanten in Grundwasserleitern: Habilitationsschrift. Institut für Geowissenschaften, Christian-Albrechts-Universität zu Kiel.

Schilling, F., Ossing, F., Würdemann, H., CO2SINK Team, 2009. Public acceptance for geological CO_2-Storage. Geophysical Research Abstracts. Vol. 11, EGU2009-13801-2, 2009.

Schneider, R., Crotogino, F., 2010. New developments in Europe´s salt cavern projects, in: Hou, M.Z., Xie, H., Yoon, J.S. (Eds.), Underground storage of CO_2 and energy. CRC Press, Taylor & Francis Group, Boca Raton, Fla., pp. 199–205.

Schreiber, B.C., Bąbel, M., 2007. Evaporites through space and time. Geol. Soc. Sp. 285 (1). doi:10.1144/SP285.

Schulze, F., Keimeyer, F., Schöne, R., Westphal, I., Janssen, G., Bartel, S., Seiffert, S., 2015. Unterirdische Raumplanung – Vorschläge des Umweltschutzes zur Verbesserung der über- und untertägigen Informationsgrundlagen, zur Ausgestaltung des Planungsinstrumentariums und zur nachhaltigen Lösung von Nutzungskonflikten:

Teilvorhaben 2: planerische und rechtliche Aspekte. Umweltbundesamt, Dessau-Roßlau, 324 pp.

Shen, L., Chen, Z., 2007. Critical review of the impact of tortuosity on diffusion. Chem. Eng. Sci. 62 (14), 3748–3755. doi:10.1016/j.ces.2007.03.041.

Šmigáň, P., Greksák, M., Kozánková, J., Buzek, F., Onderka, V., Wolf, I., 1990. Methanogenic bacteria as a key factor involved in changes of town gas stored in an underground reservoir. FEMS Microbiol. Lett. 73 (3), 221–224. doi:10.1111/j.1574-6968.1990.tb03944.x.

Somerday, B.P., Gangloff, R.P. (Eds.), 2012. Mechanisms, modelling and future developments. Woodhead Pub, Cambridge, U.K, Phildelphia, Pa, 500 pp.

Soyk, D., 2015. Diagenesis and reservoir quality of the Lower and Middle Buntsandstein (Lower Triassic), SW Germany. Ph.D. Thesis, University of Heidelberg.

Steefel, C.I., DePaolo, D.J., Lichtner, P.C., 2005. Reactive transport modeling: An essential tool and a new research approach for the Earth sciences. Earth Planet. Sc. Lett. 240 (3–4), 539–558. doi:10.1016/j.epsl.2005.09.017.

Stone, H.B.J., Veldhuis, I., Richardson, R.N., 2009. Underground hydrogen storage in the UK. Geol. Soc. Sp. 313 (1), 217–226. doi:10.1144/SP313.13.

Stumm, W., Morgan, J.J., 1981. Aquatic Chemistry: An introduction emphasizing chemical equilibria in natural waters, 2nd ed. John Wiley & Sons, Inc., New York, 780 pp.

Szabó, Z., Hellevang, H., Király, C., Sendula, E., Kónya, P., Falus, G., Török, S., Szabó, C., 2016. Experimental-modelling geochemical study of potential CCS caprocks in brine and CO_2-saturated brine. Int. J. Greenh. Gas Con. 44, 262–275. doi:10.1016/j.ijggc.2015.11.027.

Taylor, J.B., Alderson, J.E.A., Kalyanam, K.M., Lyle, A.B., Phillips, L.A., 1986. Technical and economic assessment of methods for the storage of large quantities of hydrogen. Int. J. Hydrogen Energy 11 (1), 5–22.

Thorstenson, D.C., Parkhurst, D.L., 2002. Calculation of individual isotope equilibrium constants for implementation in geochemical models: U.S. Geological Survey Water-Resources Investigations Report 02-4172, 129 pp.

Thorstenson, D.C., Parkhurst, D.L., 2004. Calculation of individual isotope equilibrium constants for geochemical reactions. Geochim. Cosmochim. Ac. 68 (11), 2449–2465. doi:10.1016/j.gca.2003.11.027.

Tian, H., Pan, F., Xu, T., McPherson, B.J., Yue, G., Mandalaparty, P., 2014. Impacts of hydrological heterogeneities on caprock mineral alteration and containment of CO_2 in geological storage sites. Int. J. Greenh. Gas Con. 24, 30–42. doi:10.1016/j.ijggc.2014.02.018.

Tian, H., Xu, T., Li, Y., Yang, Z., Wang, F., 2015. Evolution of sealing efficiency for CO_2 geological storage due to mineral alteration within a hydrogeologically heterogeneous caprock. Appl. Geochem. 63, 380–397. doi:10.1016/j.apgeochem.2015.10.002.

Timmers, P.H., Suarez-Zuluaga, D.A., van Rossem, M., Diender, M., Stams, A.J., Plugge, C.M., 2016. Anaerobic oxidation of methane associated with sulfate reduction in a natural freshwater gas source. ISME J 10 (6), 1400–1412. doi:10.1038/ismej.2015.213.

Timmers, P.H.A., Gieteling, J., Widjaja-Greefkes, H.C.A., Plugge, C.M., Stams, A.J.M., Lens, P.N.L., Meulepas, R.J.W., 2015. Growth of anaerobic methane-oxidizing archaea and sulfate-reducing bacteria in a high-pressure membrane capsule bioreactor. Appl. Environ. Microbiol. 81 (4), 1286–1296. doi:10.1128/AEM.03255-14.

Truche, L., Berger, G., Destrigneville, C., Guillaume, D., Giffaut, E., 2010. Kinetics of pyrite to pyrrhotite reduction by hydrogen in calcite buffered solutions between 90 and 180°C:

Implications for nuclear waste disposal. Geochim. Cosmochim. Ac. 74 (10), 2894–2914. doi:10.1016/j.gca.2010.02.027.

Truche, L., Jodin-Caumon, M.-C., Lerouge, C., Berger, G., Mosser-Ruck, R., Giffaut, E., Michau, N., 2013. Sulphide mineral reactions in clay-rich rock induced by high hydrogen pressure. Application to disturbed or natural settings up to 250 °C and 30 bar. Chem. Geol. 351, 217–228. doi:10.1016/j.chemgeo.2013.05.025.

Tuttle, J.H., Dugan, P.R., Randles, C.I., 1969. Microbial sulfate reduction and its potential utility as an acid mine water pollution abatement procedure. Appl. Microbiol. 17 (2), 297–302.

U.S. Environmental Protection Agency, 1999. MINTEQA2/PRODEFA2, A geochemical assessment model for environmental systems: User manual supplement for version 4.0. National Exposure Research Laboratory, Ecosystems Research Division, Athens, Georgia, 76 pp.

van Berk, W., Fu, Y., Schulz, H.-M., 2015. Creation of pre-oil-charging porosity by migration of source-rock-derived corrosive fluids through carbonate reservoirs: one-dimensional reactive mass transport modelling. Petrol. Geosci. (21), 35–42. doi:10.1144/petgeo2014-065.

van Berk, W., Hansen, C., 2006. Hydrogeochemische Stoffflussmodelle: Leitfaden zur Modellierung der Beschaffenheitsentwicklung von Grund- und Rohwässern. Springer-Verlag, Berlin, Heidelberg, 226 pp.

Van Pham, T.H., Aagaard, P., Hellevang, H., 2012. On the potential for CO_2 mineral storage in continental flood basalts - PHREEQC batch- and 1D diffusion-reaction simulations. Geochem. T. 13 (5).

Vaughan, P.J., 1987. Analysis of permeability reduction during flow of heated, aqueous fluid through westerly granite, in: Tsang, C.-F. (Ed.), Coupled processes associated with nuclear waste repositories. Acad. Pr, Orlando, Fla., pp. 529–539.

Verdon, J.P., Stork, A.L., 2016. Carbon capture and storage, geomechanics and induced seismic activity. J. Rock Mechan. Geotechnol. Eng. 8 (6), 928–935. doi:10.1016/j.jrmge.2016.06.004.

Verma, A., Pruess, K., 1988. Thermohydrological conditions and silica redistribution near high-level nuclear wastes emplaced in saturated geological formations. J. Geophys. Res. 93, 1159–1173. doi:10.1029/JB093iB02p01159.

Vinograd, J.R., McBain, J.W., 1941. Diffusion of electrolytes and of the ions in their mixtures. J. Am. Chem. Soc. 63 (7), 2008–2015. doi:10.1021/ja01852a063.

Vögele, S., Rübbelke, D., Mayer, P., Kuckshinrichs, W., 2018. Germany's "No" to carbon capture and storage: Just a question of lacking acceptance? Appl. Energ. 214, 205–218. doi:10.1016/j.apenergy.2018.01.077.

Wakita, H., Nakamura, Y., Kita, I., Fujii, N., Notsu, K., 1980. Hydrogen release: New indicator of fault activity. Science 210 (4466), 188–190. doi:10.1126/science.210.4466.188.

Wang, T., Yang, C., Yan, X., Daemen, J.J.K., 2015. Allowable pillar width for bedded rock salt caverns gas storage. J. Petrol. Sci. Eng. 127, 433–444. doi:10.1016/j.petrol.2015.01.040.

Ware, R.H., Roecken, C., Wyss, M., 1985. The detection and interpretation of hydrogen in fault gases. PAGEOPH 122 (2–4), 392–402. doi:10.1007/BF00874607.

Whitman, W.B., Bowen, T.L., Boone, D.R., 2006. The methanogenic bacteria, in: Dworkin, M., Falkow, S., Rosenberg, E., Schleifer, K.-H., Stackebrandt, E. (Eds.), The Prokaryotes. A handbook on the biology of bacteria. Springer, New York, pp. 165–207.

Wolery, T.J., 1992. EQ3/6, A software package for geochemical modeling of aqueous systems: Package overview and installation guide (Version 7.0). Lawrence Livermore National Laboratory, Livermore, California, 66 pp.

Wollenweber, J., Alles, S., Busch, A., Krooss, B.M., Stanjek, H., Littke, R., 2010. Experimental investigation of the CO_2 sealing efficiency of caprocks. Int. J. Greenh. Gas Con. 4 (2), 231–241. doi:10.1016/j.ijggc.2010.01.003.

Yang, C., Jing, W., Daemen, J.J.K., Zhang, G., Du, C., 2013. Analysis of major risks associated with hydrocarbon storage caverns in bedded salt rock. Reliab. Eng. Syst. Safe. 113, 94–111. doi:10.1016/j.ress.2012.12.017.

Yekta, A.E., Pichavant, M., Audigane, P., 2018. Evaluation of geochemical reactivity of hydrogen in sandstone: Application to geological storage. Appl. Geochem. 95, 182–194. doi:10.1016/j.apgeochem.2018.05.021.

Zander-Schiebenhöfer, D., Donadei, S., Schneider, G.-S., 2014. Mögliche Nutzungskonkurrenzen bei Energiespeichern im Untergrund. Akademie für Geowissenschaften und Geotechnologien e.V. 30, 37–42. doi:10.7788/figurationen-2014-0104.

Zgonnik, V., Beaumont, V., Deville, E., Larin, N., Pillot, D., Farrell, K.M., 2015. Evidence for natural molecular hydrogen seepage associated with Carolina bays (surficial, ovoid depressions on the Atlantic Coastal Plain, Province of the USA). Prog. Earth Planet. Sci. 2 (31). doi:10.1186/s40645-015-0062-5.

Zimmermann, G., Jacob, G., Lautenschläger, K.-H., Richter, G., Teschner, J., 1986. Wissensspeicher, 7th ed. Dt. Verl. für Grundstoffindustrie, Leipzig, 71 pp.

ZoBell, C.E., 1958. Ecology of sulfate reducing bacteria. Prod. Monthly 22 (7), 12–29.